Evaluation of Pipeline Performance Subjected to Slope Instabilities

by

Mohammad Katebi

A Thesis submitted to the Faculty of Graduate Studies of

The University of Manitoba

in partial fulfilment of the requirements of the degree of

DOCTOR OF PHILOSOPHY

Department of Civil Engineering

University of Manitoba

Winnipeg

Declaration of Authorship

I, Mohammad KATEBI, declare that this thesis titled, "Evaluation of pipeline performance subjected to slope instabilities" and the work presented in it are my own. I confirm that:

- This work was done wholly or mainly while in candidature for a research degree at this University.
- Where any part of this thesis has previously been submitted for a degree or any other qualification at this University or any other institution, this has been clearly stated.
- Where I have consulted the published work of others, this is always clearly attributed.
- Where I have quoted from the work of others, the source is always given. With the exception of such quotations, this thesis is entirely my own work.
- I have acknowledged all main sources of help.
- Where the thesis is based on work done by myself jointly with others, I have made clear exactly what was done by others and what I have contributed myself.

Abstract

Mohammad KATEBI

Evaluation of pipeline performance subjected to slope instabilities

The horizontal soil-pipe interaction in slopes is characterized in this research program for inclusion in pipeline guidelines. For this purpose, a series of full-scale experiments were conducted at the Advanced Soil-Pipe Interaction Research (ASPIRe™) testing facility at the University of British Columbia, Vancouver, BC, Canada. The experimental data indicated that the soil load is an increasing function of the slope grade for soil springs inside the landslide boundaries and a decreasing function of the slope grade for soil springs outside the landslide boundaries. The lateral force-displacement responses of pipes installed below sloping ground were presented and compared to those arising from the level ground condition. The experimental results suggest that the values of the horizontal bearing capacity factor can be two-fold higher than those estimated using pipeline guidelines. A finite element model was calibrated against the experimental data and was implemented in an extensive parametric study to extend the results to deep embedment conditions for loose, medium and dense sands. The horizontal bearing capacity factors are presented in dimensionless graphs as a function of the slope grade and pipe burial depth, which can be used in pipeline guidelines as a benchmark for the design.

Acknowledgements

I want to start by thanking my supervisor, Dr. Pooneh Maghoul, who supported and guided me throughout this endeavour. She was always accessible for me, being day or night, weekdays or weekends. She gave me encouragement and provided me with the opportunity to choose this field of research so I am deeply indebted and appreciative of her.

Next on my appreciation list is my co-supervisor, Dr. Dharma Wijewickreme, who provided me with necessary resources to perform the full-scale experiments at the UBC testing facility. I am truly thankful and appreciative of him as his support had a remarkable impact on the success of this research project.

I would like thank Dr. James Blatz, who mentored me conducting two research projects, presented in Chapter 3 and 4. His experience and knowledge gave me the vision required to complete this research with satisfactory results.

I want to thank Dr. Kshama Roy who has provided me with expertise required to perform the numerical part of the work in Chapter 2. I am very appreciative of him as he has been very supportive.

I would like to thank Hongwei Liu for that the research presented in chapter 4 is completed with his collaboration.

I would like to thank Dr. Hamid Karimian for his inputs. The discussion we had in the international pipeline conference in Calgary (2018) was very insightful and helped me to see the bigger picture and the industry need.

I would also like to thank the technical staff, Doug Hudniuk, Scott Jackson, Sylvain Picard and Simon Lee, and the undergraduate students, Eric Hebbard, Bradley Jeffrey, Yufeng Qiu, Diao Ruoshi, Parsa Taghvaei, Catalina Ospina who helped me with the test preparation and the setup of the large-scale testing equipment at UBC. Their hard work made this project finished in time.

I am grateful for the scholarships and awards that I received during this program. These include Natural Sciences and Engineering Research Council of Canada (NSERC), Mitacs Accelerate award, the University of Manitoba Graduate Enhancement of Tri-Council Stipends (GETS), TransCanada Pipelines Graduate Fellowship in Engineering, FGS Research Completion Scholarship (2019), Edward R. Toporeck Graduate Fellowship in Engineering (2020), and the University of Manitoba Travel Awards.

Last but not least, I want to thank my wife and parents who have walked with me in the long journey of education.

List of Publications

Journal papers:

- Katebi M., Wijewickreme D., Maghoul P., Roy K., 2020. Lateral force-displacement response of buried pipes in slopes. In: *Géotechnique (ICEPublishing)*, manuscript no. 20-P-284, under review.

- Katebi M., Maghoul P., Blatz J., 2019. Numerical analysis of pipeline response to landslides: case study. In: *Canadian Geotechnical Journal (Canadian Science Publishing), 56(12): 1779-1788.* (Katebi et al., 2019b)

Conference papers:

- Katebi M., Wijewickreme D., Maghoul P., Roy K., 2020. Effects of slope grade on soil-pipe interaction: full-scale experiments. In: *International pipeline conference 2020.*

- Katebi M., Maghoul P., Blatz J., Roy K., Wijewickreme D., A study on the effects of slope grade on the soil-pipeline interaction loading. In: *Geostjohns2019 conference.* (Katebi et al., 2019a)

- Katebi M., Hongwei L., Maghoul P., Roy K. The optimum pipeline burial depth considering slow downslope soil movement and seasonal temperature variation. In: *International pipeline conference 2018.* (Katebi et al., 2018)

Contributions of authors

Chapter 2: Katebi, M., Wijewickreme, D., Maghoul, P., Roy, K.

- Katebi: project conceptualization, methodology development, laboratory work, modelling simulations, results interpretation, original drafting and revising the paper.
- Wijewickreme: project conceptualization, criticized methodology, supervision of the laboratory work, funding acquisition, review and edit.
- Maghoul: project conceptualization, criticized methodology, supervision of the modelling simulations, funding acquisition, review and edit.
- Roy: supervision of the modelling simulations, industry partner and supervisor (NSERC Engage & MITACS Accelerate), review and edit.

Chapter 3: Katebi, M., Maghoul, P., Blatz, J.

- Katebi: methodology development, modelling simulations, results interpretation, original drafting and revising the paper.
- Maghoul: project conceptualization, criticized methodology, supervision of the modelling simulations, funding acquisition, review and edit.
- Blatz: field data, data interpretation, review and edit.

Chapter 4: Katebi, M., Hongwei, L., Maghoul, P., Blatz, J.

- Katebi: project conceptualization, methodology development, modelling simulations, results interpretation, original drafting and revising the paper.
- Hongwei: thermal analysis
- Maghoul: project conceptualization, criticized methodology, supervision of the modelling simulations, review and edit.
- Blatz: review and edit.

List of Copyrighted Materials

Materials used in chapter 2, 3 and 4 of this thesis are reproduced, with modifications from following publications:

- Katebi M., Wijewickreme D., Maghoul P., Roy K., 2020. Lateral force-displacement response of buried pipes in slopes. In: *Géotechnique (ICEPublishing)*, manuscript no. 20-P-284, under review.
- Katebi M., Wijewickreme D., Maghoul P., Roy K., 2020. Effects of slope grade on soil-pipe interaction: full-scale experiments. In: *International pipeline conference 2020.*
- Katebi M., Maghoul P., Blatz J., 2019. Numerical analysis of pipeline response to landslides: case study. In: *Canadian Geotechnical Journal (Canadian Science Publishing), 56(12): 1779-1788.* (Katebi et al., 2019b)
- Katebi M., Hongwei L., Maghoul P., Roy K. The optimum pipeline burial depth considering slow downslope soil movement and seasonal temperature variation. In: *International pipeline conference 2018.* (Katebi et al., 2018)

Contents

List of Tables

List of Figures

List of Abbreviations

FEM	**F**inite **E**lement **M**odel
GPS	**G**lobal **P**ositioning **S**ystem
MC	**M**ohr **C**oulomb
MMC	**M**odified **M**ohr **C**oulomb
NEB	**N**ational **E**nergy **B**oard
NPS	**N**ominal **P**ipe **S**ize
PE	**P**lastic **S**train
PSI	**P**ipe **S**oil **I**nteraction
RTK	**R**eal **T**ime **K**inematic
SI	**S**lope **I**nclinometer
UTM	**U**niversal **T**ransverse **M**ercador
VW	**V**ibrating **W**ire

List of Symbols

α	adhesion factor in chapter 1 and 3
α	slope angle in chapter 2
α	thermal expansion coefficient in chapter 4
α_L	linear expansion coefficient
γ'	effective unit weight of soil
γ	total unit weight of soil
θ_i	volumetric ice content of a soil
θ_r	residual volumetric water content
θ_s	saturated volumetric water content
θ_w	unfrozen volumetric water content
θ_{wo}	initial volumetric water content
μ	soil-pipe interface friction coefficient
ν	Poisson's ratio
ν_{air}	kinematic viscosity of air
ξ	burial depth ratio
ρ	density
ρ^{ph}	soil density considering the phase change
ρ_i	density of ice
ρ_s	density of soil skeleton

ρ_w	density of water
σ_B	longitudinal stress due to bending
σ_L	longitudinal stress in the pipe wall
σ_P	longitudinal stress due to internal pressure
σ_T	longitudinal stress due to temperature change
σ_X	longitudinal stress in the pipe wall
σ_y	Ultimate tensile strength of steel
ϕ'	internal friction angle of soil
ϕ'_μ	soil-pipe interface friction angle
ϕ_{crit}	critical state friction angle
ψ	dilation angle
c	soil cohesion
C_{pp}^{ph}	apparent heat capacity of the soil considering the phase change
C_p^{ph}	specific heat capacity considering the phase change
C_{pi}	specific heat capacity of ice
C_{ps}	specific heat capacity of the soil skeleton
C_{pw}	specific heat capacity of water
C_{u}	coefficient of uniformity
D	outside pipe diameter
D_{50}	average particle size
e_{max}	maximum void ratio
e_{min}	minimum void ratio
E	elastic modulus
E_{i}	initial Young's modulus
F_a	maximum axial soil on the pipe
F_h	horizontal load per unit length of pipe

$\bar{F}_h$	dimensionless horizontal load per unit length of pipe
G_s	specific gravity
h_{conv}	convection heat transfer coefficient
k_0	coefficient of earth pressure at rest
k_a	thermal conductivity of air
k_i	thermal conductivity of ice
k^{ph}	thermal conductivity of the soil considering phase change
k_s	thermal conductivity of soil skeleton
k_w	thermal conductivity of water
K	coefficient of lateral earth pressure
L_{anchor}	anchor length of pipe
L_f	latent heat
$\bar{L}$	characteristic length of the ground affected by the wind in the wind's direction
$N_\mathrm{c}, N_\mathrm{q}, N_\gamma$	bearing capacity factors
N_qh	horizontal bearing capacity factor for sand
N_ch	horizontal bearing capacity factor for clay
N_qv	uplift bearing capacity factor for sand
N_cv	uplift bearing capacity factor for clay
P_{max}	maximum operating pressure
Pr	Prandtl number of air
q_{conv}	surface convection heat flux
Q	heat source
Re_L	Reynolds number
S_u	undrained shear strength of soil
t	pipe wall thickness in chapter 2
t	time in chapter 4

t_u	ultimate axial force
T	temperature of the soil
T_0	freezing temperature
T_a	ambient air temperature
T_s	temperature on the ground surface
V	wind speed at the ground surface
x_u	ultimate relative displacement
Y	transverse pipe displacement
$\bar{Y}$	normalized horizontal displacement of the pipe
Y_{p}	critical pipe displacement (the displacement at the peak load)

Dedicated to my son who is one man I
love more than any other

Chapter 1

Introduction

Pipelines are commonly used for transporting oil and gas from production sites to facilities and storage tanks. Pipeline infrastructure is an integral component of oil and gas transportation networks in Canada, and its integrity has an important impact on the economy of the country. In Canada, there is an aggregate of 242,000 km of oil and gas pipelines, which is considered the second-longest pipeline network in the world. Pipelines are often installed below ground to mitigate damage from external forces such as third party accidents and natural hazards. They traverse regions with a variety of terrains, topographic and geological conditions and may be exposed to geohazards such as landslide, fault, soil settlement, heave, lateral spreading and liquefaction. Pipeline incidents are often environmentally damaging and extremely costly to clean-up and remediate. In Canada, according to the National Energy Board (NEB) database, about 750 incidents have occurred since 2008 on major pipelines, including 454 gas and oil leaks, 25 cases of serious injury, six deaths, 13 explosions and seven cases of adverse environmental effects. Loss-of-containment events are often environmentally damaging and extremely costly to clean-up and remediate. Also, civil, criminal or regulatory penalties from a pipeline loss of containment may be very high (Oswell, 2016).

The relative displacement of pipe and soil is translated into external forces on the pipe,

and the pipe response depends on various factors such as the pipe and soil materials, the extend of the ground displacement, loading direction, displacement rate, interface behaviour and operational conditions. Current pipeline guidelines such as PRCI (2017) and ALA (2001) provide useful information on how to assess the conditions of existing buried pipes and the system demand and capacity for stress-based design of these systems. Pipe elongation, buckling, fracturing and plastic collapse are examples of pipeline failure modes. The relative soil-pipe displacement may be developed through a variety of conditions. Revie (2015) categorize these conditions into four main groups:

- environmental conditions such as water level condition or soil weight
- operational conditions such as pipe weight and thermal expansion
- construction activities such as mining, blasting and road building
- geohazards such as landslides, liquefaction, and faults

The estimation of pipeline performance in ground displacements has been the focus of research for the past four decades. In industry practice, pipeline response subject to ground displacements is typically assessed with finite element models that account for soil-pipe interaction with discrete independent soil springs. Soil springs, commonly called p-y curves, are nonlinear load-displacement relations defined in four principal directions: longitudinal axial, horizontal lateral, vertical uplift and vertical bearing. The four independent soil springs are shown in Fig. 1.1. The displacement mechanisms associated with each soil spring are shown in Fig. 1.2. In real-life problems, the pipe can be exposed to a combination of various loading conditions, and so the separation of these mechanisms are not very realistic. Despite the advances in computing power and modelling techniques, the soil-pipe interaction problems with real-life conditions are still beyond the capability of existing three-dimensional continuum techniques. Herein, we list some of the limitations of the three-dimensional continuum models that have to be overcome in order to be considered

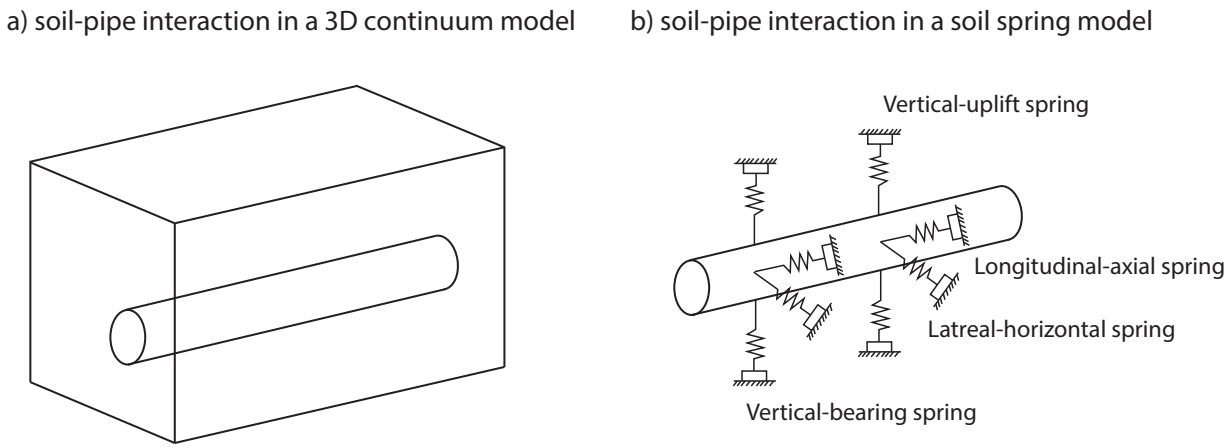

FIGURE 1.1: Soil spring versus 3D continuum model

superior to the simplistic representation of soil-pipe problems using beam/shell elements and soil springs (PRCI, 2017):

- Pipelines are often very long, and the axial strain in the pipe wall can extend to hundreds of metres away from the area. As a result, large model size and high computing costs make three-dimensional continuum models unattractive, especially for industry practice.

- Most conventionally used three-dimensional continuum models have difficulty modelling large relative displacements between pipe and soil. This is because these models are often based upon finite element or finite difference methods in which the interface is represented by a discrete mesh of solid elements that get excessively distorted in large deformation.

- There is limited validation of three-dimensional continuum models against real-life case studies. The potential benefit of the three-dimensional continuum models is their ability to investigate the pipeline behaviour subject to complex loading scenarios. However, the current validation of these models are based upon the laboratory works with simple loading conditions.

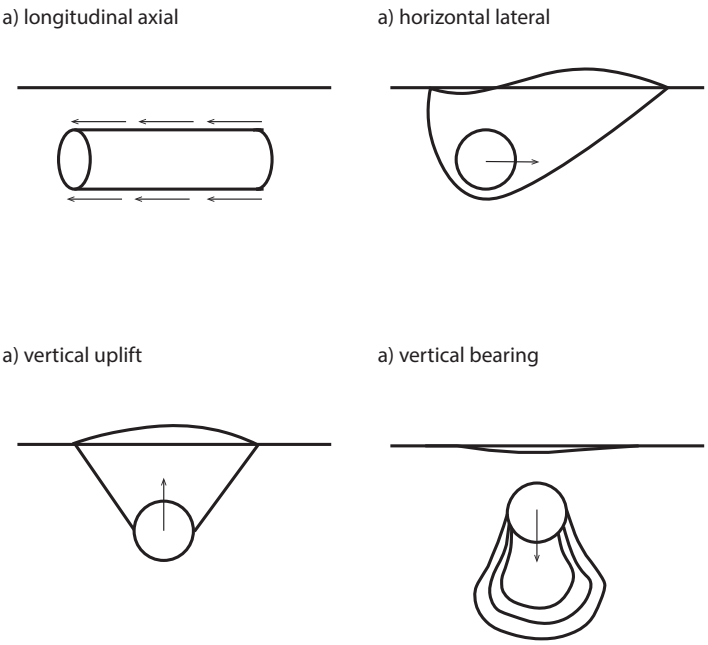

FIGURE 1.2: Four main soil-pipe interaction mechanisms associated with independent soil springs

- The use of more advanced constitutive models requires more specific soil properties. Considering the extent of pipelines and that they traverse different topographies and geological conditions, the additional cost for a more detailed geotechnical investigation is a limiting factor.

In light of the above, the soil springs have remained relevant in the past four decades and proved to be sufficient for most soil-pipeline interaction problems. For example, O'Rourke et al. (2005) performed a series of centrifuge modelling to measure the axial and bending strain along a pipe, which was subjected to an offset deformation in a split-box. They constructed a beam-type finite element model using the soil springs in the longitudinal and horizontal directions and defined the soil springs based upon the recommendations by ASCE (1984). The pipe model was considered with pinned boundary conditions in the finite element model at the location of the split-box sidewalls. The offset in the split-box was modelled by

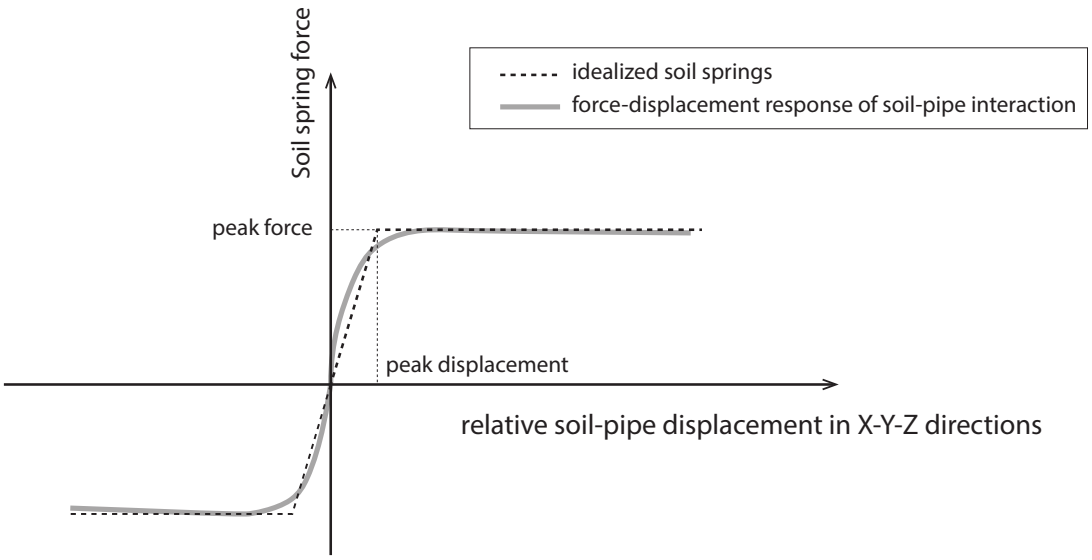

FIGURE 1.3: Force-displacement response of soil-pipe interaction and idealized soil springs

moving the fixed end of all the soil springs and the pinned boundary condition in one side of the fault. Results showed that the axial and bending strains from Finite element simulations match remarkably well with the measured strain in the tests with lower offset values. For higher offset values, a reasonable agreement was observed between the experimental data and the numerical models except for the axial strain, which was less in the physical tests compared to the simulation results.

Fig. 1.3 shows a typical force-displacement response for the soil-pipe interaction measured in the laboratory versus the idealized soil springs (bilinear, multilinear or hyperbolic functions) used in a finite element model. Relevant information regarding the soil springs based upon the engineering guidelines such as PRCI (2017), ALA (2001), and ASCE (1984) is presented in the following that can be used for constructing beam-type finite element models with soil springs.

1.1 Axial longitudinal soil springs

The peak soil force in the axial-longitudinal direction, F_a, is based upon the friction force equation, which is customized for sand- and clay-pipe interaction, in Eq. 1.1a and 1.1b, respectively.

$$F_a = \pi D H \gamma' \frac{1 + K_0}{2} \tan\left(\phi'_\mu\right) \tag{1.1a}$$

$$F_a = \pi D \alpha S \tag{1.1b}$$

where D is the outside pipe diameter, H is the vertical distance from the centre of the pipe to the ground surface, γ' is the effective soil unit weight, K is the effective coefficient of horizontal earth pressure at rest at the side of a pipe, ϕ'_μ is the interface friction angle at the soil-pipe interface, α is adhesion factor, and S is the shear strength of soil backfill. Eq. 1.1b has been the primary formula for axial soil load calculation for a long time. Early evidence of its usage is in the work of Newmark and Hall (1975), in which the longitudinal soil force on a pipe in a strike-slip fault set up is calculated. The displacement at the peak load (Y_p) is 3 mm for cohesive soils, 5 mm for cohesionless soils, 8 mm for stiff cohesive soils and 10 mm for soft cohesive soils according to PRCI (2017). Leonards (1965) presented the interface friction angle, ϕ'_μ, between soil and a wide range of construction material based on static and dynamic tests. It is Noted that $(1 + K_0)/2$ is the average radial pressure on the pipe. The value of K_0 is reported in the literature to be between 0.35 to 0.47 for normally consolidated soil. However, K_0 could be higher, considering the effects of soil compaction during backfilling. Trautmann and O'Rourke (1985) suggested using $K_0 = 1$ as a conservative estimate. Note that K_0 cannot be higher than one because in that case, the slippage between soil and pipe occurs within the soil (not in the soil-pipe interface), and the internal soil friction angle determines the soil load on a pipe. Suggested values of K_0 and α can be found in industry guidelines such as PRCI (2017), ASCE (1984) and ALA (2001). Wijewickreme et al. (2009) studied the effects of

constrained dilation of dense sand during the interface shearing on the peak axial loading and concluded that the axial soil loading can be more than twice the values suggested by guidelines.

1.2 Horizontal lateral soil springs

The early evaluation of pipeline response subject to lateral soil displacement was based upon published studies on retaining walls, laterally loaded piles and anchor plates (Hansen, 1961; Smith, 1962; Ovesen, 1964; Kostyukov, 1967; Ovesen and Strømann, 1972; Neely et al., 1973; Das and Seeley, 1975; Murray and Geddes, 1989). The first well-known experimental study of soil restraint on buried pipes was carried out by Audibert and Nyman, 1978. They examined the method suggested by Hansen (1961) and performed a series of small-scale tests on 25, 60, and 114-mm diameter pipes in loose and dense sands. The experimental results were validated against a field test conducted on a 230-mm diameter pipe. The force-displacement data trends were fitted by a hyperbolic function. The study covered a wide range of burial depth ratios, ξ = 1.5 to 24.5, and the results were in good agreement with those of Hansen (1961) and Das and Seeley (1975). Trautmann and O'Rourke (1985) performed a series of full-scale experiments to study the lateral soil restraint of buried pipes. The tests were performed in loose, medium, and dense sands (corresponding to friction angles of 31°, 36°, and 44°) with the burial depth ratio (ξ) ranging from 1.5 to 11. A good agreement was observed compared to the analytical solution of Rowe and Davis (1982) when the sand was medium or dense. However, the soil restraint in the tests with loose sands was higher than that of the analytical solution. Their work was used in ASCE (1984) and ALA (2001) guidelines for the estimation of lateral soil springs.

Nyman (1984) studied the soil restraint in the oblique (horizontal-vertical) direction through a series of full-scale tests. A method was proposed based on the peak uplift and horizontal soil restraints and the oblique loading angle for estimating the oblique

force-displacement relationship. Hsu (1996) performed an extensive experimental study on the oblique soil restraint. Several parameters, including the pipe diameter, loading rate, burial depth ratio, and loading angle, were investigated. The hyperbolic equations, initially proposed by Kondner (1963), were modified for the estimation of the oblique soil restraint. Paulin (1998) described the C-CORE large-scale testing facility in St. John's, Newfoundland, Canada and investigated soil-pipe interaction in axial and lateral directions for sand and clay. The results were compared to that of ASCE (1984) and Rowe and Davis (1982) in a relative format. They observed that the relative density has a prominent effect on the soil-pipe interaction. For example, the post peak lateral soil restraint at large displacement was about 80% higher in dense sand in relation to that in loose sand according to the experiments. The post peak axial soil restraint at large displacement was about 160% higher in dense sand compared to that in loose sand. Comparing these finding to the literature, they realized that the commonly used methods from the literature overpredict the soil restraint in loose sand. In dense sand, however, the results of the experiments were in reasonable agreement with the prediction of the state-of-the-art literature methods. According to the experimental results on clay, the lateral soil restraint was significantly influenced by the strength of the soil. They reported that the lateral peak loads predicted using ASCE (1984) were 100% higher than the values measured in the experiments in soft clay and 150% higher than the values measured in stiff clay tests. They also reported that the suggestions in the literature and guidelines significantly overpredict the adhesion factors, α. Hsu et al. (2001) and Hsu et al. (2006) performed a series of full-scale experiments on loose and dense sands to measure the oblique soil restraint in the axial-horizontal direction. They concluded that the axial and horizontal soil loads on the oblique pipes could be calculated by multiplying the corresponding cosine and sine values of the oblique angle with the associated longitudinal soil load of axial pipe and the horizontal soil load of the lateral pipe, respectively.

Yimsiri et al. (2004) conducted finite element analysis of horizontal and uplift loading for higher burial depth ratios up to 100. The numerical model was calibrated against the

experiments of Trautmann (1983). The results were used to present a design chart for deep embedment conditions. Eq. 1.2a and 1.2b are examples of the industry practice for prediction of the peak soil force per unit length of the pipe for sand and clay, respectively, in the horizontal-lateral direction, F_h.

$$F_h = N_{qh} \times \gamma' HD \tag{1.2a}$$

$$F_h = N_{ch} \times cD \tag{1.2b}$$

where N_{qh} and N_{ch} are the horizontal bearing capacity factor for cohesionless and cohesive soils respectively and c is the cohesion of the cohesive soil. Values of N_{qh} and N_{ch} can be found in PRCI (2017), ASCE (1984), and ALA (2001). For example, PRCI (2017) presents N_{qh} as a function of burial depth ratio and internal soil friction angle in Fig. 1.4 based upon the work of Yimsiri et al. (2004). The peak displacement can be calculated using Eq. 1.3 according to PRCI (2017).

$$Y_{\mathrm{p}} = 0.04(H + 0.5D) \leq 0.1D \text{ to } 0.15D \tag{1.3}$$

Karimian (2006) conducted an extensive full-scale testing program on large diameter pipes to study the pipe response in lateral and axial loading conditions and to examine the effectiveness of the widely accepted methods to reduce soil loads on buried pipes. Numerical model was implemented to enhance the understanding of soil-pipe interaction in axial and lateral directions. The study elucidated that the normal stress on the pipe was increased substantially after loading the pipe. Accordingly, the increase in normal stress was associated with dilation of constrained dense sand in the shear zone. They reported that the thickness of the active shear zone was about 2 mm, which is in agreement with 10 times d_{50} according to studies on direct shear tests. They presented a series of charts and formulas for estimation of an equivalent lateral earth pressure that can replace K_0 in Eq. 1.1a. Ha et al. (2008) performed four centrifuge tests to study the effects of pipe-fault orientation on buried pipes. Using the

data from strain gauges and tactile pressure sensors, they calculated the force-displacement relations of soil-pipe interaction in the lateral direction. They showed that the p-y relations are stiffer at points closer to the fault and softer at points further away. It was found that the peak force of stiffer p-y relations (those closer to the fault) was comparable with the recommendations of ASCE (1984). Oliveira et al. (2010) performed centrifuge tests on lateral soil-pipe interaction. Soft clay from Rio de Janeiro site, where more than 1×10^6 litre of crude oil were spilled into Guanabara Bay in January 2000, was used for the tests. An analytical model was proposed for lateral soil-pipe interaction for buried pipes with depth ratios less than one. The model was in good agreement with recommendations of ALA (2001).

Daiyan et al. (2011) performed a series of centrifuge modelling as well as a numerical study on oblique (axial-lateral) soil-pipe interaction. They found that the peak values of the axial and lateral soil restraints are a function of the relative soil-pipe movement's attack angle. Tian and Cassidy (2011) performed the lateral soil-pipe interaction tests in calcareous sands. They reported that the berms build up alongside a pipe in large displacement can affect the force-displacement behaviour of soil-pipe interaction. In their experiments, the pipe was displaced up to five times the pipe diameters to model the berm effect. They used the physical modellings to validate a model that includes the hardening of the yield surface in the horizontal soil-pipe interaction loading. Monroy-Concha (2013) described major modification to an existing soil chamber and conducted soil-pipe interaction testing in lateral, oblique (axial-lateral) and uplift direction for sand, crushed gravel and crushed limestone. The effectiveness of geotextiles to reduce the soil load on buried pipes were investigated. Tests on geotextile-lined trenches showed no reduction of soil load on the pipe as the shear resistance was observed not to merely dependant on the geotextile interface.

Roy et al. (2015) performed finite element analyses of soil-pipe interaction and compared the effectiveness of the Mohr-Coulomb (MC) and Modified Mohr-Coulomb (MCC) model in predicting the lateral soil restraint in dense sand. A number of important features of stress-strain relation and volume change behaviour of dense sand was considered in the

MMC model. They concluded that the MC model can be used to match the peak force of the experimental studies. However, the MCC model is more capable of simulating the force-displacement of soil-pipe interaction. The effects of pipe diameter, burial depth and soil properties were numerically investigated. It was observed that the mobilized internal friction and dilation angles are not constant along the shear failure surface. Saiyar et al. (2016) studied soil-pipe interaction under normal faulting through centrifuge modellings. They argued that the empirical models, currently being used as the standard design practice, overestimate peak strain for flexible pipes. This overestimation is the result of defining soil springs based upon soil-pipe interaction experiments of rigid pipes. They concluded that reducing soil restraint stiffness can satisfactorily account for pipe flexibility with the advantage of using the simple soil spring models.

A series of full-scale physical model testing was undertaken by Wijewickreme et al. (2017) to evaluate soil–pipe interaction behaviour by testing the performance of the 400-mm diameter (nominal pipe size, NPS 16) pipe specimens buried in moist sands and crushed limestone trench backfill. The oblique soil restraint values were found to depend significantly on the internal friction angle (ϕ') of soil when the pipe movement was closer to the horizontal axis; whereas, the soil restraint was less sensitive to ϕ' when the oblique movement was higher than about 35° with respect to the horizontal axis. Zhou et al. (2017) investigated the total deflection of buried HDPE pipes with special consideration on the peaking behaviour. They reported that the relative flexural stiffness, compactor type, and soil's unit weight significantly affect the induced deflection in the pipe. Tsatsis et al. (2018) studied pipeline behaviour subject to a rotational slide occurring in the direction of the pipe. They found that the amount of bending induced in the pipe is strongly related to the pipe position relative to the slip-line at the pipe-slip-line intersection.

Ansari et al. (2019) presented results of a series of physical tests on lateral soil-pipe interaction in loose, medium and dense sand. Parameters including lateral pipe displacement, depth ratio, sand bed density, pipe placement method and the pipe-pinch connection set-up

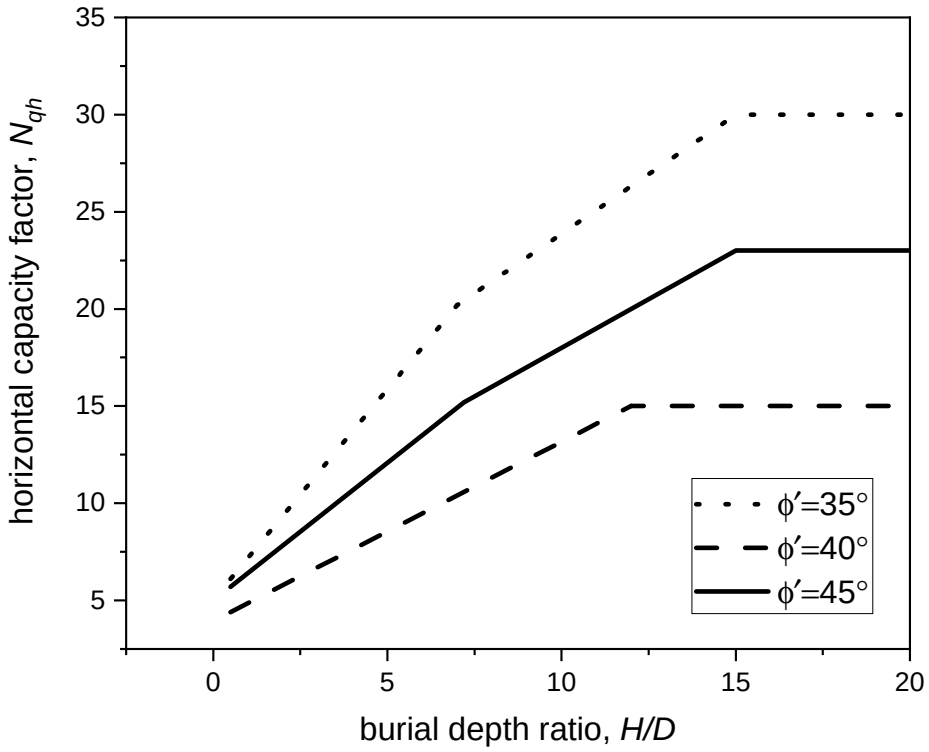

FIGURE 1.4: Horizontal capacity factor versus burial depth ratio (PRCI, 2017)

were investigated. Results were compared to published studies to conclude on the scatter results of different testing facilities. Zhang and Askarinejad (2019) studied the lateral soil forces acting on the buried pipes subject to slope instabilities by conducting a series of small-scale tests in a centrifuge testing facility. They performed six tests on dense coarse sands and two tests on medium-dense fine sands. The force-displacement relationships of lateral soil-pipe interaction were derived and compared to those from previous studies performed on flat ground conditions. They proposed a geometric factor that links the horizontal soil load in sandy slopes to that in the flat ground. According to their findings, the slope grade has an inverse effect on the lateral soil restraint.

1.3 Vertical uplift soil springs

Early evaluation of uplift soil force on pipelines was based upon a limit equilibrium solution on "inclined slip surfaces" shown in Fig. 1.5, which is one of the simplest methods for calculating the uplift capacity of buried structures (Vermeer and Sutjiadi, 1985). According to this analytical model, the vertical capacity of a buried object per unit length is equal to the weight of the lifted block, as shown in Eq. 1.4. This analytical model is based upon the assumption that frictional soil obeys normality. Normality requires that the shear surface occurs at an angle in which the normal stress and the shear stress cancel each out in the vertical direction (θ=ϕ=ψ). In other words, in a frictional material obeying normality, there is no energy dissipation on the shear surfaces. It is worth pointing out that $-\frac{\pi D}{8H}$ is half of the pipe area that is subtracted from the area of the trapezium (see Fig. 1.5).

$$\frac{F_u}{\gamma' HD} = [1 - \frac{\pi D}{8H} + Ktan(\phi')\frac{H}{D}] \tag{1.4}$$

where F_u is the maximum force per unit length of pipe, and K is the coefficient of lateral earth pressure. The advantage of this model is its simple analytical essence, but the values of K should be determined empirically, which is a very complex topic. Trautmann et al. (1985) conducted full-scale experiments on uplift soil-pipe interaction to measure the maximum soil forces on the buried pipe. They used Cornell Sand Filter with three test densities of 14.8, 16.4 and 17.7 kN/m^3 corresponding to internal friction angles of 31°, 36° and 44°. They normalized the maximum soil force to soil density, pipe burial depth, diameter and length and presented the results in a format convenient for design. Yimsiri et al. (2004) extended the research for deep embedment conditions with conducting finite element analysis. They presented a design chart, shown in Fig. 1.6, for deeply buried pipes. Based on these studies, PRCI (2017) offered using Eq. 1.5a for sand and Eq. 1.5b for clay to estimate the maximum uplift soil load per unit length of a pipe. The suggested values of N_{qv} and N_{cv} can be found

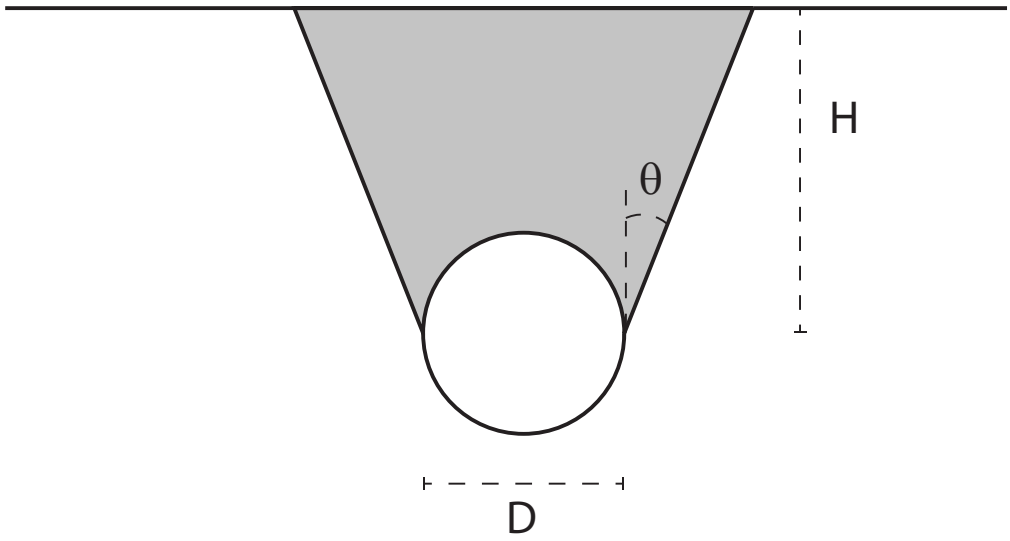

FIGURE 1.5: Inclined slip surface in uplift loading

in PRCI (2017).

$$F_u = N_{qv}\gamma' HD \tag{1.5a}$$

$$F_u = N_{cv}cD \tag{1.5b}$$

where N_{qv} is the vertical uplift factor for cohesive soil and N_{cv} is the vertical uplift factor for cohesionless soil.

1.4 Vertical-bearing soil springs

The vertical-bearing soil springs presented in PRCI (2017) are based on the assumption of a continuous strip footing and is defined by Eq. 1.6. PRCI (2017) offered formulas to estimate the appropriate values of bearing capacity factors, N_c, N_q and N_γ as a function of internal friction angle of soil. The peak displacement is reported 0.1D and 0.2D for granular and

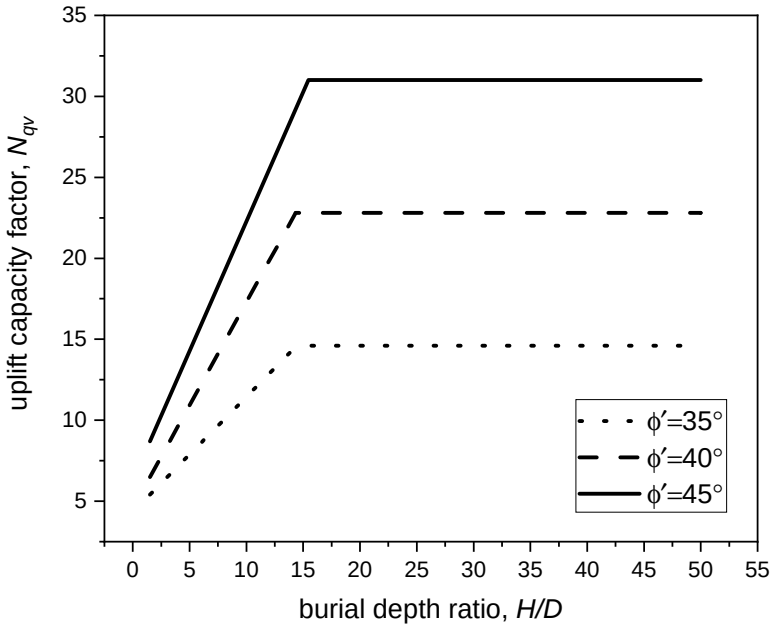

FIGURE 1.6: Uplift capacity factor versus burial depth ratio (Yimsiri et al., 2004)

cohesive soil, respectively (PRCI, 2017).

$$Q_d = N_c c D + N_q \gamma' H D + N_\gamma \gamma' \frac{D^2}{2} \tag{1.6}$$

1.5 Pipeline design for thermal loads

According to CSA-Z662-15 and ASME B31.8 (2003), the effects of temperature variation on the pipe deformation should be included in the design of pipelines. A pipe is considered "restrained" or "unrestrained" for the purpose of design. A pipe is "restrained" if the axial displacement of the pipe is prevented due to the soil-pipe interaction or supports (ASME B31.8, 2003). A pipe that is free to move in the axial direction or flex at bends is considered "unrestrained". Examples of unrestrained pipes include above-ground and buried pipes (in soft soil) that can accommodate thermal expansion due to flexibility or expansion joints. For a restrained pipe, the thermal stress due to a temperature change can be calculated

using Eq. 1.7 (ASME B31.8, 2003).

$$\sigma_T = E\alpha\Delta T \tag{1.7}$$

where E is the Young's modulus of the pipe, α is the thermal expansion coefficient and ΔT is the temperature change in the pipe wall. The pipe wall temperature variation can be estimated by a heat-transfer analysis over a typical year. In the pipeline context, a heat transfer includes the heat exchange between the pipe, soil and the atmosphere. The reader is directed to Chapter 4 for more information on this topic.

1.6 Objectives of the thesis

The main objective of this research is to characterize the horizontal soil springs for pipes that are installed below sloping ground (see Fig. 1.7 b,c). It is important to note that the soil springs offered by pipeline guidelines are based upon level ground conditions (see Fig. 1.7 a). For this purpose, a comprehensive experimental program with associated numerical modelling was undertaken using a large scale testing equipment at the University of British Colombia, Vancouver, BC, Canada. Two sets of experiments were performed: 1) pulling the pipe to the left as shown in Fig. 1.7 b, and 2) pulling the pipe to the right as shown in Fig. 1.7c. It is important to note that this is the first study aiming at presenting soil springs in a quantitative and comprehensive manner for sloping grounds that can be included in pipeline guidelines for design purposes.

The next objective of this research program is to analyze the field data, collected for four consecutive years from three at-risk Manitoba Hydro pipelines subjected to slow landslides, and to draw conclusion on the pipeline performance and the monitoring program.

The last project is aimed at developing a practical way to determine the pipe burial depth in sloping ground with ground displacement and temperature variation such that the combined

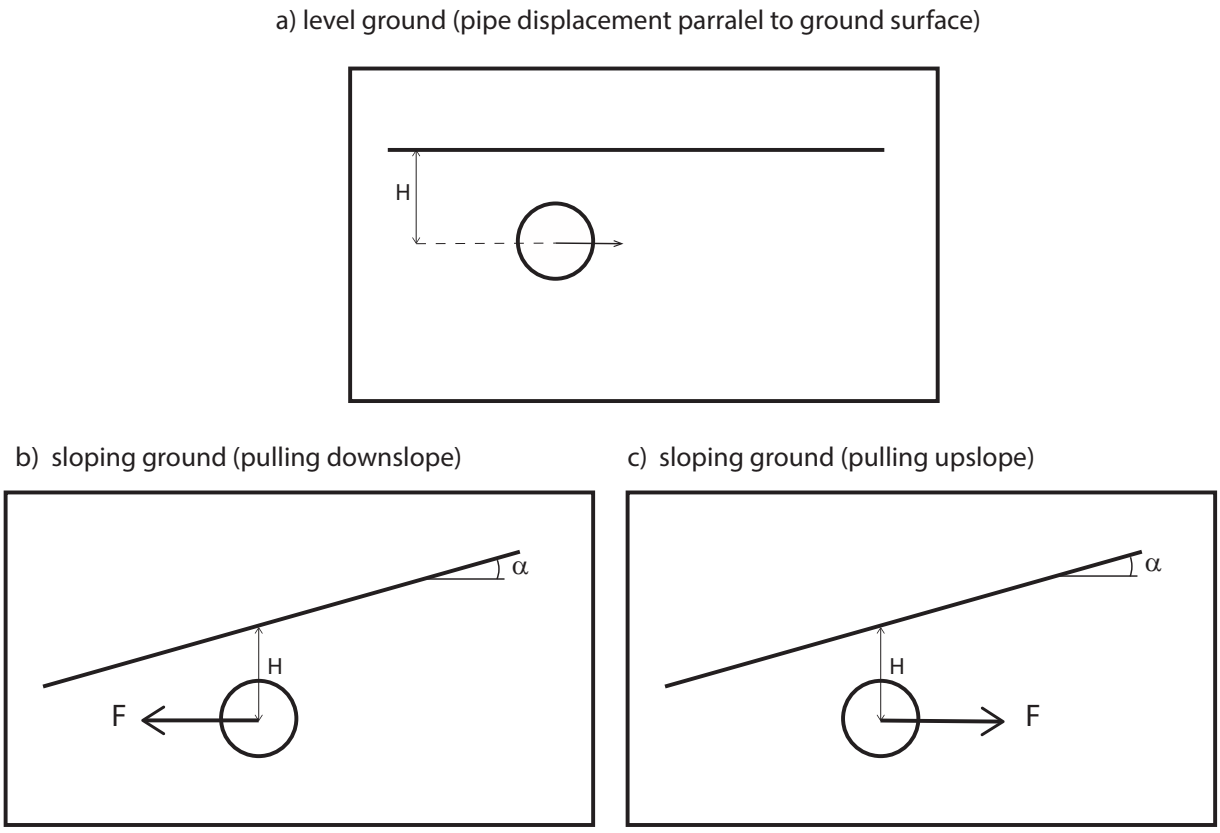

FIGURE 1.7: Level ground assumption in horizontal soil springs

loading on the pipe is minimized.

1.7 Structure of the thesis

This thesis is presented in five chapters and four appendices.

- Chapter 1: a brief background is presented on soil-pipe interaction with a focus on the industry practice for estimating soil springs in axial, horizontal, uplift and downward directions.

- Chapter 2: The horizontal soil springs are developed for sloping ground in this chapter. This is a standalone chapter in which the slope grade effects on horizontal soil springs are examined and characterized for industry use. The chapter includes an abstract,

introduction (problem definition), a literature review (on horizontal soil springs), description of full-scale experimental work, numerical modelling, results, and conclusion.

- Chapter 3: The behaviour of buried pipes in slow landslides is evaluated using a finite element method in three landslide areas of Manitoba Hydro pipeline network, and results are compared to four years of field monitoring data. This chapter is a standalone chapter with an abstract, introduction, description of a field monitoring program, numerical modelling, results and conclusion.

- Chapter 4: This chapter presents a methodology for selecting the appropriate depth of cover for buried pipes in sloping ground, considering the seasonal temperature variation and ground displacement. This chapter is a standalone chapter with an abstract, introduction, description of numerical modelling and developing equations, solved examples and conclusion.

- Chapter 5: This chapter presents a summary of the main findings in this dissertation and provides recommendations for future work.

- Appendix A: details of the equipment used in the experimental work are presented in this appendix. This appendix includes the names and specifications of the testing chamber, loading system, control system, data acquisition system, instrumentation and photography equipment.

- Appendix B: this appendix presents photographs from all ten experiments at the peak displacement. Pictures of plastic-strain contours from the numerical simulations are presented for comparison to the shear failure surface observed during the tests.

- Appendix C: additional photos are presented in this appendix to show the soil chamber, test preparation, the pipe position, loading system, conveyor belt and the compaction tools.

- Appendix D: force-time response of all ten experiments are presented in this appendix with the load cells and string pots measurements.

Chapter 2

Lateral force-displacement response of buried pipes in slopes

2.1 Abstract

A series of full-scale experiments were conducted to estimate lateral soil constraints on the pipes buried in slopes at different burial depths. The experimental data indicated that the soil force on the pipe increases with increasing slope grade and burial depth ratio (normalized with respect to pipe diameter). The lateral soil force versus relative pipe displacement response observed from the experiments is presented and compared to those arising from level ground conditions. The study was extended to larger burial depth ratios by simulating pipes in loose, medium and dense sandy slopes using a numerical (finite element) model that was initially calibrated using the results from physical modelling. The findings from the study in terms of the variation of peak lateral soil restraint as a function of the slope grade and burial depth ratio are presented for consideration in pipeline design.

2.2 Introduction

As explained earlier, the response of pipelines subjected to ground movements is typically investigated using numerical techniques such as the finite element method in which the soil-pipe interaction is modelled using a series of orthogonal discrete soil springs. The analysis of a given soil-pipe interaction scenario is typically undertaken considering non-linear soil springs in three orthogonal directions: horizontal (lateral), vertical (bearing and uplift) and, longitudinal (axial), as shown in Fig. 2.1. The force-displacement curves of these soil springs, also commonly called p-y curves, are intended to describe the soil force development as a function of relative soil-pipe displacements.

To establish benchmarks for presenting the results and compare with cases involving different pipe sizes and depths, the concept of dimensionless load and normalized displacement has been used to interpret soil forces on pipelines. As previously suggested by Hansen (1961) and used by Audibert and Nyman (1978), Rowe and Davis (1982), Trautmann (1983), and Burnett (2015), the dimensionless horizontal load per unit length of pipe ($\bar{F}_h$) is expressed using the relationship given in Eq. B.1. The normalized horizontal displacement of the pipe ($\bar{Y}$) during the soil-pipe interaction is defined according to Eq. B.2.

$$\bar{F}_h = F_h / (\gamma' HDL) \tag{2.1}$$

$$\bar{Y} = Y / D \tag{2.2}$$

where F_h is the horizontal load per unit length of pipe, H is the vertical distance from the centre of the pipe to the ground surface, D is the outside diameter of the pipe, γ' is the effective unit weight of soil, and Y is the transverse pipe displacement.

In the current design guidelines (e.g. ALA, 2001; PRCI, 2017), the peak value of the dimensionless horizontal load per length ($\bar{F}_h$) is termed the lateral soil restraint (N_{qh}). N_{qh},

which essentially represents a horizontal "bearing capacity factor", depends on the internal friction angle of soil (ϕ') and the pipeline centreline depth (H) to diameter (D) ratio, $\xi = H/D$. The normalization process implicitly assumes that the peak soil force is linearly correlated with γ', H, and D. The value of N_{qh} has been primarily developed to address the cases of buried pipeline in level ground based upon bearing capacity mechanics considerations supported by experimental data. As mentioned previously, the force-displacement curves for the soil springs are developed initially based on the underlying assumption that the ground surface is perfectly horizontal. However, pipelines often cross natural slopes or riverbanks, where the ground surfaces are inclined. Therefore, there is a need for a comprehensive investigation to assess the effects of slope grade on pipeline design.

With this background, a comprehensive investigation was undertaken to study the significant effect of the ground inclination (i.e. slope grade) on soil-pipe interaction. For this purpose, the Advanced Soil Pipe Interaction Research (ASPIRe™) full-scale testing facility at the University of British Columbia, Vancouver, Canada, was used to study the performance of buried pipelines in slopes subjected to ground displacements. The full-scale experiments for physical modelling of soil-pipe interaction under close-to-field conditions with precision instruments provided the opportunity to investigate the mechanics of the problem and generate valuable data for calibration/validation of numerical models. The experimental data was then used to develop calibrated finite element simulations and study the problem numerically, considering various combinations of slope grades and burial depth ratios. The study aims to characterize soil springs as a function of slope grade and burial depth ratio in loose, medium and dense sands. This chapter is organized as follows: the literature is reviewed to provide a brief background of research studies on lateral soil-pipe interaction. The testing program, equipment, soil and pipe material properties, and details on test preparation are described. The force-displacement response from the experimental work is presented and discussed. A finite element (FE) model is developed to investigate the peak lateral soil restraint for deep embedment conditions. The FE modelling procedure,

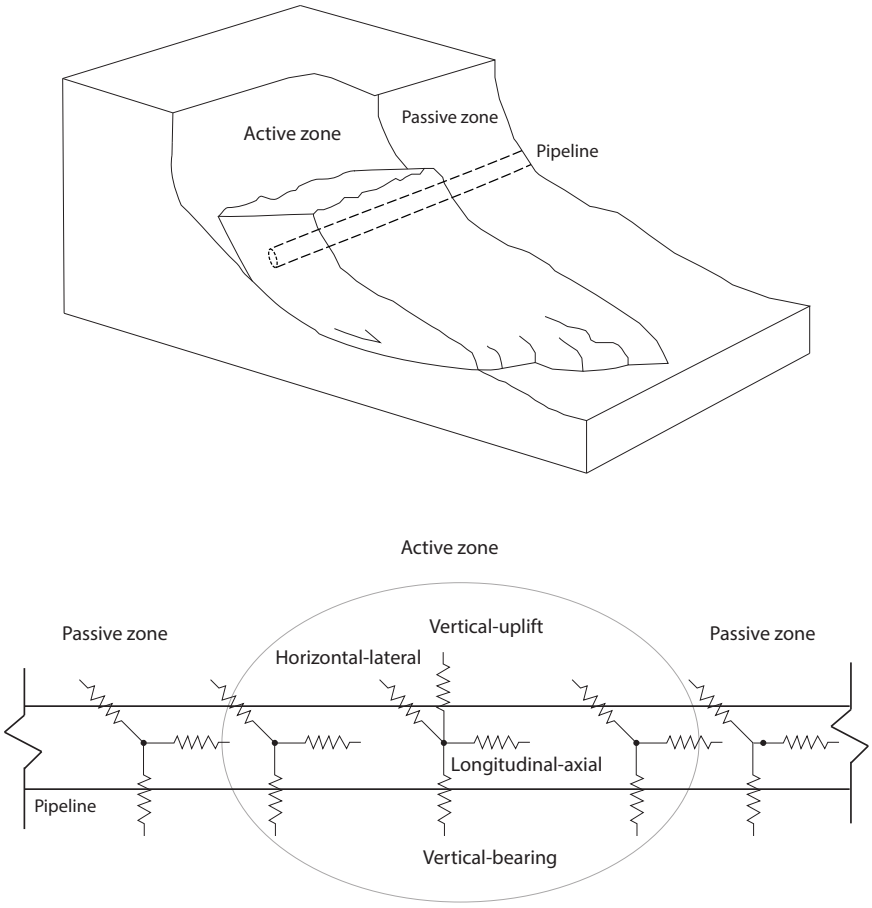

FIGURE 2.1: Soil spring model

soil model, and calibration of the FE model with the physical experiment conducted in the present study are explained. Finally, the variation of N_{qh} as a function of slope grade and burial depth ratio (ξ) are presented graphically for consideration in pipeline design.

2.3 Experimental study

In this section, the testing equipment is briefly explained, and some critical aspects of the full-scale experiments are presented. More detailed description of the equipment and related photos are presented in Appendix A and C, respectively. The reader is encouraged to read

TABLE 2.1: Summary of horizontal load tests ($\xi = H/D$ and α are shown in Fig. 2.2b)

Test #	ξ	$\tan(\alpha)$	N_{qh}	Y_p / D
1	1.6	25%	11.3	0.06
2	1.6	40%	15.4	0.08
3	2.0	0	8.3	0.05
4	2.0	25%	12.8	0.1
5	2.0	40%	16	0.08
6	2.4	-40%	4.2	0.05
7	2.4	-25%	6	0.12
8	2.4	0	9.8	0.12
9	2.4	25%	13.3	0.08
10	2.4	40%	15.5	0.15

previous studies including Karimian (2006), Wijewickreme et al. (2009), and Monroy-Concha (2013) for further information on the equipment.

2.3.1 Testing program

A total of 10 full-scale experiments (detailed in Table 2.1) are conducted in this research program to investigate the influence of ξ and $\tan(\alpha)$ (shown in Fig. 2.2b) on soil pipe interaction. As notable, the experiments were performed to simulate both positive and negative slope situations with respect to pipe movements. In the experiments, the pipes are subjected to displacement-controlled lateral loading conditions at a constant displacement rate of 2.5 mm/sec. This loading rate is selected with consideration of the hydraulic pumps capacity and actuators maintenance costs. The same displacement rate was used in the lateral soil-pipe interaction testing performed by Karimian (2006) with the same sand backfill, after showing that the test results were not sensitive to the loading rates between 2 and 50 mm/s. The insensitivity of the results to the loading rate is most likely due to dry condition of the experimental soil.

2.3.2 Testing equipment

The testing equipment comprises a 3.85 m $\times$ 2.5 m $\times$ 2.5 m steel-frame soil chamber, built for soil-pipe interaction studies in axial, horizontal, vertical, and oblique directions. The details of the facility are shown in Fig. 2.2 through several photos. The plan and lateral view of the equipment are provided in Fig. 2.3 with the identification numbers listed in Table 2.2. This unique set-up enables the user to simulate both positive and negative slope situations with respect to pipe movements, as illustrated in Fig. 2.3(b). Note that for the cases with the negative slope grades, the pipe is displaced towards the toe of the slope (Fig. 2.3b).

The facility is equipped with two hydraulic actuators with an individual actuator capacity of 418 kN. These actuators were positioned on the south side of the chamber (Note: a longer dimension of the chamber is parallel to the north-south direction), and they are connected using the steel cables to the two ends of the test pipe segment laterally placed in the east-west direction as shown in Fig. 2.3(b). Soil forces and pipe movements were measured using two load cells and two string potentiometers. The load cells had the individual capacity of 250 kN and were installed on the actuator cylinders. The string potentiometers were positioned on a steel frame structure on the north side of the chamber and connected to the pipe using an 80-cm-long extension wire passing through a small hole on the north wall of the chamber. The walls of the chamber are made of treated plywood stiffened with timber cross-beams. The interface friction between the soil and vertical sidewalls of the soil chamber during lateral pipe movements were minimized by having the west side wall lined with stainless steel sheets and the east side (front) wall with Plexiglas materials (i.e., which would also promote low interface friction with soil). The chamber sidewall friction force on the pipe was reported less than 5% of the measured peak lateral soil restraint according to Karimian (2006). The dimensions of the chamber and size/position of the pipe were chosen such that the shear failure surface does not interfere with the chamber walls. The thickness of the pipe wall was selected so that the assumption of a rigid pipe would be reasonable under the applied

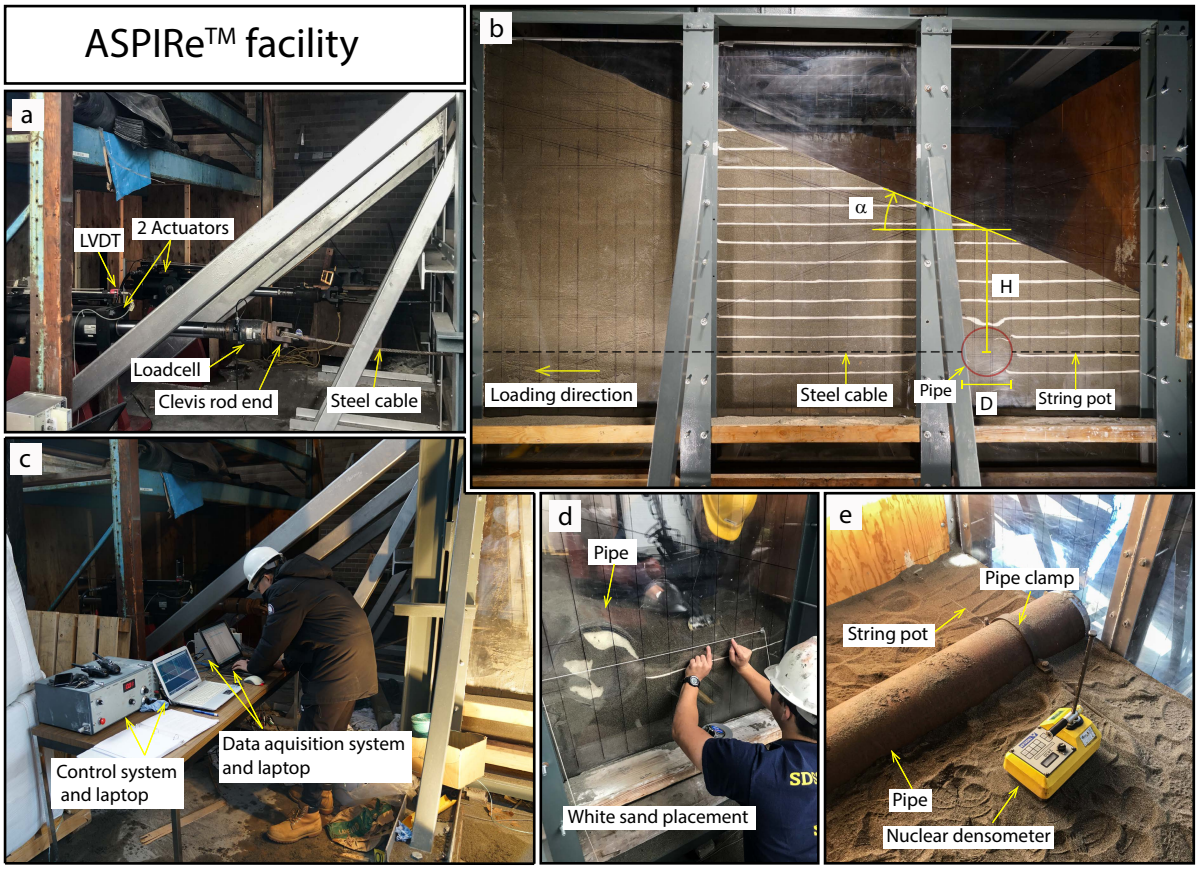

FIGURE 2.2: Advanced Soil-Pipe Interaction Research facility at the University of British Columbia a) actuators b) test configuration c) electronics d) white sand placement e) pipe position

loads—in turn, to enable the assumption of a plane strain soil deformation mechanism (with respect to the north-south vertical plane).

2.3.3 Soil and pipe materials

The experiments were performed using the Fraser River sand as the backfill material. The Fraser River sand is dredged from the Fraser River in the Lower Mainland of British Columbia in Canada. It has wide usage in the construction sector and been used for geotechnical engineering research test materials at UBC for more than thirty years. The sand has an average particle size (D_{50}) of 0.26 mm; coefficient of uniformity (C_u) of 1.6, which classifies the sand as uniformly graded (Fig. 2.4). Its specific gravity (G_s) is 2.71, with the minimum

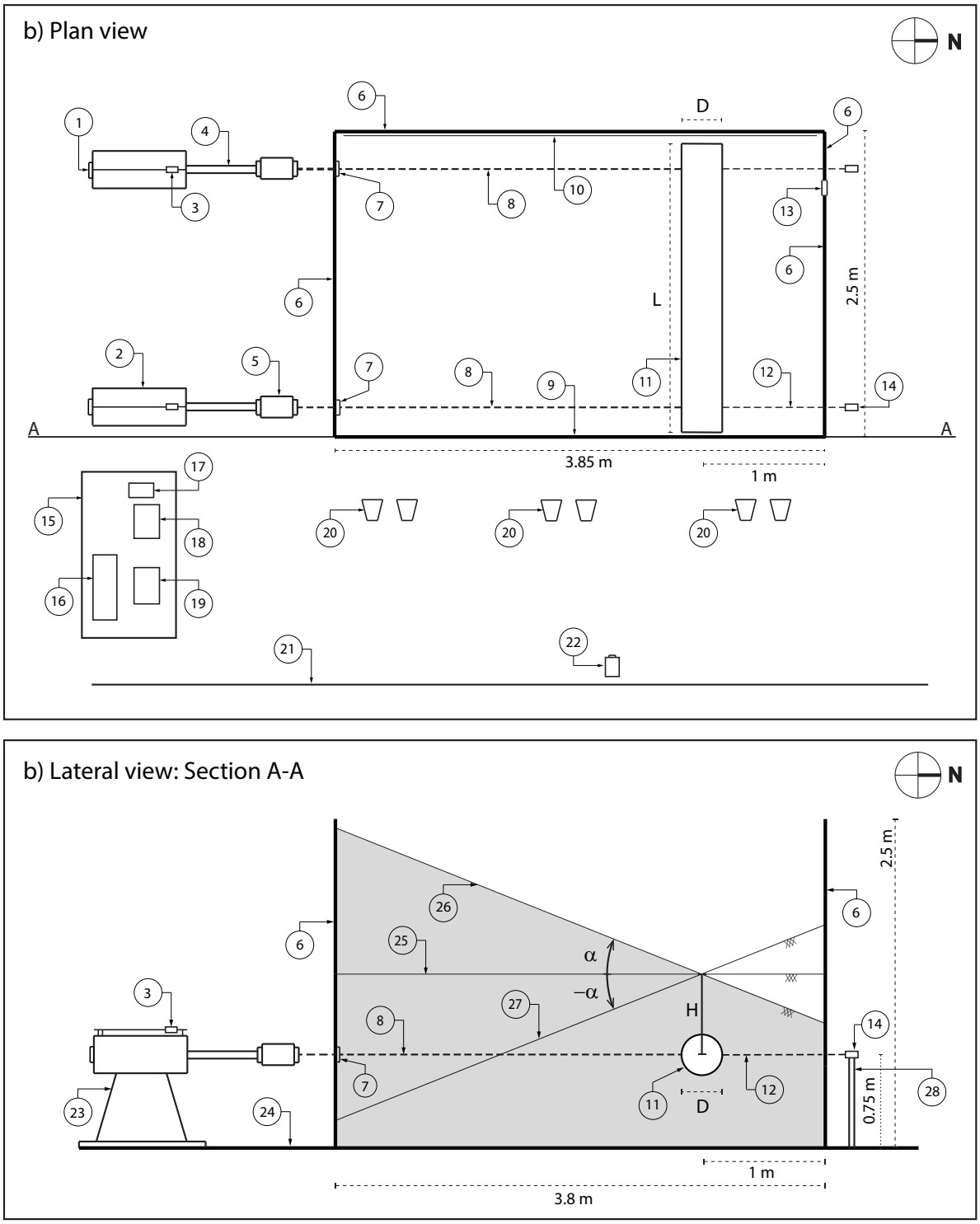

FIGURE 2.3: Plan and lateral view of the testing equipment—identification is described in Table 2.2

TABLE 2.2: Description of the testing equipment (identification in Fig. 2.3)

#	Description	#	Description
1	Servo controller	15	desk
2	Hydraulic actuator	16	Control system
3	LVDT	17	Data acquisition system
4	Hydraulic cylinder	18	Laptop for data acquisition
5	Load cell	19	Laptop for Controller
6	Plywood wall	20	500 W Halogen work light
7	Foam	21	Matte black tarp
8	25-mm Steel cable	22	Camera
9	Plexiglass wall	23	Loading pedestal
10	Stainless steel	24	Steel foundation
11	Pipe	25	Soil surface (flat ground)
12	80-cm extension wire	26	Soil surface (positive slopes)
13	Access hole	27	Soil surface (negative slopes)
14	String potentiometer	28	Steel stand for string pot

and maximum void ratios (e_{min} and e_{max}) of 0.62 and 0.94, respectively (Karimian, 2006). The sand particle sphericity is low to medium, and its angularity is from angular to sub-rounded (Garrison et al., 1969). The Fraser River sand is composed of 40% quartzite and chert, 11% feldspar, 45% unstable rock fragments (mostly fragments of volcanic rocks), and 4% other minerals (Garrison et al., 1969). The maximum dry density of the sand at the optimum water content of 19.5% is 1625 kg/m^3 (Fig. 2.5). The water content of the sand used in the experiments was below 2%. Further geotechnical information on the Fraser River sand can be found in Uthayakumar (1996), Sivathayalan (2000), and Karimian (2006).

A steel pipe segment with an outside diameter of 324 mm (Nominal Pipe Size, NPS 12), the wall thickness of 6.35 mm (Sch. 20), and length of 2.4 m was used for the experimental study. The pipe had a rusty uncoated sand-blasted surface. Based on the direct shear tests performed by Karimian (2006), the Fraser River sand/ sand-blasted steel interface friction angle was found to be about 0.85 of the internal friction angle of soil (ϕ').

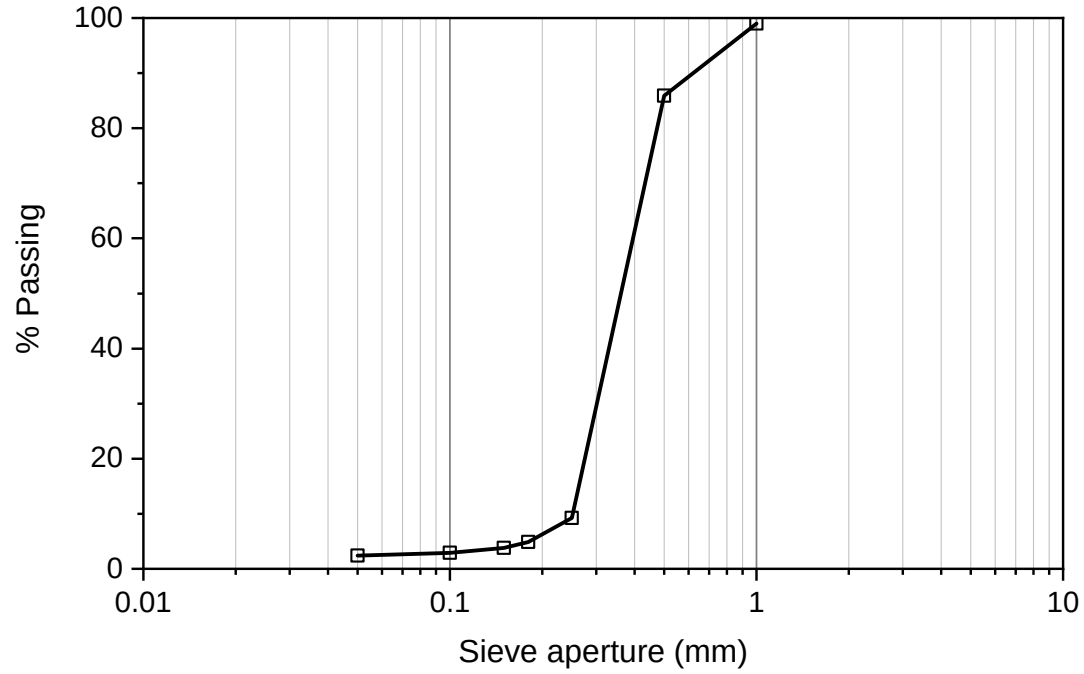

FIGURE 2.4: Grain size distribution of the Fraser River sand

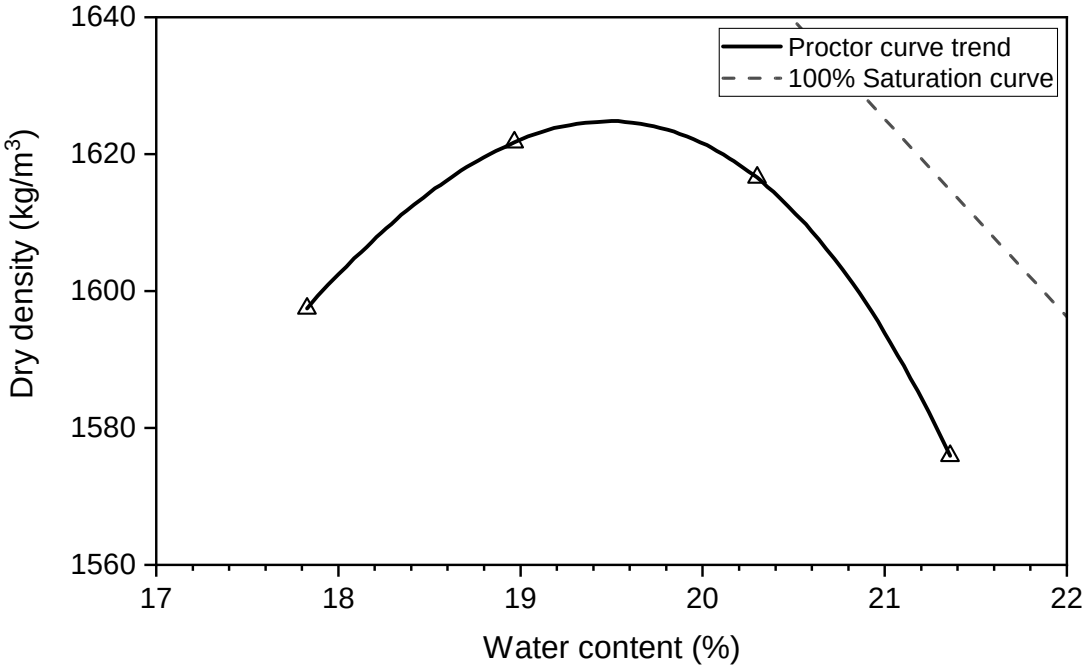

FIGURE 2.5: Results of compaction tests on Fraser River sand

2.3.4 Test chamber preparation

The preparation of the test chamber was carried out in three steps. First, the soil was deposited up to the invert elevation of the pipe. The pipe was placed on the sand bed, and connections to the actuators and string potentiometers were made. The pipe was plugged from both ends with the wooden caps and silicone caulk to prevent potential ingress of sand particles into the pipe cavity. Next, the filling was resumed layer-by-layer (using 15-cm lifts), and each lift was compacted with a static roller to reach the desired burial depth ratio. The soil compaction was performed with a tamper in the vicinity of the chamber boundaries and pipe. The total unit weight of soil was targeted at γ=16 kN/m^3. The soil density was measured using the metallic bowls of known volumes located at three arbitrary points in each layer; the bowls were buried in each layer before the compaction and excavated after the compaction. The unit weight was calculated by weighting the bowls before and after the process. These values were cross-checked with nuclear densitometer measurements, with the density measurements between the two methods resulting in values within 2% of each other. In the tests involving sloping ground, the soil above the desired line of the ground surface was carefully excavated by hand to create the required slope. After completing a given test, the soil was emptied to the invert elevation of the pipe. This was accomplished using a 0.3 m $\times$ 0.45 m opening in the northern wall of the soil chamber. A conveyor belt, aligned immediately below this opening, was used to transfer the soil to bulk bags for storage and later usage.

2.4 Lateral soil restraints: experimental force-displacement response

The force-displacement response of soil-pipe interaction is examined in a dimensionless form as defined in Eq. B.1, B.2. From a quality control point of view, an initial test with a

level ground surface was performed for comparing the results of the current experimental setup with respect to a similar test previously performed by Monroy-Concha (2013). The results from the two tests are compared in Fig. 2.6, and showing a very good agreement, thus confirming the repeatability of the testing methodologies employed at the ASPIRe™ testing facility.

The actual force, normalized force and pipe displacement measurements of the buried pipe for all ten experiments are presented in Appendix D through a number of figures. These data are presented in the form of $\bar{F}_h - \bar{Y}$ in Fig. 2.7, 2.8, 2.9 and 2.10 with the use of solid lines; each figure, 2.7 through 2.10, corresponds to a specific ξ value. In an overall sense, the graphical shape of the observed lateral force versus displacement is similar to those typically observed in previous lateral soil restraint tests (Wijewickreme et al., 2017; Trautmann and O'Rourke, 1985). Initially, the $\bar{F}$ values rise up rapidly until the peak normalized soil restraint is reached at a certain displacement, followed by the lateral soil restraint reaching a near-constant value or post-peak drop.

A peak dimensionless force (N_{qh}) in the order of 8 to 9 is noted for the cases with the level ground (α=0°) and ξ=1.6-2.4. This is also consistent with the pure lateral test results conducted by Trautmann and O'Rourke (1985). The values of N_{qh} rise up by almost two-fold in the tests where the pipe is displaced in the sloping ground with a grade of 40%. Fig. 2.9 presents $\bar{F}_h - \bar{Y}$ response of soil-pipe interaction for the slope grades of -25% and -40% (tests 6 and 7, respectively) where the N_{qh} value is reduced by about 30%, from about 6 to 4, as the ground slope is decreased from -25% to -40%. The results clearly show the significant influence of the ground slope on the ensuing horizontal bearing capacity factor N_{qh}, which can be a pivotal consideration for the design of pipelines traversing sloping ground in mountainous areas, river banks, etc.

Another important parameter of value from the force-displacement relations, for soil pipe-interaction evaluations, is the displacement corresponding to the peak force, commonly called the critical pipe displacement (Y_p). PRCI (2017) suggest using Eq. 2.3 to predict the

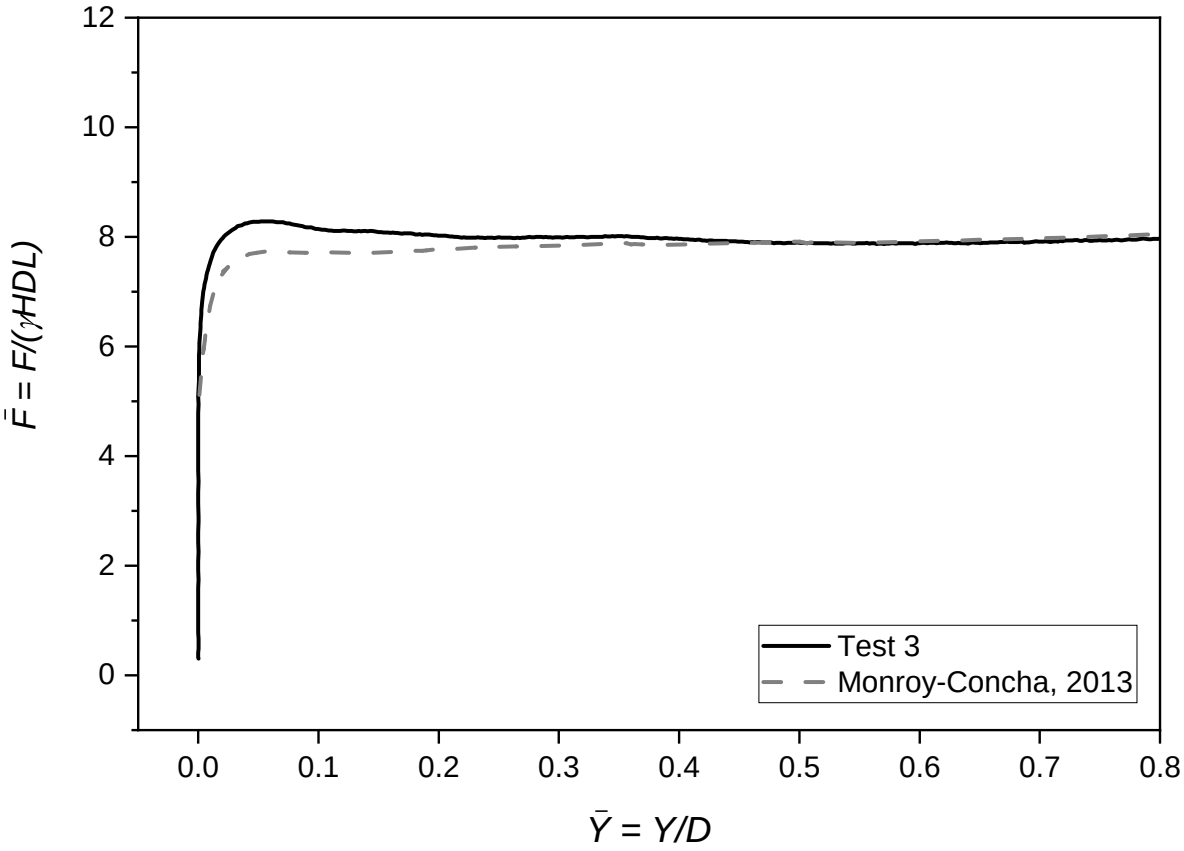

FIGURE 2.6: Test verification—results of test 3, compared to a similar test from Monroy-Concha (2013)

critical pipe displacement. As this equation has been recommended only for level ground conditions, it would also be useful to examine its applicability for sloping ground conditions. Table B.1 details Y_p/D based on the experimental results presented in Fig. 2.7 to 2.10. Using Eq. 2.3, Y_p will be 0.08D, 0.10D and 0.12D for ξ =1.6, 2.0 and 2.4, respectively. Eq. 2.3 suggests that Y_p is an increasing function of H; however, this was not observed in the experiments. Y_p seems to lie between 0.05D to 0.15D with no clear pattern from one test to another. In essence, the experimental results did not provide conclusive evidence for a clear trend for the variation of Y_p.

$$Y_p = 0.04(H + 0.5D) \leq 0.1D \text{ to } 0.15D \tag{2.3}$$

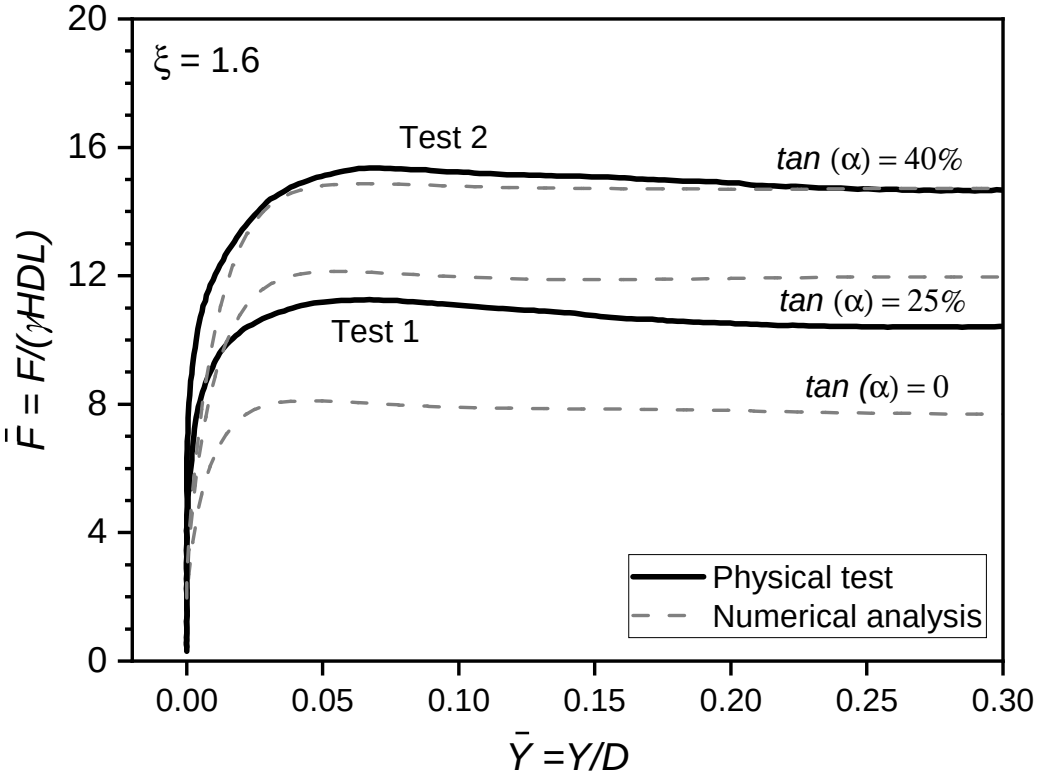

FIGURE 2.7: Lateral Force-displacement response of soil-pipe interaction for burial depth ratio of 1.6

2.5 Numerical study

The full-scale experimental program successfully illustrated the significance of sloping grounds on soil-pipe interaction behaviour. However, higher burial depth ratios (ξ values) could not be investigated experimentally due to the chamber size's physical limitation. Under real-life conditions, there can be cases where a pipeline needs to be buried several metres below the ground surface to meet operational requirements or to traverse in certain geological and topographical conditions. For example, in western Canada, it is a common practice to bury the gas pipelines 1.2-1.5 m below the ground surface. In such cases, ξ can vary from 10 to 13 for NPS 4 (D=114.3 mm) pipeline. Yimsiri et al. (2004) reported that ξ

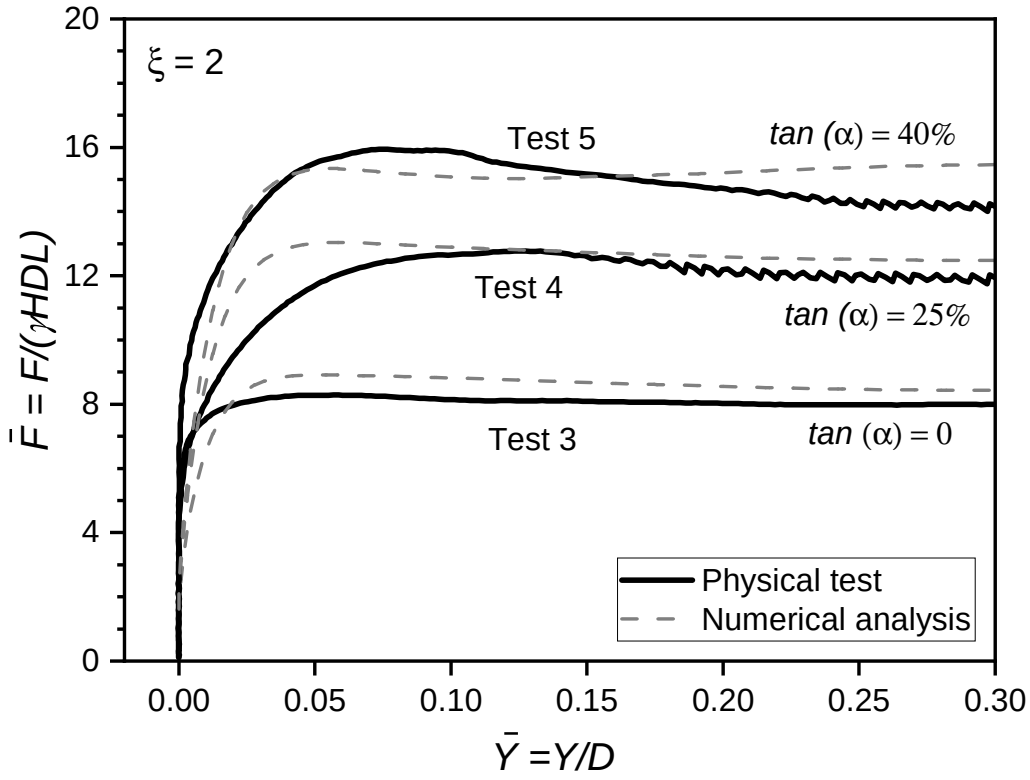

FIGURE 2.8: Lateral Force-displacement response of soil-pipe interaction for burial depth ratio of 2

could be as high as 40-80 for cases where pipelines are buried under large embankments. Therefore, it is important to investigate the soil force development in slopes under higher ξ values. A finite element (FE) model is developed using Abaqus/Explicit to investigate the horizontal bearing capacity factor for burial depth ratios higher than 2.4 under the inclined ground surface condition. The soil's initial stress condition is estimated in a general static step in Abaqus/Standard and then imported into the explicit model as a predefined field from the general static model's output database. The soil-pipe interaction is modelled using the surface-to-surface contact method with penalty constraint formulation as available in Abaqus FE software. The normal interaction of the soil and pipe is modelled with "hard" contact pressure-overclosure formulation. The tangential behaviour of the interaction is

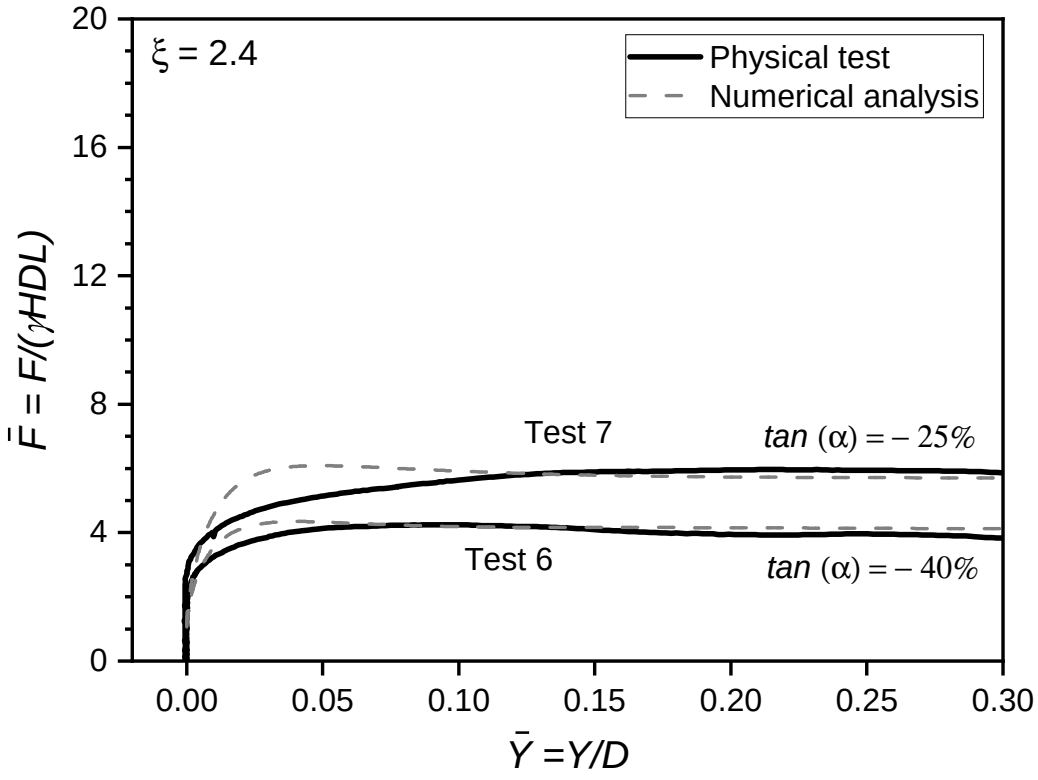

FIGURE 2.9: Lateral Force-displacement response of soil-pipe interaction for burial depth ratio of 2.4 (negative slope grades)

modelled with "penalty" friction formulation with friction coefficient of 0.81. In other words, the soil-pipe interface friction coefficient (μ) is defined as $\mu = \tan(\phi'_\mu)$, where ϕ'_μ is the interface friction angle that depends on pipe surface roughness and the angle of internal friction (ϕ') of the soil. To be consistent with experimental results, ϕ'_μ=39° (i.e. μ=0.81) is used in the numerical simulations. Fig. 2.12 shows the typical FE mesh used in the present study. Note that a mesh sensitivity analysis is conducted, and an approximate mesh size of 2 cm is found suitable for the analysis. As shown in Fig. 2.12(a), a structured mesh is generated by zoning the soil domain. An adaptive meshing algorithm available in the Abaqus FE software is used for the complete soil domain to avoid any mesh distortion issue. Fig. 2.12(b) shows the FE mesh after the pipe is displaced at the desired location ($\bar{Y}$=0.3).

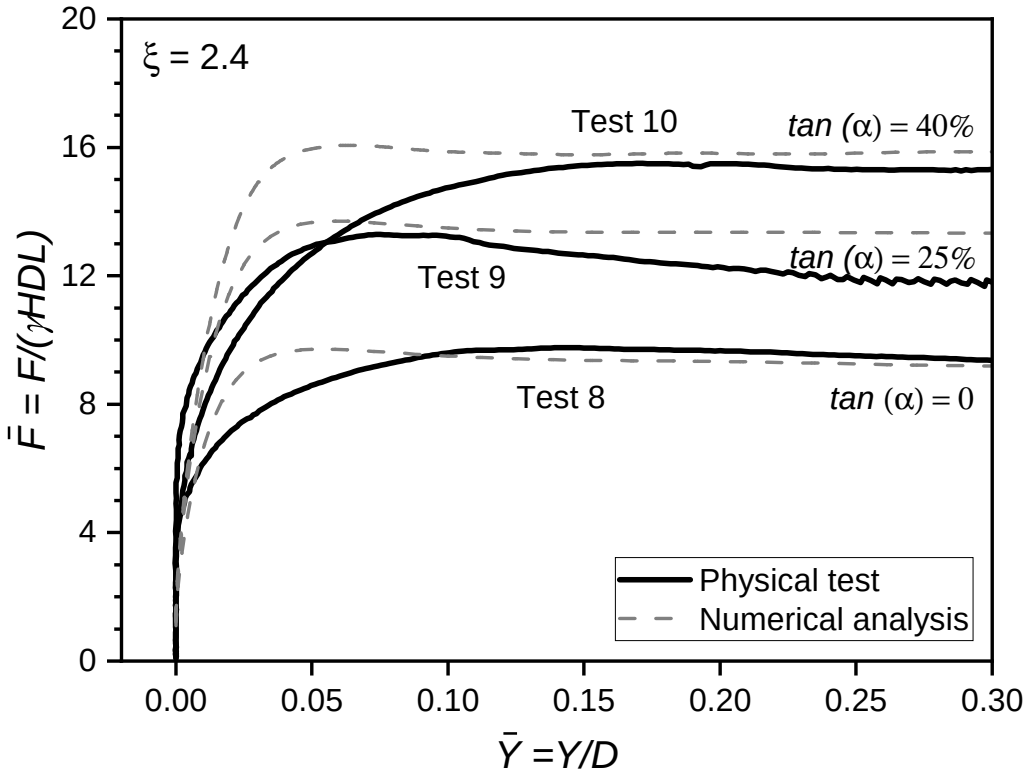

FIGURE 2.10: Lateral Force-displacement response of soil-pipe interaction for burial depth ratio of 2.4

The soil is modelled with 4-node bilinear plane-strain quadrilateral elements with reduced integration and hourglass control (i.e CPE4R in Abaqus FE software). The pipe is modelled as a rigid body according to the experiments. The bottom of the FE domain is restrained from any vertical movement, while all the vertical faces are restrained from any lateral movement. The physical experiment was conducted at a pipe displacement rate of 2.5 mm/sec. For numerical simulations, 200 mm/sec is used to make the simulations computationally efficient. For all the numerical analyses, kinetic energy (ALLKE) and internal energy (ALLIE) are checked. ALLKE represents a very small fraction of the ALLIE showing that the quasi-static condition is satisfied at this loading rate. A sensitivity analysis was conducted to ensure that the results of the simulations with 200 mm/sec resemble that with 2.5 mm/sec.

Further evaluation of the numerical model includes studying the response's energy content. According to Fig. 2.11a, the kinetic energy (E_{KE}) is a small fraction of the internal energy (E_I) throughout the majority of the analysis ensuring that the inertia forces were negligible. Artificial strain energy (E_{AE}) was checked to be 1-2% of the internal energy; if not, it may be an indication of hourglassing problems, which can be resolved by reducing the mesh size; see Fig. 2.11b. Internal work by penalty contact (E_{PW}) was monitored to be a small fraction of the external work (E_W); see Fig. 2.11c. The energy balance of the system was investigated using Eqn. 2.4; see Fig. 2.11d. Note that E_I is the internal energy (including elastic, inelastic and artificial strain energy), E_{VD} is the energy absorbed by the viscous dissipation, E_{FD} is the frictional dissipation energy, E_{KE} is the kinetic energy, E_W is the work of external forces, and E_{TOT} is the total energy in the system.

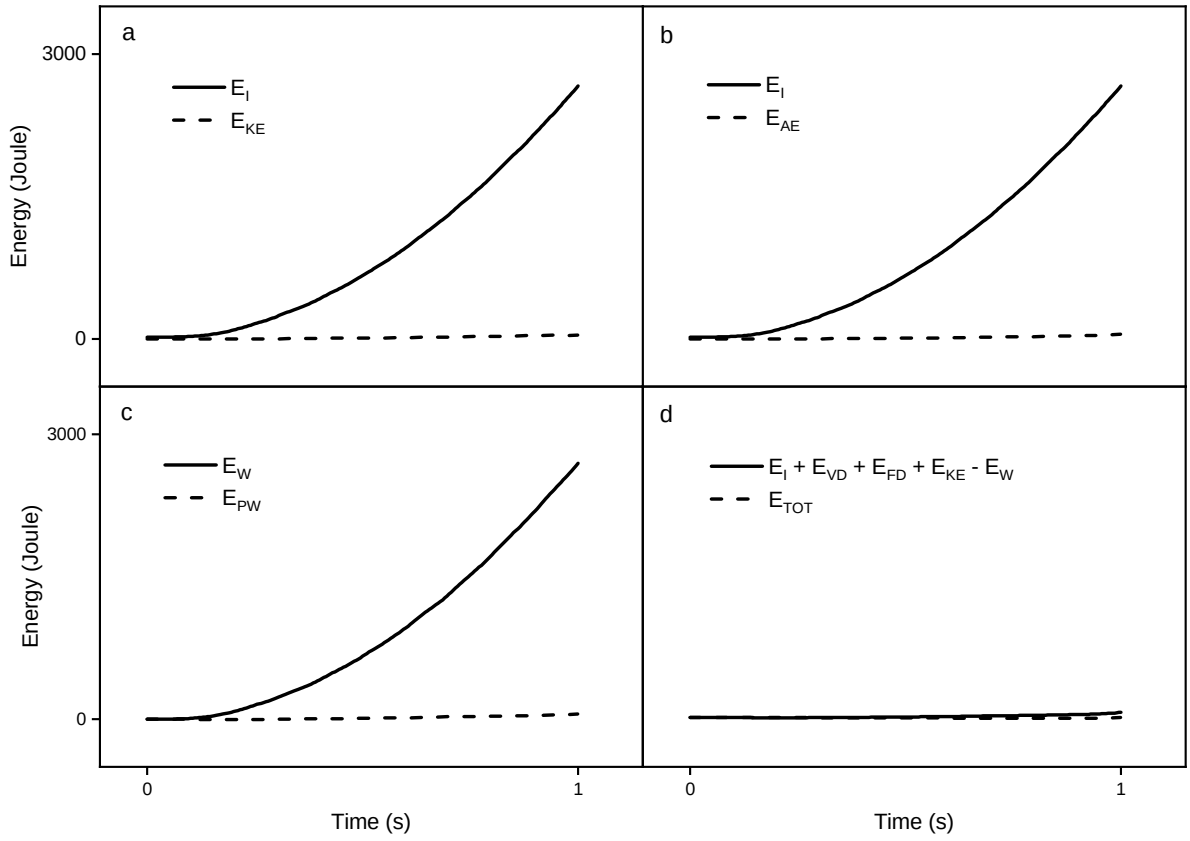

FIGURE 2.11: Evaluation of the numerical response of test 6

$$E_I + E_{VD} + E_{FD} + E_{KE} - E_W = E_{TOT} = constant \tag{2.4}$$

In Fig. 2.13, the plastic strain (PE) from the numerical simulation is overlaid on a photograph of the deformed soil of test 8. PE is shown in a green tone that is in good agreement with the shear failure surface in the physical test.

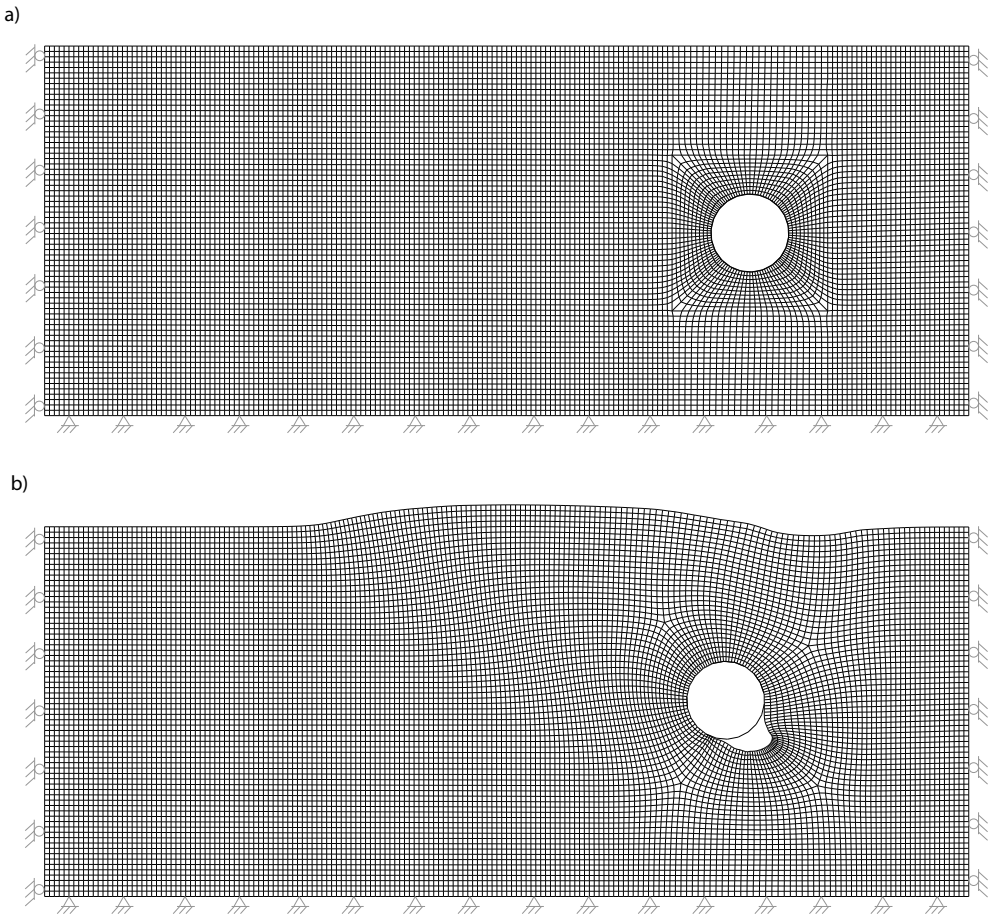

FIGURE 2.12: Typical finite element mesh (test 8)

2.5.1 Soil model

The finite element modelling is performed using the classical elastic-perfectly plastic Mohr-Coulomb (MC) soil model as available in the Abaqus FE software. The initial stage of the

loading is dominated by elastic behaviour, while the plastic deformation occurs as the applied shear stress exceeds the shear strength of the soil. This mechanism is also observed in the soil-pipe interaction tests: a linear force-displacement response followed by a perfectly plastic behaviour after the critical pipe displacement (Fig. 2.7 to 2.10). The MC model is commonly used to predict the horizontal bearing capacity factor for soil (sand)-pipe interaction with and without modifications (Yimsiri et al., 2004; Guo and Stolle, 2005; Xie, 2008; Daiyan et al., 2011; Jung et al., 2013; Roy et al., 2015). In the MC model, angles of internal friction (ϕ') and dilation (ψ) are given as input, which remain constant during FE analysis. Note that for dense sand, both ϕ' and ψ vary with plastic shear strain and mean effective stress by showing a pre-peak hardening and post-peak softening behaviour (Bolton, 1986; Mitchell and Soga, 2005). As constant values of ϕ' and ψ are used, the MC model cannot capture the post-peak softening behaviour of dense sand (Roy et al., 2015; Roy et al., 2018). However, by choosing appropriate equivalent (lower than the peak but higher than the critical) values of ϕ' and ψ for the plane strain conditions, the MC model can reasonably capture the peak dimensionless force (Yimsiri et al., 2004; Guo and Stolle, 2005; Roy et al., 2018). As the horizontal bearing capacity factor (N_{qh}) is the primary focus, the classical MC model is used in the present study. The parameters of the MC model used in this numerical study are selected based upon previous studies on the Fraser River sand, which are detailed in Table 2.3. Specifically, the soil friction angle (ϕ'=46°) of is chosen for the numerical simulation by examining the triaxial tests performed under low effective confining stress levels by Karimian (2006). The dilation angle (ψ=16°) is calculated using $\phi' = \phi_{crit} + 0.8\psi$ (Bolton, 1986). Note that similar values of equivalent ϕ' and ψ were used to simulate the soil-pipe interaction using the MC model by previous researchers (Yimsiri et al., 2004; Roy et al., 2018). In the present study, ϕ'_{crit}=33° is used based on the triaxial tests conducted by Uthayakumar (1996) and Sivathayalan (2000). The initial Young's modulus (E_i) of the dense sand is 65 MPa, according to Karimian (2006) at the confining stress and sand density resembling conditions in these experiments. In an elastic-perfectly plastic model, a secant elastic modulus can be used to estimate the peak

TABLE 2.3: Properties of the Mohr-Coulomb model for the dense sand

Soil properties	dense sand
Internal friction angle of soil (ϕ')	46°
Dilation angle (ψ)	16°
Secant elastic modulus (E_{sec})	21 MPa
Total unit weight of soil (γ)	16 kPa
Poisson's ratio (ρ)	0.3
Soil-pipe interface friction coefficient (μ)	0.81

force. Using $E_{\text{sec}} = 1/3E_{\text{i}}$ (Byrne et al., 1987), the secant modulus of 21 MPa is used in this numerical analysis.

2.5.2 Model calibration and the parametric study

The numerical model developed in Abaqus/Explicit is first calibrated against one reference test (Test 8: ξ = 2.4) with a flat ground surface by selecting appropriate soil properties as discussed in Section 2.5.1. The comparisons of the force-displacement response and the soil deformation mechanism between the numerical simulation and the physical test are presented in Fig. 2.13(a) and 2.13(b). A good agreement is achieved in predicting the peak dimensionless force (Fig. 2.13a) and the soil failure mechanism (Fig. 2.13b). Further comparison between the physical soil failure mechanism and the plastic shear bands estimated numerically is presented in Appendix B. Note that the peak dimensionless force (i.e. horizontal bearing capacity factor N_{qh}) is the primary focus of the present study, which is predicted reasonably well with the MC model. More examples of the deformation pattern between the numerical and experimental simulations are presented in Fig. 2.14, which will be discussed in the next section. After the model is calibrated against an experiment with a flat ground surface, a comprehensive parametric study is conducted with 45 simulations including the slope grades of -40%, -25%, 0, 25%, 40% and the burial depth ratios of 1.6, 2, 2.4, 3, 4, 5, 6, 7 and 8. The force-displacement responses of the numerical models with associated physical

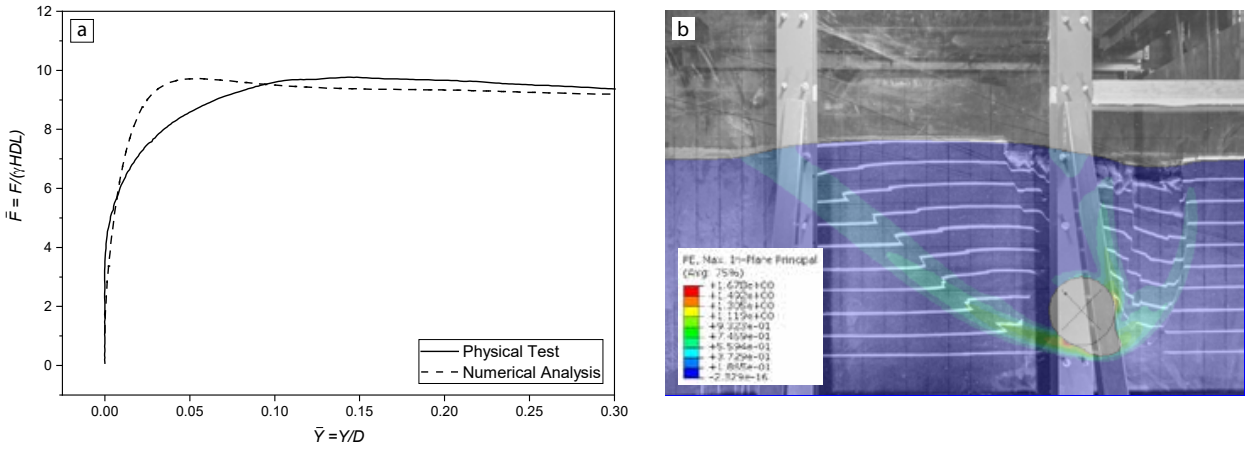

FIGURE 2.13: Calibration of the numerical analysis against a reference test (test 8) a) force-displacement response b) The plastic strain from the numerical simulation overlaid on a photograph of the deformed soil

tests are presented in Fig. 2.7 to 2.10. Similar to the calibrated model response with the physical test, Fig. 2.7 to 2.10 shows that the present numerical model can successfully predict the peak dimensionless force of all the experiments with less than 10-15% error.

2.6 Soil deformation mechanism

As indicated earlier, the experimental program involved conducting ten full-scale physical modelling experiments. For brevity, the photographs from five tests are presented in Fig. 2.14, which vividly illustrate the effects of slope grade on the soil failure mechanism. Further photos can be found in Appendix B. The resultant displacement vectors from the numerical analysis at about the same pipe displacement, for tests 6, 7, 8, 9, and 10, are also presented beside the photographs taken from the physical tests in Fig. 2.14 to assist with the interpretation. For all the five tests (ξ=2.4 and $\tan(\alpha)$=-40%, -25%, 0, 25%, 40%), the physical soil failure pattern is in good agreement with the deformation vectors obtained from the numerical models. Fig. 2.14 clearly shows that the shear failure surface is primarily dependent on the slope grade with a more elevated failure surface for a steeper slope. This mechanism

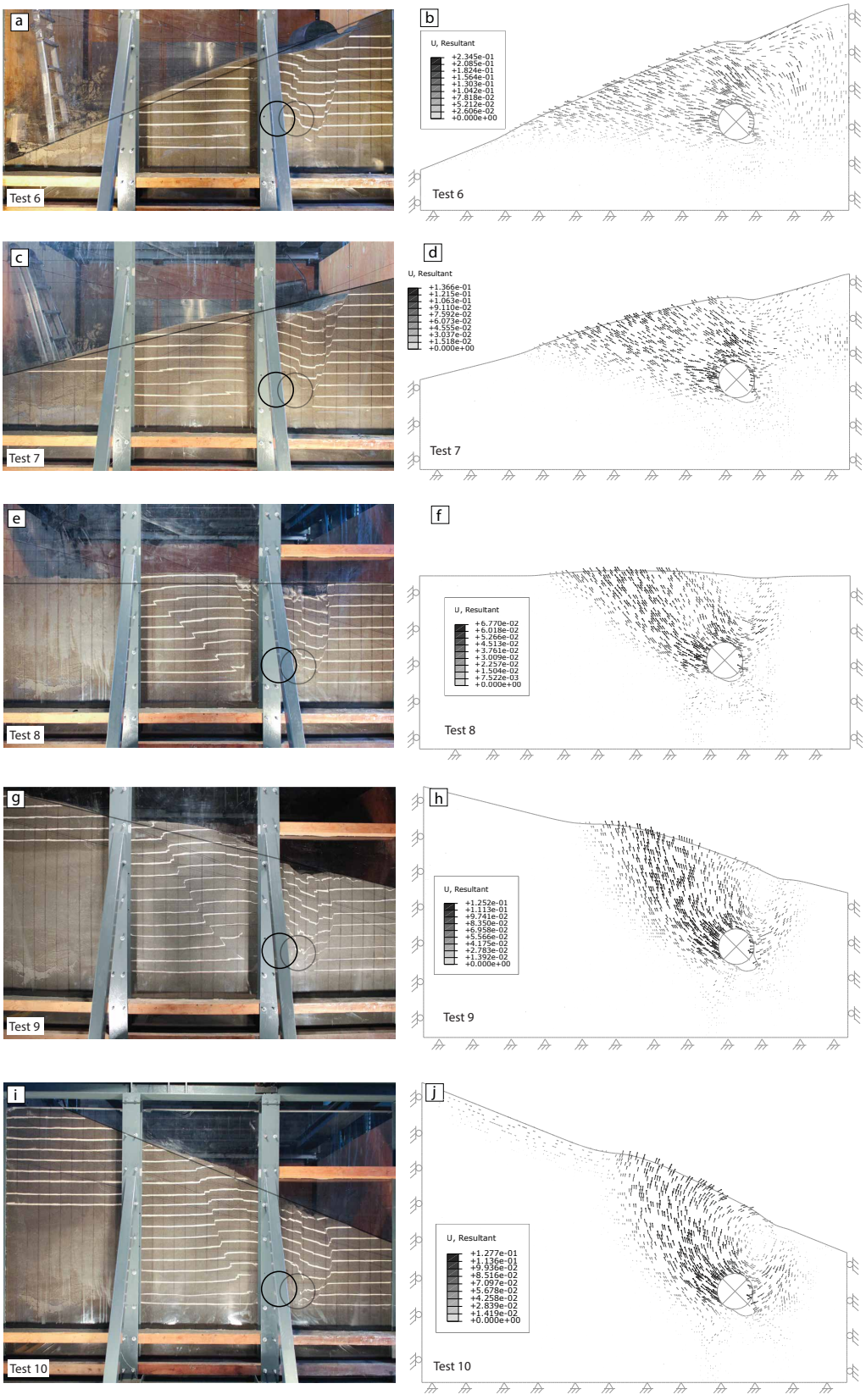

FIGURE 2.14: Soil deformation in numerical and experimental study: a, c, e, g, i) photographs of the physical test configuration b, d, f, h, j) resultant displacement vectors and the numerical model configuration

can be observed from the resultant vectors as the intercept angle of the vectors with the horizontal plane is increased by the slope grade. As stated earlier, the pipe had the freedom to move vertically while being displaced horizontally. According to the study, the vertical displacement of the pipe is also dependent on the slope grade. In test 6, for example, the ratio of the vertical to the horizontal displacement of the pipe is about 1/3 (see Fig. 2.14a,b) whereas in test 10, this ratio is 2/3 (see Fig. 2.14i,j). Interestingly, similar conclusions can be drawn from the displacement vectors obtained from the numerical models. For example, the soil displacement vector components, vertical to horizontal, have the same ratio of 1/3 and 2/3 in front of the pipe in tests 6 and 10, respectively, according to Fig. 2.14(b) and Fig. 2.14(d). Fig. 2.14(a) shows that the white sand lines placed for visual observation of deformation patterns at the front transparent walls are not distorted in front of the pipe (test 6). It is evident from Fig. 2.14(b) that the likely reason lies in the intercept angle of the resultant vectors with the horizontal plane. As the intercept angle is small for this particular example, it appears that a more substantial deformation is required for producing noticeable distortion in the horizontally placed white sand stripes.

2.7 Horizontal bearing capacity factor for the dense sand

The horizontal bearing capacity factor, N_{qh}, is one of the key parameters in numerically analysing the pipelines subjected to ground displacements. N_{qh} is the maximum values of the $\bar{F}_h - \bar{Y}$ curves, as shown in Fig 2.7 to 2.10. N_{qh} for all the cases, including 45 numerical simulations and ten full-scale physical model tests, are presented in Fig. 2.15. The line for N_{qh} representing the level ground condition presented by Trautmann and O'Rourke (1985) is also plotted for comparison. Note that for Cornell Filter sand, Trautmann and O'Rourke (1985) used ϕ'=44° for their numerical simulation with the MC model while ϕ'=46° is used for the Fraser River sand in the present study.

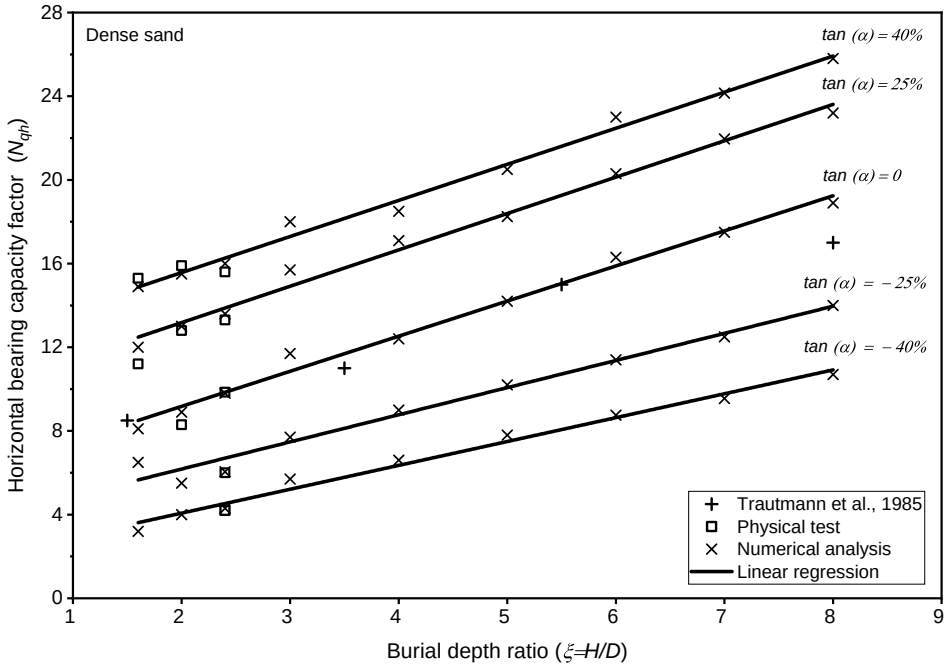

FIGURE 2.15: Horizontal bearing capacity factor versus burial depth ratios for dense sand

Fig. 2.15 includes useful information as highlighted below:

- The peak dimensionless forces from the full-scale experiments are superimposed with that obtained from numerical studies, thus illustrating their agreement in a mutual sense.
- It is apparent from this illustration that the horizontal bearing capacity factor (N_{qh}), as expected, is an increasing function of the slope grade and burial depth ratio.
- N_{qh} can be selected using the linear regressions, which are performed on the numerical data and presented with solid black lines.

The study investigates only five slope grades, -40%, -25%, 0, 25%, and 40%; as such, five lines are representing the horizontal bearing capacity factors for each slope case. The intermediate slope grades can be linearly interpolated as a clear trend was observed between the slope grades, burial depth ratios, and bearing capacity factors. The lines corresponding to the negative slope grades can be used for the definition of soil springs in the passive zones

(see the passive zone in Fig. B.1). For example, in a case with a burial depth ratio of 5 and a slope grade of 25%, it is recommended to use the lines corresponding to tan(α)=25% and tan(α)=-25% for the active and passive zones, respectively. This results in estimating N_{qh} of 18 for the active zone and 10 for the passive zone. This is about a 30% increase in N_{qh} for the passive zone and a 40% decrease for the active zone, compared to level ground conditions. Increasing the soil load in the active zone is essential for the safe design of pipelines in sloping grounds. Decreasing the soil load in the passive zone provides the opportunity to reach an economical design by distributing the soil loads on a more extended section of the pipe, which in turn prevents the chance of strain localization, especially around the boundaries of the slide zone where the ground displacements change abruptly. Note that a lower value of N_{qh} in the passive zone is due to the reverse behaviour of soil-pipe interaction in this zone. The soil loads the pipe in the active zone while it resists the pipe displacement in the passive zone in case of a slope movement. As a result, the active zone's amplifying effects are attenuating in the passive zones. This distinctive definition of soil springs in the passive and active zones is considered essential to reach an economical and safe solution by implementing "softer" soil springs in the passive zone and "stiffer" soil springs in the active zone.

2.8 Horizontal bearing capacity factor for loose and medium sands

The numerical model, calibrated using the physical tests, is used to extend the results of the study to the loose and medium sands. The loose and medium sand properties, used in the simulations, are presented in Table 2.4. The horizontal bearing capacity factors for the loose and medium sands for slope grades of -40%, -25%, 0, 25% and 40% are presented in Fig. 2.16 and Fig. 2.17 as a function of burial depth ratio. N_{qh} for flat ground conditions,

TABLE 2.4: Properties of the Mohr-Coulomb model for the loose and medium sands

Soil properties	Loose sands	Medium sands
Internal friction angle of soil (ϕ')	31 °	36 °
Dilation angle (ψ)	0°	3.75°
Secant elastic modulus (E_{sec})	10 MPa	15 MPa
Total unit weight of soil (γ)	14.8 kPa	15.7 kPa
Poisson's ratio (ρ)	0.3	0.3
Soil-pipe interface friction coefficient (μ)	0.81	0.81

presented by Trautmann and O'Rourke (1985) for the loose and medium sands, are shown in these graphs for comparison. According to Fig. 2.16, the predicted N_{qh} for flat ground is in good agreement with that of Trautmann and O'Rourke (1985) for $\xi = 3.5$ and $\xi = 5.5$. N_{qh} is about 10-15% lower for $\xi = 1.5$ and $\xi = 8$ compared to that of Trautmann and O'Rourke (1985). For the medium sand, according to Fig. 2.17, N_{qh} for flat ground is in good agreement for $\xi = 1.5$ and $\xi = 3.5$. N_{qh} is about 10% lower for $\xi = 5.5$ and $\xi = 8$ compared to that of Trautmann and O'Rourke (1985).

2.9 Conclusion

The current formulations describing soil-pipe interaction have been focused mainly considering the performance of buried pipelines in level ground subjected to relative ground displacements. The applicability of such formulations becomes questionable when assessing the behaviour of pipelines that traverse perpendicular to ground slopes encountered in mountainous areas and river banks, etc. With this background, research was undertaken to study the soil-pipe interaction mechanisms with respect to pipelines buried in sloping ground. Ten full-scale experiments were performed on a 324-mm diameter pipe buried in a sandy slope investigating the lateral soil restraint against pipe displacements. The experimental work was followed by comprehensive numerical analysis to assess pipes having

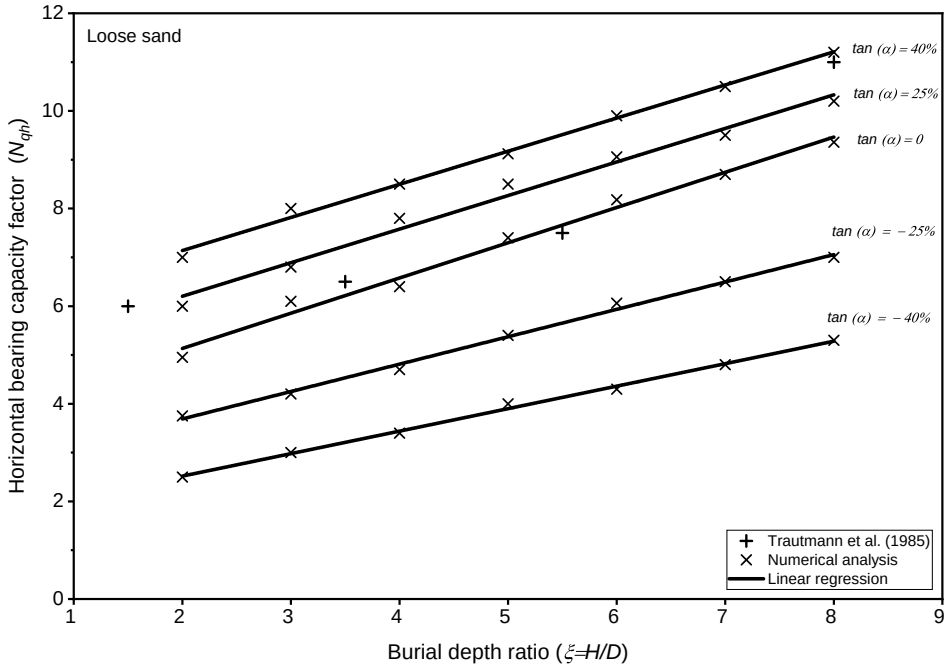

FIGURE 2.16: Horizontal bearing capacity factor versus burial depth ratios for loose sand

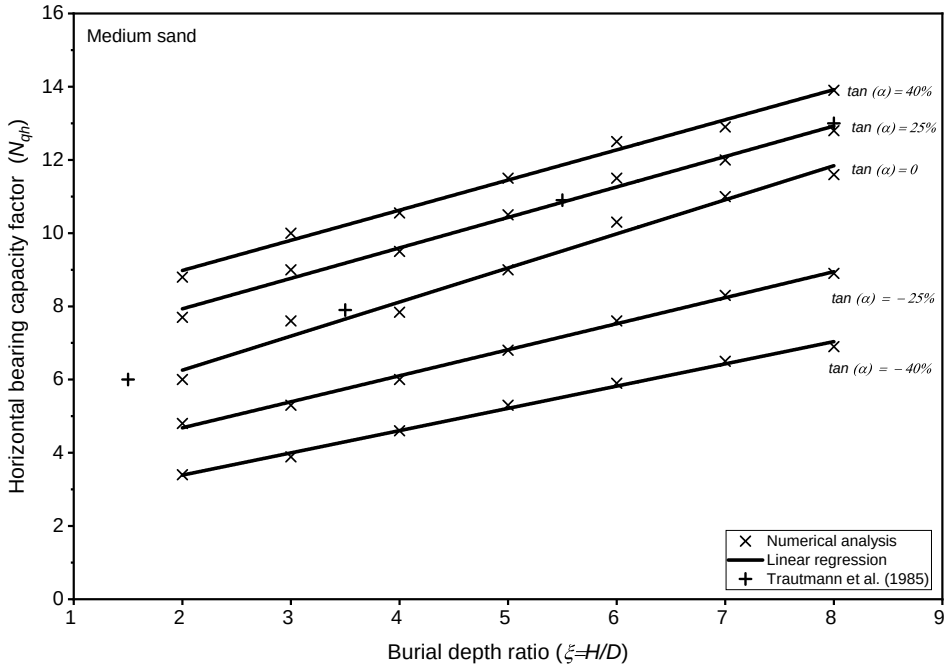

FIGURE 2.17: Horizontal bearing capacity factor versus burial depth ratios for medium sand

deeper embedment conditions in loose, medium and dense sandy slopes. The development of soil restraint on pipes buried in slopes are defined as a function of two key variables, slope grade and burial depth ratio.

The results demonstrated that the soil restraint was significantly affected by the slope grade in addition to burial depth ratio, highlighting the importance of accounting for the slope grade in soil-pipe interaction analysis and associated engineering design. The variation of bearing capacity factors, graphically presented as a function of burial depth ratios (i.e., ξ between 1.6 and 8) and slope grades (i.e., $\tan(\alpha)$ between -40% to 40%), could be useful in developing soil springs for evaluating pipeline response in slopes. It is also critical to understand the soil-pipe interaction behaviour in the longitudinal and vertical directions for sloping grounds to fully incorporate the slope grade effects in pipeline modelling and design.

Chapter 3

Numerical analysis of pipeline response to slow landslides: case study

3.1 Abstract

A numerical analysis is carried out to study the behaviour of pipelines subjected to slow landslides at three at-risk landslide zones of Manitoba Pipeline Network. The pipeline's longitudinal axis is parallel to the slow landslides at all three research sites. The ground displacements monitored for 5 years are imposed on the pipe using a special purpose soil–pipe interaction element (PSI element) using Abaqus/Standard. The stiffness of PSI elements is defined based on soil–pipe interface properties according to PRCI (2017). The results of the numerical analysis are compared with the instrumentation data to draw recommendations for future monitoring programs in slow landslide zones.

3.2 Introduction

A program started in 2010 at the University of Manitoba to monitor the strain in the pipelines subjected to slow landslides (Ferreira, 2016). For this purpose, over 10 Manitoba pipeline network locations visited in fall 2009, three at-risk landslide areas at St-Lazare Assiniboine River valley, Plum River Crossing, and Harrowby Assiniboine River valley were selected. The pipelines at these sites are ductile steel gas transmission lines with the minimum yield strength of 241 MPa for the oldest sections to a maximum of 345 MPa for the newest sections. The pipelines have been under operation for more than 30 years at Harrowby, and more than 50 years at Plum River and St-Lazare. The ground displacement, temperature of the ground at the pipe's burial depth, temperature of the outer wall of the pipe, groundwater conditions, and longitudinal strain in the pipe's outer wall were instrumented from 2010 to 2015 with hourly measurements to analyze the behaviour of pipelines subjected to slow soil movements. In this study, Abaqus/Standard, a finite element method (FEM) software, is used to model the soil–pipeline interaction under the effects of ground displacements. The pipeline is represented by Timoshenko beam elements, and the soil–pipeline interaction is simulated by using a special-purpose soil–pipe interaction element (PSI element) in Abaqus/Standard. PSI elements reflect force transfer between the pipeline and soil as a result of their relative movements on the pipeline through their stiffness. The stiffness is defined based on soil–pipe interface properties according to PRCI (2017). The results of the numerical simulations are compared with field data of Ferreira (2016) to examine the behaviour of pipelines subjected to slow landslide movements and to provide some recommendations for future monitoring programs in landslide zones.

3.3 Field monitoring program

As noted earlier, three at-risk landslide areas of the Manitoba pipeline network are chosen for the field monitoring program: St-Lazare Assiniboine River valley, Plum River Crossing, and Harrowby Assiniboine River valley. The pipelines at these sites are parallel to the slope and the slopes are undergoing ongoing soil creep. At the Plum River research site, the pipeline is also subjected to localized river bank landslide activities.

These research sites were instrumented for 5 years, from September 2010 to August 2015, with hourly monitoring of ground movements, longitudinal pipe strain, pipe and soil temperatures, and groundwater levels to assess the behaviour of pipelines subjected to slow landslides. A total of seven slope inclinometers (SIs), six temperature gauges, 23 strain gauges, and 10 vibrating wire (VW) piezometers were installed in the three research sites (Ferreira, 2016).

Uniaxial strain gauges were installed on the pipes as the ground deformations are parallel to the pipeline's longitudinal axis. Two uniaxial strain gauges were attached to each pipe, one at the top and another at the bottom.

One of the challenges of an instrumentation of this kind is to measure the initial conditions of the pipe before the instalment of strain gauges. It has been known that the pipelines at St-Lazare and Plum River have been subjected to slow landslides many years before the instalment of strain gauges. Therefore, the assessment of initial conditions for the interpretation of measured data is extremely difficult.

The pipelines were cut and replaced at Plum River and St-Lazare, which created an opportunity for the research team to measure the strain release after the cut. It was reported that the pipeline moved instantly after the cut, which is a clear sign of the presence of accumulated strain in the pipe. However, no strain release was picked up by the strain gauges installed on the pipes: the reasons are explained in detail in section 3.4.5. In addition, a pipe push test was carried out on the abandoned portion of the pipe to estimate the

undrained shear strength of the soil–pipe interface. The results of the instrumentation are explained and discussed in section 3.3.4. In the following section, a brief description of each research site is given.

3.3.1 St-Lazare research site

Site location

St-Lazare research site is located on the southern side of Assiniboine River, which is about 1.3 km southwest of St-Lazare town. The research site is located between STA:0 + 00 with the Universal Transverse Mercator (UTM) coordinates of E335617 m, N5589666 m and STA:4 + 25 with the UTM coordinates of E335973 m, N5589898 m. The slope is approximately 55 m high and 300 m wide (5.5H:1V) as shown in Fig. 3.1.

The pipeline at the St-Lazare research site has been under operation for more than 50 years. The pipeline was installed with an open-cut method on 5 October 1965, with the burial depth of 1 m and was backfilled with the excavated material. The pipeline burial depth in the valley varies from a minimum of 0.75 m to a maximum of 4.9 m, which is illustrated in Fig. 3.1b. The pipeline is a thin-walled ($D/t > 20$) ductile steel pipe with 168.3 mm diameter (D) and 4.78 mm wall thickness (t). The material Poisson's ratio (ν), linear expansion coefficient (α_L), Elastic modulus (E), yield strength (σ_y) and maximum operating pressure (P_{max}) are detailed in Table 3.1.

Site investigation and instrumentation

Three boreholes were drilled for the installation of the SIs and site investigation to the depth of 27.1, 11.1, and 20.5 m in the top, middle, and bottom of the slope, respectively. The inclinometers were installed in September 2010. The ground displacement rate was expected to be extremely slow, and as a result, the first inclinometer reading was scheduled

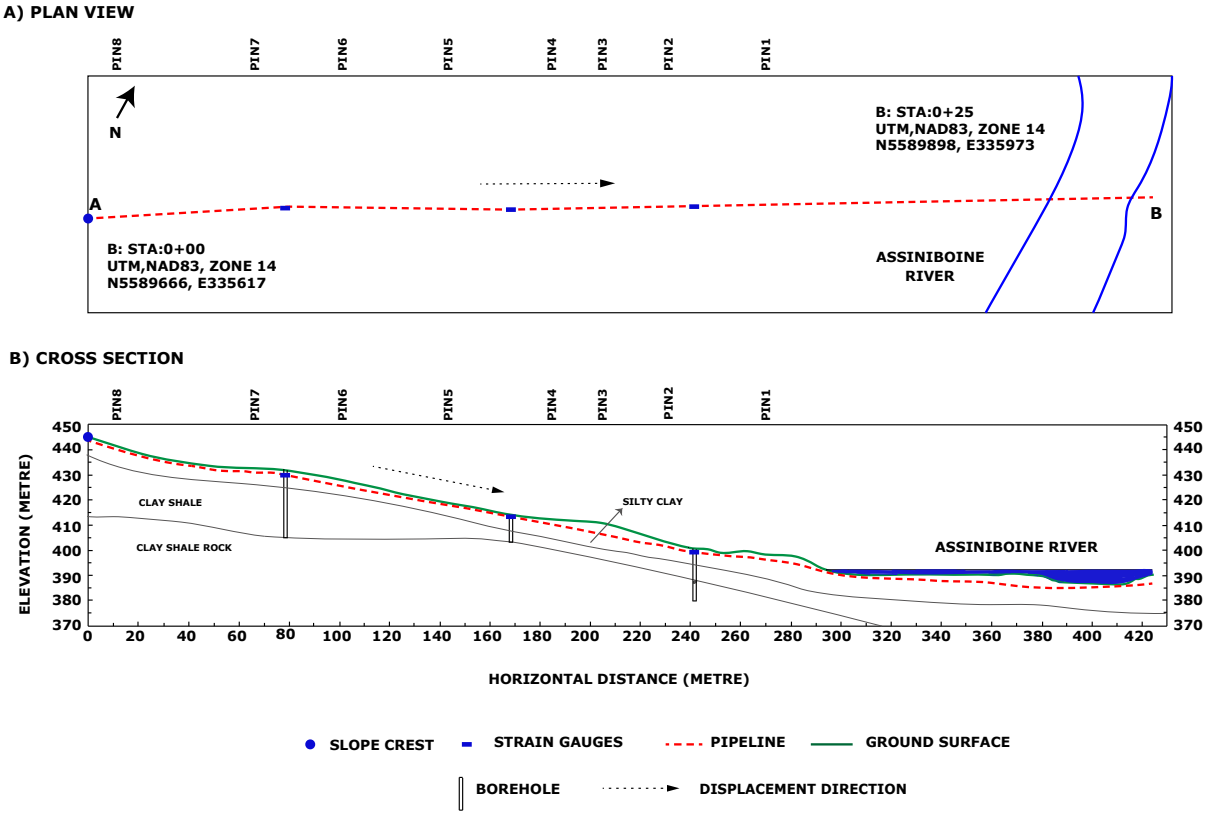

FIGURE 3.1: St-Lazare site plan and cross section (Ferreira, 2016).

TABLE 3.1: Pipeline properties used for the numerical simulation.

Parameters	St-Lazare	Plum River	Harrowby
D (mm)	168.3	88.9	88.9
t (mm)	4.78	3.17	3.18
ν	0.3	0.3	0.3
α_L	12×10^{-6}	12×10^{-6}	12×10^{-6}
E (GPa)	207	207	207
σ_y (MPa)	345	241	290
P_{max} (kPa)	7230	6070	3450

for June 2011. However, the inclinometer movement exceeded expectations (i.e., the ground displacement was much faster).

The thickness of the moving ground can be estimated from the depth at which the inclinometers are impassible with the SI probes. These depths are approximately 7.3 m at the top of the slope and 4 m at the bottom of the slope. According to Fig. 3.1, the SI at the top and bottom of the slope are approximately 80 and 240 m away from the slope crest, respectively.

The ground displacement monitoring then relied on surface monitoring using 12.5 mm rebars with RTK GPS survey equipment. The resolution of the survey was $\pm$ 5 mm in the horizontal and $\pm$ 10 mm in the vertical direction. It was considered that the downslope ground movement would far exceed any lateral movements associated with frost action. As a result, the pins were installed simply by pushing them into the ground without any effort to control the effect of frost action on pin movements. The pin monitoring results for St-Lazare research site are presented in Table 3.2. The negative values represent upslope movements, which is likely due to the effect of frost heave, and freeze–thaw cycles at the ground surface.

Strain gauges were installed approximately 80, 170, and 240 m away from the slope crest according to Fig. 3.1. One temperature gauge was attached to the pipeline wall to measure the pipe temperature, and another used in the ground at the elevation of the pipe to measure the ground temperature.

According to VW piezometer data, the water table fluctuates between the depth of 2 m to a maximum depth of 6 m over the 5 years of monitoring at the St-Lazare research site.

3.3.2 Harrowby Research Site

Site Location

The Harrowby research site is approximately 37 km to the north of the St-Lazare research site and located about 12 km to the west of Russell, Manitoba. The plan view and cross

TABLE 3.2: Monitoring pin results: downslope soil movement at St-Lazare (mm) (Ferreira, 2016)

Reading interval	PIN8	PIN7	PIN6	PIN5	PIN4	PIN3	PIN2	PIN1
2011-05-31—2013-06-18	547.1	268.3	246.7	146.4	54.7	41.7	23.5	25
2013-06-18—2013-10-10	-42.9	-19.8	-16.9	-44.4	-219.9	-25.8	-30.6	-347
2013-10-10—2014-05-29	26.5	32.4	25.6	37.9	—	—	34.7	38.8
2014-05-29—2014-10-07	66.3	18.2	68.1	9.9	137.8	-11.9	-8.9	—
2014-10-07—2015-06-10	-14.9	-3.5	-28	-28.9	—	-48	17	3.9
2015-06-10—2015-09-02	-0.1	14.8	8.9	13.9	—	-19.5	-9.4	—

section of the research site are presented in Fig. 3.2. The research site is located between the approximate UTM coordinates of E327346 m, N5626147 m and E327820 m, N5626276 m. The valley wall is about 75 m deep and 500 m wide with a slope of 6.7H:1V. The pipeline at Harrowby is a steel gas transmission line with a burial depth of 1 m along its right-of-way. The burial depth varies from a minimum of 0.8 m on the slope to a maximum of 4.1 m under the river as shown in Fig. 3.2. The properties of the steel pipe are detailed in Table 3.1. There are many indicators of historical landslides in the area, and heavy rainfall is known to trigger movements in the area. The pipeline is parallel to the slope as can be seen from the topographic contours of the plan view. The pipeline was installed with an open-cut method and backfilled with the excavated material. The pipeline has been in operation for more than 30 years.

Site investigation and instrumentation

Three boreholes were drilled at the Harrowby research site at the top, middle, and bottom of the slope to a depth of 30, 11, and 30 m, respectively (Fig. 3.2). The top, middle, and bottom boreholes, as well as the strain gauges, are located 140, 290, and 410 m down the crest of the slope, respectively. Three inclinometers installed in November 2010 became inoperable before the first reading in June 2011. The depth to the shearing surface can be estimated from the depth at which the SIs are impassable with SI probes. The depth is 3.7, 18.3, and 11 m at

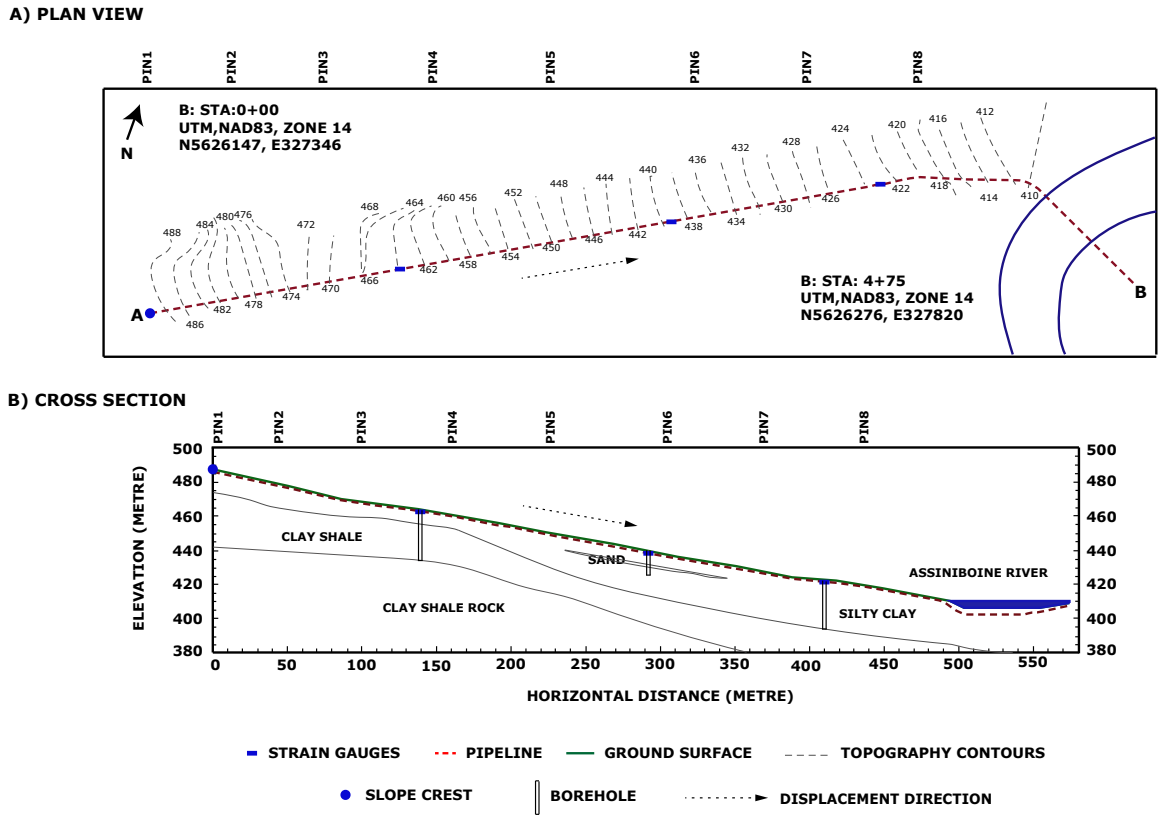

FIGURE 3.2: Harrowby site plan and cross section (Ferreira, 2016).

the top, middle, and bottom of the slope, respectively. The SIs are located 140, 290, and 410 m away from the slope crest as shown in Fig. 3.2.

The ground displacement was monitored using surface pins with RTK GPS survey equipment from June 2011 to September 2015. The pin monitoring results of the Harrowby research site is presented in Table 3.3. Similar to St-Lazare site, the effect of frost action on pins' movements was not assessed. The negative values in Table 3.3, which represents the upslope ground displacements, are likely due to the effect of frost action on the pins.

TABLE 3.3: Monitoring pin results: downslope soil movement at Harrowby (mm)(Ferreira 2016).

Reading interval	PIN8	PIN7	PIN6	PIN5	PIN4	PIN3	PIN2	PIN1
2011-05-31—2013-06-18	0.3	67.3	75.7	82.3	107.2	199.9	149.8	135.4
2013-06-18—2013-10-10	-8.6	-3.2	13.5	4.9	-5.3	2.4	-3.8	0.4
2013-10-10—2014-05-29	15.4	7.4	10.3	12	10.9	-7.2	15.5	-2.5
2014-05-29—2014-10-07	-12.6	12.6	24.4	5.6	3.2	25.7	21.4	15.5
2014-10-07—2015-06-10	15.8	2.4	13.2	5.2	18.5	4.7	29.6	24.7
2015-06-10—2015-09-02	4.7	-7.8	-14.5	10.4	6.3	-3.7	-4.9	10.0

3.3.3 Plum River Research Site

Site Location

The Plum River research site is located about 10 km south of Morris, Manitoba and just at the southwest area of the town of St. Jean Baptiste. The valley is about 4 to 5 m deep with a slope of 3.7H:1V. The plan view and cross section of Plum River research site are presented in Fig. 3.3.

The pipeline at Plum River is a steel gas transmission line with the properties detailed in Table 3.1. This pipeline has been under operation for more than 50 years. The burial depth of the pipeline is 1 m along its right-of-way. The burial depth varies from a minimum of 0.7 m on the slope to a maximum of 2.5 m under the river.

Site investigation and instrumentation

A borehole to the depth of 11.8 m was drilled for the site investigation and installation of a SI. The SI installed in August 2010 became inoperable within 2 months before the first reading. The impassable depth of the inclinometers with the SI probe is 3.86 m, which shows the depth to the ground movements. The ground displacement at Plum River research site was not instrumented after the inclinometer failure. However, the pipe's longitudinal

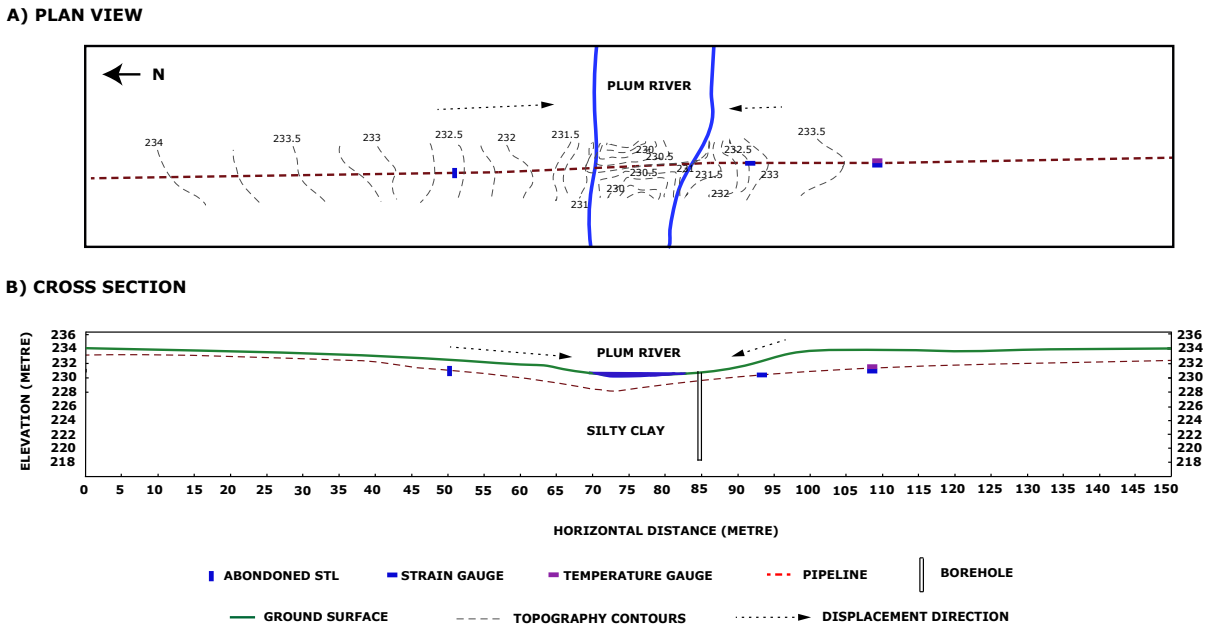

FIGURE 3.3: Plum River site plan and cross-section (Ferreira, 2016).

deformation was instrumented using two sets of strain gauges; one at X = 93 m and another at 110 m as shown in Fig. 3.3. A temperature gauge was installed at X = 110 m.

3.3.4 Instrumentation results

The results of the strain gauges of all three research sites along with an estimation of thermal stress are presented in Fig. 3.4. It is worth mentioning that the thermal stress shown by the red curve in Fig. 3.4 is calculated based on the data from the temperature gauges attached to the pipeline's wall. Katebi et al. (2018) carried out a thermal analysis using COMSOL Multiphysics to estimate the ground temperature profile using weather data from Brandon, MB, from 2011-09-20 to 2016-08-24. This established the boundary conditions at the ground surface. The numerical simulation suggested that the temperature of the pipe wall is mainly influenced by seasonal weather conditions.

According to Fig. 3.4, the axial stress captured by the strain gauges fluctuates between

winter and summer and resembles the induced thermal stress. For example, the strain gauge at X = 93 m at Plum River was installed in April 2012 so compressive stress is generated in the pipe each summer. As another example, the strain gauge at X = 293 m at Harrowby was installed in September 2011. Tensile stress is induced in the pipe in winter due to the contraction of the steel. These rises and falls in the stress profile due to the seasonal temperature variation is illustrated in Fig. 3.4; however, no strain due to gradual landslide is visible from the curves. The reason of this will be discussed in detail in section 3.4.

The initial rise of the stress at the beginning of the instrumentation following installation for two cases, shown by the green and purple colours in Fig. 3.4, is due to the effect of backfilling on the pipeline. The curves then follow the same trend driven by seasonal effects, rising in winter and falling in summer.

As mentioned earlier, the strain gauges did not show any strain release when the pipelines were cut at Plum River and St-Lazare research sites. However, an instant movement of the pipe after the cut was observed. The strain gauges were installed in summer, and the pipe was cut in summer. Comparing the temperature of the pipe after the installation of the temperature gauge with the temperature of the pipe just before the cut showed that almost no thermal stress existed in the pipe at the time of the cut. As a result, the movement of the pipe clearly shows that there was accumulated elastic strain locked in the pipe.

3.4 Numerical simulation

A numerical study is carried out using Abaqus/Standard to analyze the stress induced in a buried pipeline due to ground deformations in slow landslides. The pipeline is modelled using Timoshenko beam element using PIPE21, which is a planar pipe element. PIPE21 is used for the simulation because the slopes are all parallel to the pipe and the transverse relative movements of soil and pipe are considered negligible according to the instrumentation. We note that the Timoshenko beams are good for dealing with large axial strain, but

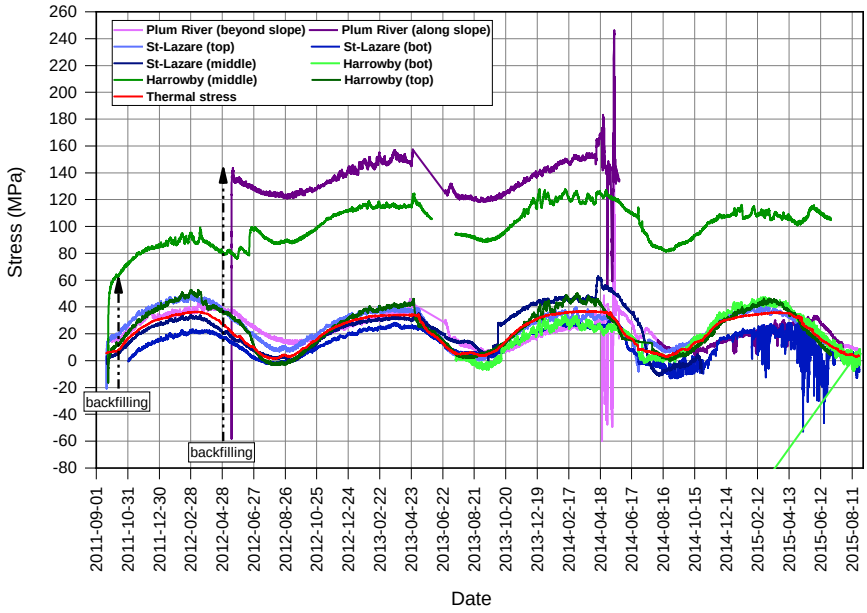

FIGURE 3.4: Longitudinal stress captured by the strain gauges (Ferreira, 2016) and the thermal stress.

the axial strain due to torsion should be small. The soil–pipeline interaction is modelled using PSI elements. A PSI element is a special-purpose element that has only displacement degrees of freedom at its nodes. The far-field edges of the PSI elements resemble the surface deformation of the ground, and the close-field edges of the PSI elements share nodes with the pipe elements as shown in Fig. 3.5 (Abaqus Manual, 2017). The ground displacements, measured during the instrumentation from 2010 to 2015 (Tables 3.2 and 3.3), are imposed on the pipeline through PSI elements. The force on the pipeline due to the ground deformation is transferred to the pipeline through the stiffness of the PSI elements along the pipeline's length. The interaction between pipe and soil can numerically be modelled in four different directions: axial (longitudinal), transverse horizontal, vertical upward, and vertical downward. The stiffness of the PSI elements in these directions can be determined using PRCI (2017). The ground deformation in the transverse horizontal direction is considered to be negligible because the pipeline's longitudinal axis is parallel to the slow landslides at all

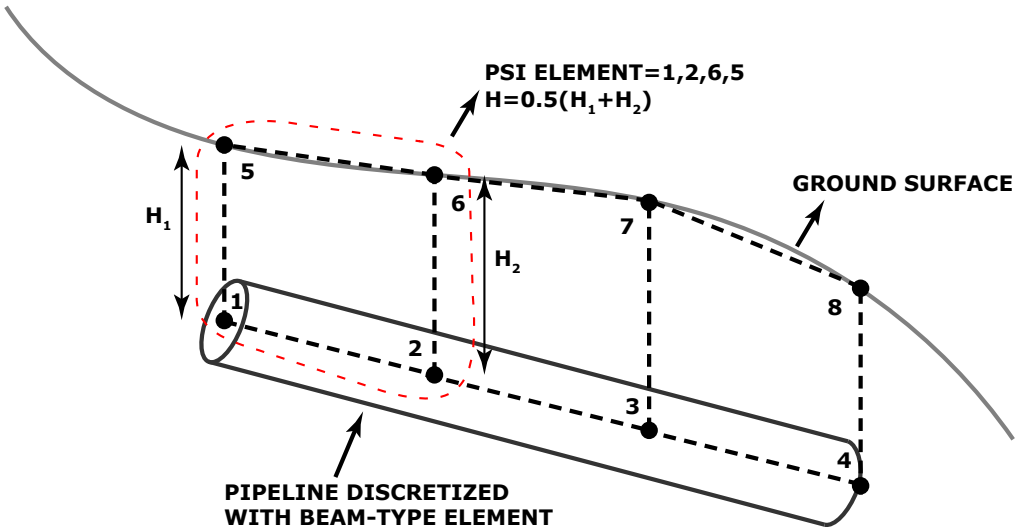

FIGURE 3.5: Pipeline-soil interaction (PSI) element.

three research sites. Also, the soil uplift in the lower reach of the slope and the soil subsidence in the upper reach of the slope, which usually occurs in landslides, are not considered in the numerical simulation for simplicity and given that the instrumentation did not measure them.

The axial soil–pipeline interaction based on the total and effective stresses is estimated using Eq. 1.1a and 1.1b, respectively, according to PRCI (2017). The peak displacements (Y_p) of 5 mm for sand and 10 mm for clay are used in the simulation according PRCI (2017).

3.4.1 Effects of ground displacement rate on soil–pipeline interface

The active shear zone of the soil-pipe interface is about $\sim$ 2 mm thick according to Wijewickreme et al. (2009). The excess pore-water pressure can be dissipated through the soil–pipe interface depending on the landslide speed and the drainage properties of the interface. The rate of landslide movement in which the interface behaves in a drained manner is important

to select the appropriate model for the interface. In this study, Eq. 3.1 is used to determine the degree of drainage condition of the interface according to Paulin (1998):

$$V_n = \frac{vD}{c_v} \tag{3.1}$$

where V_n is a normalized displacement parameter; v is the displacement rate; and c_v is the consolidation coefficient. The loading is drained if $V_n < 0.1$, and undrained if $V_n > 10$. The values of consolidation coefficient are usually between 1 m^2/year to 10 m^2/year. If we use the lower-bound value of 1 m^2/year for the consolidation coefficient, the maximum rate of displacement in which the interface is drained would be 50 mm/month at St-Lazare and 93 mm/month at Harrowby and Plum River. The maximum displacement rates monitored were 3.75 mm/month at St-Lazare research site, and 5.2 mm/month at Harrowby research site. Therefore, a drained model is considered appropriate for the interface. It is worth noting that the full-scale field tests on longitudinal soil–pipe interaction carried out by Cappelletto et al. (1998) suggested that whatever the nature of the soil, clay or sand, the use of an effective stress model yields better prediction of longitudinal soil loads on a pipeline in landslide areas. According to their work, the excess pore-water pressure is easily dissipated through the thin soil–pipe interface along the pipe's longitudinal axis even when the backfill material is cohesive. For the aforementioned reasons, the drained model (Eq. 1.1a) is used for the numerical simulation.

3.4.2 Domain Extent and Boundary Conditions

The pipeline should be simulated with sufficient length to ensure that the imposed pipe loading is balanced out by the soil–pipe interaction outside of the landslide zone. To estimate the necessary length of the pipe for simulation, Eq. 3.2 introduced by PRCI (2017) can be used.

$$L_{anchor} = \frac{\pi D t \sigma_y}{F_a} \tag{3.2}$$

where F_a is the maximum axial soil on the pipe, L_{anchor} is the necessary length of the pipeline outside the landslide zone to balance out the axial soil force, t is the pipe wall thickness, and σ_y is the pipe yield strength.

The extent of the model should be long enough such that the boundary conditions at both ends of the model do not affect the results of the analysis. Furthermore, the length of the pipeline should be sufficient so that the axial strain originating from the landslide dissipates within boundaries in the model.

Using Eq. 3.2, the minimum length of the anchor at each side of the landslide is calculated to be 585 m. The computation of the analysis is not affected much by increasing the extent of the anchor zones because the pipeline behaviour at these locations is elastic. As a result, the pipeline length of 2000 m is used to ensure that the noted boundary conditions are satisfied. Both ends of the pipeline are fixed to prevent the pipe from rigid motion.

3.4.3 Pipeline and soil properties

The pipeline and soil properties used in the numerical analysis are presented in Tables 3.1 and 3.4, respectively. The Atterberg limits of soils at the three research sites are provided in Table 3.5. In this table, LL stands for liquid limit and PL stands for plastic limit. In Table 3.4, γ is the total unit weight of soil, k_0 is the coefficient of earth pressure at rest, ϕ' is the drained internal friction angle of soil, μ is the friction factor of the soil–pipe interface, and x_u is the ultimate relative displacement of the soil–pipe interface. As was presented earlier, the effective stress model is used for the soil– pipeline interface. The total unit weight of soil is used in the simulation due to the ground water table being below the pipeline, and therefore not affecting the model.

The drained internal friction angle of 15°is assumed for St-Lazare and Plum River sites in relation to the slope grades at these two sites being 10.3° and 15°, respectively. The soil creep would generally not be expected if the internal friction angles were higher than the

TABLE 3.4: Soil properties used for the numerical simulation

Research sites	γ kN/m^3	k_0	ϕ'	μ	x_u (mm)
St-Lazare	16.8	0.8	15	0.7	5
Plum River	16.9	0.8	15	0.7	5
Harrowby	17.9	0.8	13	0.7	5

TABLE 3.5: Atterberg Limits of soil (Ferreira, 2016)

Site	**Soil**	**LL**	**PL**
St-Lazare	Silty Clay	73	26
St-Lazare	Clay Shale	99	21
Harrowby	Silty Clay	65	19
Plum River	Lacustrine Clay	83	27

slope grades. However, to be conservative, the drained friction angle of 15° was assumed for the simulation in these sites. For Harrowby, the slope grade is 8.5° and the drained friction angle of 13° was used for the simulation. Correlations between drained friction angles and Atterberg limits are used according to Kanji (1974) to verify that the assumed drained friction angles are reasonable. The k_0 coefficient for clay was chosen according to Mesri and Hayat (1993).

3.4.4 Result of numerical simulation

The pipeline is modelled with 2000 beam-type 1 m long elements. The burial depth of the pipeline is assumed to be 1 m for all nodes outside of the landslide area to be consistent with Manitoba Hydro's nominal burial depth. In the valley, the varying burial depth is used for the simulation according to Figs. 3.1b, 3.2b, and 3.3b.

St-Lazare research sites

The downslope ground displacement that is used in the numerical simulation is presented in Fig. 3.6. The horizontal axis of this figure represents the distance from the slope crest (X

= 0 m) and the vertical axis shows the cumulative downslope ground movements relative to 2013-10-10. As shown in Fig. 3.6, the displacements at the slope crest (X = 0) and toe (X = 300) are assumed to be zero. The displacements at different locations along the slope are linearly interpolated using the data in Table 3.2 and are used as boundary conditions at each PSI node in the simulation. We note that the negative values of pin displacements in Tables 3.2 and 3.3 represent upslope pin movements. The upslope movement likely occurred in the pins due to the frost action in the ground. These negative values are ignored in the numerical simulation because there is no possibility that the soil moves upslope at the pipe's burial depth. We note that the frost depth was above the pipeline during the 5 years of instrumentation so there is no need to consider the effect of frost action on the pipeline.

The displacement corresponding to the second interval, 2013- 06-18 to 2013-10-10, is not used in the simulation because they are all negative. The displacement corresponding to the first interval, 2011-05-31 to 2013-06-18, is also not considered for the simulation as the period between the readings is extensive, which makes the reading unreliable. The average ground displacement rate between 2013-10-10 and 2015-09-02 is used to estimate the cumulative ground displacement in 2023. Furthermore, by trial and error, it is found that at the minimum block-pattern displacement of 0.6 m, the ultimate interface loading capacity is reached in all PSI elements. Increasing the ground displacement from 0.6 to 0.7 m does not increase the soil loading on the pipeline because at this displacement, all interface elements are plastic. The results of the simulation for these two cases can be compared in Fig. 3.7.

The longitudinal stress (S11) is increased as the displacement accumulates over time from 2013-10-10 to 2023 as shown in Fig. 3.7. The result of the simulation shows that the longitudinal stress is at its maximum when the block-pattern displacement of 0.6 m is used. At this displacement, the soil springs used for modelling the soil–pipeline interaction become plastic and as a result, the increase of the displacement does not result in an increase of the loading.

According to the analysis, the pipeline at St-Lazare can withstand the maximum soil

loading of the 300 m moving slope with its elastic capacity, i.e., the maximum stress in the pipe is lower than the pipe's yield stress. As a result, the pipeline goes into an ultimate deformed condition after which the soil slides over the pipe all along the slope and the imposed forces are not going to be increased.

The pipeline, installed in 1965 at St. Lazard site, has been subjected to slow landslides for many years ($\sim$ 50 years) before the beginning of the instrumentation. This implies that the ultimate condition that is shown by 0.6–0.7 m block-pattern displacement has happened in the pipe before the start of the instrumentation. That the pipeline had reached its ultimate deformed condition at St-Lazare due to the gradual landslide before the start of the instrumentation justifies why the strain gauges did not pick any landslide-related strain.

Harrowby research sites

The downslope ground displacement data that are gathered from the instrumentation at Harrowby are presented in Table 3.3. The ground displacement during the first interval, 2011-05-31 to 2013-06-18, is not used in the simulation because the reading interval was too long. The negative values of pin displacements at the ground surface are likely due to frost action and consequently are not considered for the numerical simulation. Other values of pin monitoring data provided in Table 3.3 are used to estimate the ground displacement at each PSI nodes along the slope using a linear interpolation.

The downslope ground deformation at Harrowby that is used in the numerical simulation is presented in Fig. 3.8. The vertical axis is the downslope ground displacement after 2013-06-18 and the horizontal axis represents the distance from the crest. The average displacement rate between 2013-06-18 and 2015-09-02 is used to estimate the displacement in 2018 and 2024. Furthermore, two arbitrary block-pattern displacements and one triangle-pattern displacement are used to study the pipeline behaviour under different loading conditions. Results of the numerical analysis is presented in Fig. 3.9. Each curve of these figures corresponds to the displacement patterns shown in Fig. 3.8. Accordingly, the longitudinal

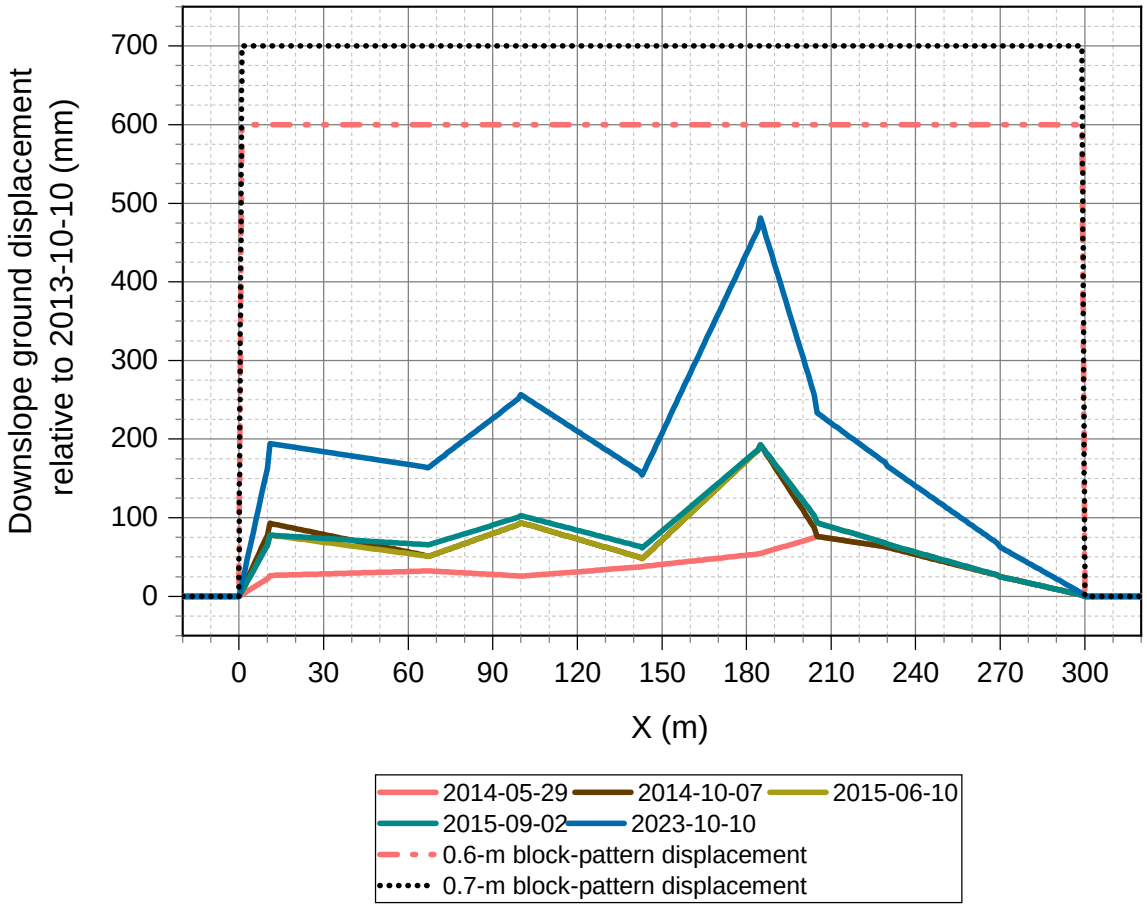

FIGURE 3.6: Downslope ground displacement versus longitudinal axis of the pipe at St-Lazare.

stress is increased as the displacement accumulates over time from 2013-06-18 to 2024. By trial and error, it is found that the maximum soil loading occurs at the 0.3 m block-pattern displacement. The longitudinal stress in the pipe is not increased as the block-pattern displacement is increased from 0.3 to 0.4 m as can be seen from Fig. 3.9. This is due to the fact that the interface is modelled using a linear elastic perfectly plastic behaviour.

We note that the pipeline at Harrowby experiences a plastic deformation under the ultimate loading condition (dashed black and yellow lines in Fig. 3.9), i.e., the maximum stress in the pipe is beyond the yield stress of the pipe. It is worth noting that the maximum

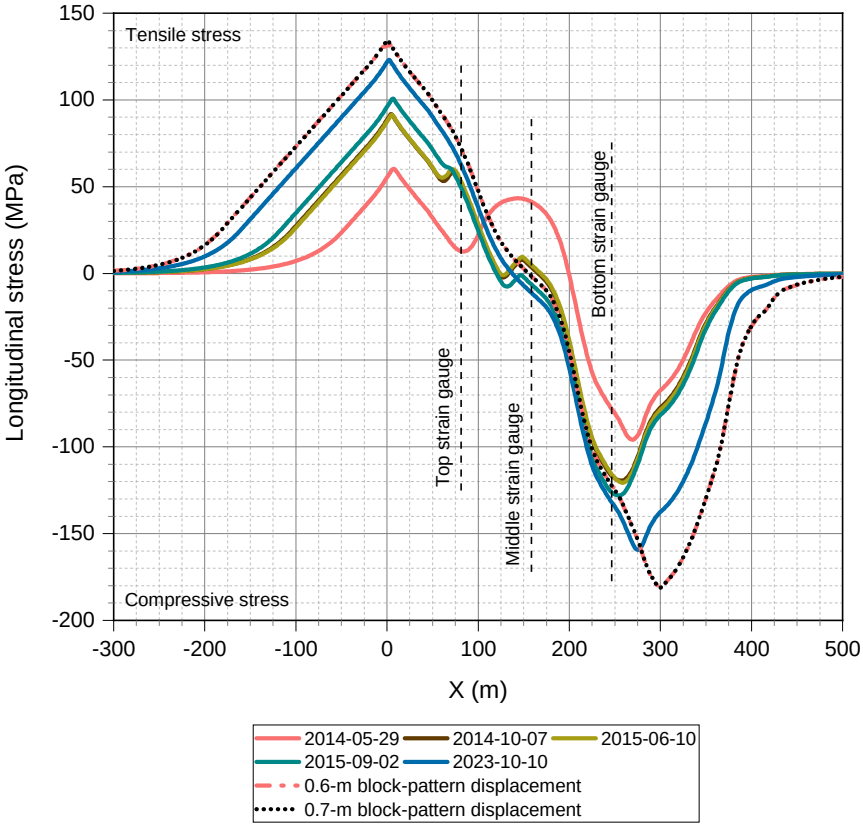

FIGURE 3.7: Longitudinal stress due to slow landslide at St-Lazare.

compressive stress shown in Fig. 3.9 is S11. The maximum Von Mises stress is slightly over the yield stress of the pipe, which leads to a plastic deformation in the pipe. The excessive deformation of the pipe at Harrowby eventually terminates the analysis due to convergence problems, which means that the pipe will rupture in time under the applied loads. This is happening because the linear elastic perfectly plastic behaviour is assumed for the steel and the steel hardening after the yield point is ignored in the analysis. To be able to solve the problem without changing the elastoplastic model, the yield stress of the pipe is increased from 290 to 350 MPa for the last two analyses (0.3 and 0.4 m blockpattern displacements). As the strain gauge data shown by green lines in Fig. 3.4 do not show any progressive trend over time, it can be interpreted that plastic deformation is not occurring in the pipe. If a plastic

deformation had occurred in the pipe, the pipe would have continued to deform by the constant soil loading, and the strain gauges would have measured that behaviour. That the numerical analysis estimated a plastic deformation in the pipe while the instrumentation and site visits proved differently is likely due to the fact that the internal friction angle of clay is chosen conservatively and the hardening of steel is ignored in the simulation. It is important to note that a pipe is designed to withstand the external loads with its elastic capacity, and careful analysis of the pipe's plastic deformation is not the intent of this study. The Harrowby site is categorized under the high-risk zone according to Ferreira (2016). This study has shown that the pipe's applied loads could yield the pipe. As such, further preventive actions are required to protect the pipe against the external loads imposed by ground displacement.

According to the black and yellow dashed lines of Fig. 3.9, which are for the ultimate loading condition, the stress decreases outside of the landslide zone until it reaches zero about 300 m away from the crest of the slope and 200 m away of the slope toe. These two zones, one at the top side of the slope (X = –300 to 0) and the other at the bottom side of the slope (X = 500 to 700), are called anchor zones. In these zones, the pipe movement is restrained by the soil–pipe interaction forces. Anchor zones are simulated using the same soil spring models assuming that the soil–pipeline interaction behaviour in the landslide zone and outside of the landslide zone is similar. At anchor zones, the far edges of the PSI elements that represent the ground displacement are fixed (zero displacement) while the near edges of the PSI elements that share nodes with the pipe are being displaced by the pipe deformation. The loading from the stable soil to the deformed pipe is estimated through the properties of soil springs and is transferred to the pipe as a resistant load to the pipe's movement. At lower reach of the slope, because the pipe is buried deeper (Fig. 3.2), the soil-pipeline interaction is stronger and so 200 m length of the pipe is deformed before the landslide forces are balanced out. In the upper reach of the slope, where the pipeline is buried shallower (Fig. 3.2), the soil–pipeline interaction is weaker that leads to a longer length of the pipeline being affected by the landslide.

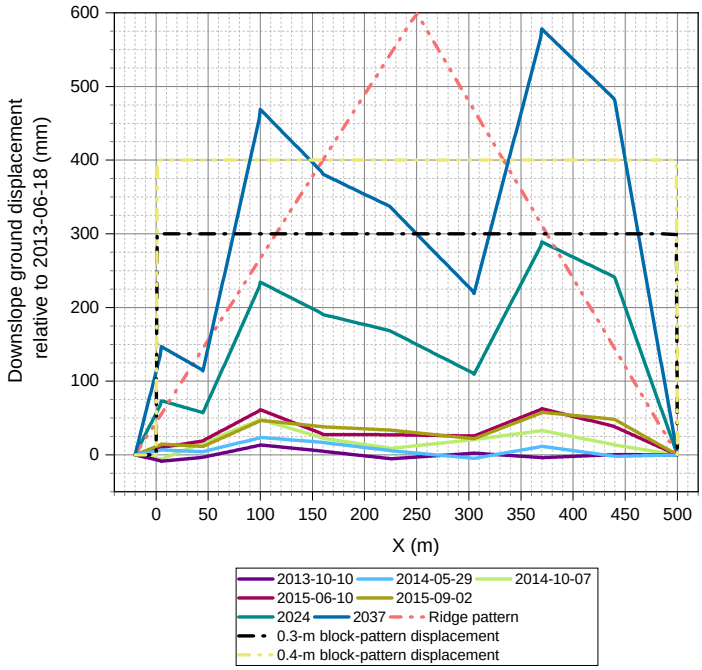

FIGURE 3.8: Downslope ground displacement versus longitudinal axis of the pipe at Harrowby.

Plum river research site

As mentioned in section 3.3.3, the ground displacement is not monitored at Plum River so the analysis is carried out with three different arbitrary displacement patterns as shown in Fig. 3.10. These three arbitrary displacement patterns are assumed with regards to the cross section of the site (Fig. 3.3). In the first analysis, a ground displacement of 1 mm in areas with a slope greater than 5% is imposed on the pipe as shown with the green line in Fig. 3.10. The analysis is repeated with an arbitrary displacement of 250 mm (yellow line) and also 1000 mm (dashed red line) for a slope greater than 5% to study the pipeline behaviour under the ultimate soil loading.

According to Fig. 3.11, the longitudinal stress is not increased as the displacement is increased from 250 to 1000 mm. This implies that at the displacement of 250 mm, the interface is plastic everywhere on the pipe and the soil slides over the pipe. The longitudinal stress

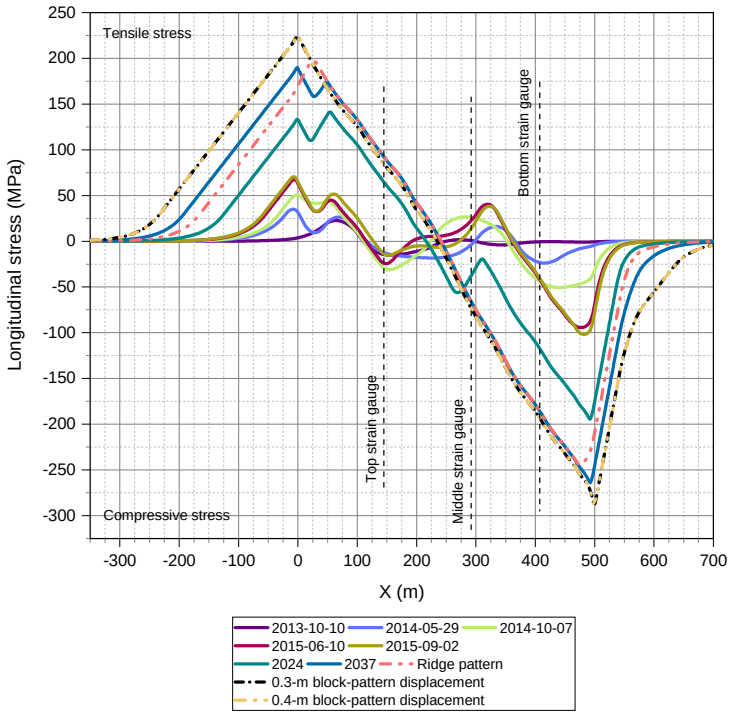

FIGURE 3.9: Longitudinal stress due to slow landslide at Harrowby.

in the pipe is very low in the ultimate case, which implies that the slow landslide is not an issue for the pipe.

Tensile stress is induced in the pipeline at both sides of the river because the pipe is surrounded by the crests of valley walls at both northern and southern sides of the river. According to Fig. 3.3, the slope (greater than 5%) in the southern side of the river is longer compared to the northern wall. This is why the stress in Fig. 3.11 is not symmetric relative to the river. It is worth mentioning that the pipeline is under compressive stress at the centre of the valley (X = 70–85 m) because the ground moves toward the river from both walls.

The effects of a 15 m long rapid landslide at the southern valley wall in Plum River research site is studied using the total stress model (Eq. 1.1b) and the peak displacement of 10 mm. This is done because some traces of river bank activities have been reported from a site visit by Ferreira (2016). The clay model is used for this purpose because the river bank

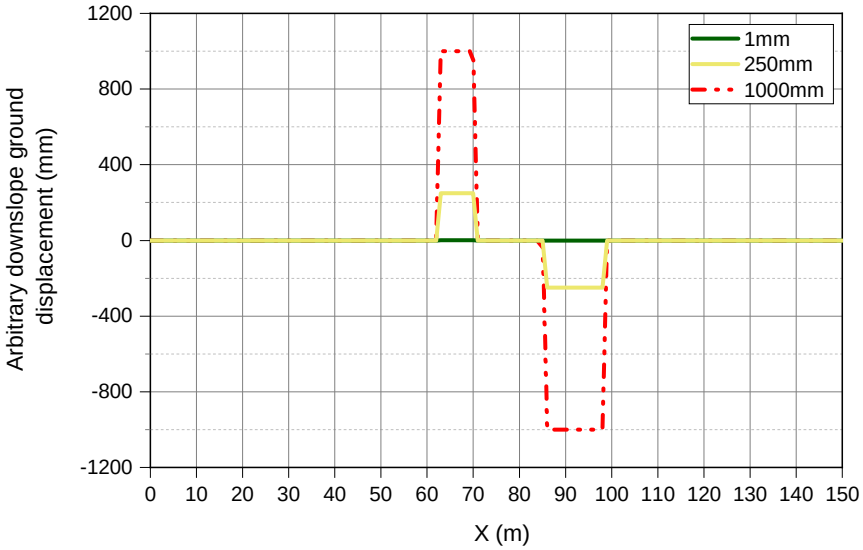

FIGURE 3.10: Downslope ground displacement versus longitudinal axis of pipe at Plum River.

activities usually occur rapidly and more importantly, the clay model gives conservative results because of the high value of the undrained shear strength of clay at this site. We note that αS_u of 45 kPa is used based on the St-Lazare push test. The results are presented in Fig. 3.12. Accordingly, the maximum tensile stress of 105 MPa occurs at the crest of the slope at X = 100 m, and the maximum compressive stress of –105 MPa occurs at the toe of slope at X = 84 m. The anchor zones are formed from X=40 to 85 m and X = 100 to 150 m according to Fig. 3.12.

The result of the rapid landslide at Plum River is somewhat symmetric because block-pattern displacements are used for the landslide and the depth of the pipeline in this location is not varying much. This analysis suggests that the pipeline at Plum River is able to withstand the soil loading from rapid river bank activities with its elastic capacity.

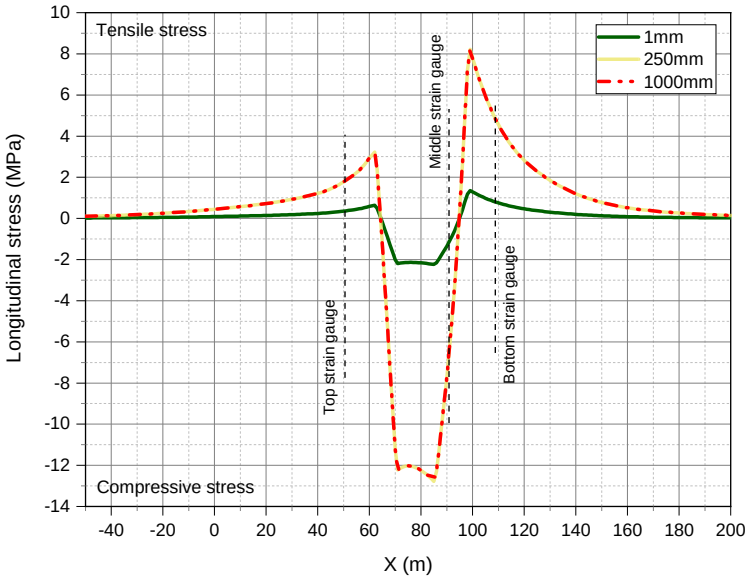

FIGURE 3.11: Longitudinal stress due to slow downslope ground displacement at Plum River.

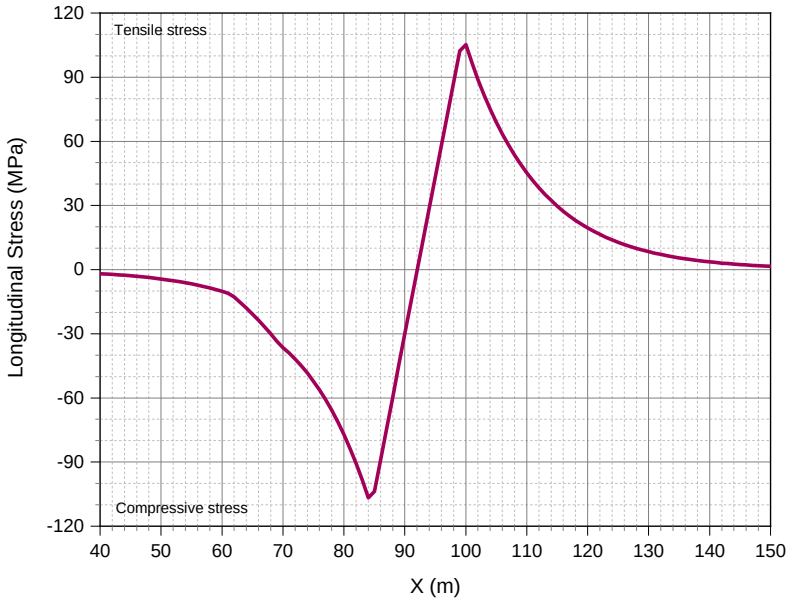

FIGURE 3.12: Longitudinal stress due to rapid landslide at Plum River.

3.4.5 Discussion and comparison

As was mentioned in section 3.3, to estimate the initial conditions of the pipeline, the research team used the opportunity of a scheduled pipeline cut in St-Lazare and Plum River research sites. However, no strain release was measured by the strain gauges. This is likely due to the anchoring effect of the pipeline in the soil. At Plum River, the pipeline was cut in a valve about 50 m away from the strain gauge. The location of the cut was beyond the crest of the slope. At St-Lazare, the location of the cut was about 100 m away from the bottom strain gauge close to the river. After the cut, the pipeline tends to move to relieve its stress while the soil resists to the pipeline's movement. As a result, depending on the soil–pipe interaction and the applied force, the strain is released only in a limited length from the cut. This length is calculated for both St-Lazare and Plum River research sites as follows: the pipeline was cut at X = 350 m and X = 0 m at St-Lazare and Plum River, respectively. According to Figs. 7 and 11, the compressive stress in the pipeline in those sections are about 130 and 0.5 MPa, respectively. The equivalent forces in these sections are calculated to be 329 kN and 450 N for St-Lazare and Harrowby research sites, respectively.

In case of a pipeline cut, the total stress model Eq. 1.1b can be used for the interface because cutting a pipeline is a rapid procedure. Using Eq. 1.1b, the soil resistance to pipeline deformation in undrained condition is equal to $F_a = 23.75$ kN/m and $F_a = 12.5$ kN/m for St-Lazare and Plum River sites, respectively. We note that αS_u of 45 MPa is used according to the St-Lazare push test. Based on this calculation, the strain release occurs only to a distance of 13.85 m at both sides of the cut at St-Lazare and 0.036 m at Plum River. The strain gauges placed 100 m away from the cut at St-Lazare and 50 m away at Plum River did not capture any strain relief simply because they were too far from the cut. This interpretation justifies the observation regarding the instant movement of the pipeline while no strain relief was measured by the strain gauges.

3.5 Conclusion

The effects of slow landslides on buried pipelines in three Manitoba pipeline sites are studied with the use of Abaqus/Standard. The pipe is simulated using Timoshenko beam elements with a linear elastic perfectly plastic behaviour. The soil–pipeline interface is modelled with PSI elements. The stiffness of PSI elements is defined according to PRCI (2017). The monitored landslide movements are imposed on the PSI elements as displacement boundaries. The pipeline behaviour subjected to the monitored ground displacement is examined. Furthermore, arbitrary blockpattern displacements are used to analyze the pipeline behaviour under different loading conditions.

It is shown that the pipelines at two of the three sites, Plum River and St-Lazare, withstand the landslide loading without experiencing any plastic deformation. At these sites, the loading due to the slow landslides increases over time as the displacements accumulate until the maximum frictional interface capacity is reached. At this stage, the soil slides over the pipe as the interface becomes plastic and as a result, the soil loading remains constant.

At Harrowby, the simulation does not converge under the ultimate loading because the pipeline at the toe of the slope experiences plastic deformation. The plastic deformation continues to increase over the analysis steps until the analysis aborts at some point due to the excessive deformation of the pipe, meaning that the pipe eventually ruptures under the applied loads. To solve the problem numerically without changing the pipe's elastoplastic behaviour, the yield stress of the steel is increased from 290 to 350 MPa, and the results are compared to the strain gauge data. Because a progressive trend cannot be seen from the green lines in Fig. 3.4, we can assume that the pipeline at Harrowby has not experienced a plastic deformation over its many years of operation. If the pipe had reached its plastic behaviour under the soil loading, the slow landslide would have induced progressive strain in the pipe and the strain gauges would have picked them up. This overestimation in the pipeline behaviour was expected to occur as the internal friction angle of the soil is chosen

conservatively and the steel hardening of the pipe is ignored in the simulation. It is important to note that the Harrowby site is categorized under the high-risk zone according to Ferreira (2016). This study has shown that the external loads in the Harrowby site could yield the pipe, and so further preventive actions are required to protect the pipe against the gradual landslide.

By comparing the stress in the pipe from the instrumentation with those of the numerical simulations, and the calculated thermal stress, we can realize that the effect of the slow landslide on the pipeline is not captured by the strain gauges. The numerical simulation suggests that the pipeline would go into an ultimate deformed condition under which the soil slides over the pipe (the interface becomes plastic). At this stage, the soil loading remains constant throughout the life of the pipe given that the pipe was able to withstand the ultimate loading condition without deforming plastically. Given the fact that the strain gauges were installed on the pipes that have already went into the ultimate deformed condition clearly explains why the strain gauges did not capture any of the soil loading effects on the pipe.

It is explained that cutting the pipeline is not a practical way to estimate the initial condition of the pipe as the pipe is anchored in the soil and the soil resistant to pipe movement prevents the release of the locked-in strain.

For instrumentation, it is said that the stress condition of the pipeline should be examined before the installation of strain gauges. If the pipeline is scheduled to be cut to capture the stress release, the position of the cut should be close to the slope, and the strain gauges should be placed next to the cut. However, this practice is not recommended. It is better to install the strain gauges either on a newly constructed pipeline or to remove the soil cover over the entire length of the pipe in the active zone and also in the passive zone to ensure the locked-in strain is released before the installation of the strain gauges.

Chapter 4

Effects of ground displacement and thermal loading on selecting pipe depth of cover in river crossings

4.1 Abstract

Thermal stress induced in a buried pipeline due to temperature variation is of great concern in Canada due to its extreme cold winter and warm summer. Thermal stress decreases by increasing the burial depth while the interaction forces due to ground displacement increase by increasing the burial depth. As a result, the optimum depth of a pipeline is of great importance to pipeline companies to minimize interactions between the pipeline and soil in case of temperature variations and ground displacements. Thermal stress is estimated from a heat transfer analysis considering the phase change in the soil using COMSOL Multiphysics. Soil-pipeline interaction based on ASCE (1984) is used for considering the effects of ground movements. The combined stress on the pipeline is estimated as a function of burial depth and is presented in a curve for design purposes. A numerical analysis by Abaqus shows the

adequacy of the presented curve.

4.2 Introduction

Pipeline transport is the most common way of gas and liquid transportation in the world, and in Canada, they are a critical part of oil and natural gas infrastructure. Pipelines are usually buried underground for protection against third party damage, natural hazards, temperature variations and coating damages. Some natural hazards that pose safety concerns to buried pipelines are landslides, soil settlement, soil heave, faults, and soil creep. Pipeline companies try to avoid constructing pipelines in areas prone to natural hazards, however, this is not always possible. For example, more than ten at-risk landslide locations in Manitoba Hydro Pipeline Network were identified during a research project (Ferreira, 2016). To be able to safely design pipelines within ground movements, the landslide mechanics and soil-pipe interactions should be understood. Much has been done by researchers on this issue but due to the complexity of the problem, soil-spring models introduced in ASCE (1984), ALA (2001) and PRCI (2017) guidelines are still in use for design purposes.

This study aims to find the optimum burial depth to minimize the combined effects of temperature variation and ground movements. The following assumptions are made for the analysis:

1. The ground displacement is parallel to the pipe's longitudinal axis.
2. The ground displacement is slow enough so that the pore water pressure can dissipate through the soil-pipe interface.
3. The pipe is made of steel.
4. Winnipeg weather data is used for the thermal analysis so the results are only applicable to similar weather conditions.

5. The landslide location is far from the compressor stations so that the weather conditions dictate the ground temperature profile.

A thermal analysis is carried out with COMSOL Multiphysics considering the phase change effects. The Winnipeg weather data is used for the boundary conditions. The thermal analysis is verified comparing with data of temperature gauges attached to a natural gas pipeline of Manitoba Hydro. The soil-pipeline interaction introduced in ASCE (1984) is used to consider the loading due to ground movements. The combined stress due to the thermal and soil loading is calculated as a function of depth, and the optimum depth is presented in a curve. The curve is used to find the optimal burial depth of pipeline for two of Manitoba Hydro's at-risk landslide sites. The combined stress on the pipeline is solved numerically using Abaqus for different burial depths for comparison.

4.3 Thermal analysis

A thermal analysis considering the phase change effects is done by COMSOL Multiphysics to estimate the temperate profiles of the ground. The governing equation by considering the phase change effects in a soil can be described as:

$$\rho^{ph} C_p^{ph} \frac{\partial T}{\partial t} = \nabla \cdot (k^{ph} \nabla T) + Q + L_f \rho_i \frac{\partial \theta_i}{\partial t} \tag{4.1}$$

where ρ^{ph} (g/m^3) is the soil density considering the phase change, C_p^{ph}(J/kgK) is the specific heat capacity considering the phase change; T (K) is the temperature of the soil; t (second) is the time; k^{ph} is the thermal conductivity(W/mK); Q (W/m^3) is the heat source ; L_f is the latent heat usually taken as 333 kJ/kg; ρ_i (kg/m^3) is the density of ice; θ_i is the volumetric ice content of a soil.

Eq. 4.1 can be rearranged into:

$$(\rho^{ph} C_p^{ph} - L_f \rho_i \frac{\partial \theta_i}{\partial T}) \frac{\partial T}{\partial t} = \nabla \cdot (k^{ph} \nabla T) + Q \tag{4.2}$$

The density of the soil (ρ^{ph}) considering the phase change can be calculated by Eq. 4.3:

$$\rho^{ph} = \rho_w \theta_w + \rho_i \theta_i + \rho_s (1 - \theta_s) \tag{4.3}$$

where ρ_w (kg/m^3) is the density of water; θ_w is the unfrozen volumetric water content; ρ_s (kg/m^3) is the density of soil skeleton; θ_s is the saturated volumetric water content.

The specific heat capacity of the soil (C_p^{ph}) is defined by Eq. 4.4:

$$C_p^{ph} = \theta_w C_{pw} + \theta_i C_{pi} + (1 - \theta_s) C_{ps} \tag{4.4}$$

where C_{pw} (J/kgK) is the specific heat capacity of water; C_{pi}(J/kgK) is the specific heat capacity of ice; C_{ps}(J/kgK) is the specific heat capacity of the soil skeleton.

The apparent heat capacity of the soil (C_{pp}^{ph}) can be defined by Eq. 4.5:

$$C_{pp}^{ph} = \frac{\rho_w \theta_w C_{pw} + \rho_i \theta_i C_{pi} + \rho_s (1 - \theta_s) C_{ps} - L_f \rho_i \frac{\partial \theta_i}{\partial t}}{\rho^{ph}} \tag{4.5}$$

The thermal conductivity (k^{ph}) can be calculated by Eq. 4.6:

$$k^{ph} = \theta_w k_w + \theta_i k_i + (1 - \theta_s) k_s \tag{4.6}$$

where k_w (W/mK) is the thermal conductivity of water; k_i (W/mK) is the thermal conductivity of ice; k_s (W/mK) is the thermal conductivity of the soil skeleton.

The unfrozen volumetric water content, θ_w, plays an important role in the thermal analysis considering the phase change. θ_w can be calculated using Eq. 4.7 (Michalowski, 1993):

$$\theta_w = \theta_r + (\theta_{wo} - \theta_r)e^{a(T-T_0)} \tag{4.7}$$

where θ_r is the residual volumetric water content; θ_{wo} is initial volumetric water content; a is a curve fitting parameter taken as 0.16; T_0 (K) is the freezing temperature which depends on the degree of saturation of the soil.

We note that T_0 can be taken as 0 °C for the saturated soil. For the unsaturated soil, the existing metric suction lowers the freezing point. In this analysis, it is assumed that the soil is initially saturated with water ($\theta_{w0} = \theta_s$= 0.5). At the ground surface, a forced convection is considered as the boundary condition. The convection term q_{conv} is temperature- and time-dependent. In this analysis, the surface convection heat flux is calculated using Eq. 4.8.

$$q_{conv}(t) = h_{conv}\ (T_a(t) - T_s(t)) \tag{4.8}$$

where T_a is the ambient air temperature and T_s is the temperature on the ground surface.

The convection heat transfer mode is comprised of two mechanisms: diffusion and advection (Incropera et al., 2007). The convection heat transfer coefficient, h_{conv}, mainly depends on ground surface conditions such as wind speed and ambient temperature (Incropera et al., 2007). The convective heat transfer coefficient for the ground surface can be calculated by the following formula (Welty et al., 2014):

$$h_{conv} = 2\frac{k_{air}}{\bar{L}}\frac{0.3387Pr^{1/3}Re_L^{1/2}}{(1+(\frac{0.0468}{Pr})^{2/3})^{1/4}}\ \ if\ Re_L \leq 5\cdot 10^5 \tag{4.9}$$

$$h_{conv} = 2\frac{k_{air}}{\bar{L}} Pr^{1/3}(0.037 Re_L^{4/5} - 871) \;\; if \; Re_L > 5 \cdot 10^5 \tag{4.10}$$

where k_{air} (W/mK) is the thermal conductivity of air; $\bar{L}$ (m) is the characteristic length of the ground affected by the wind in the wind's direction. Pr stands for Prandtl number of air, defined as the ratio of thermal diffusivity to viscosity and is taken as 0.7; Re_L is Reynolds number which can be calculated by Eq. 4.11:

$$Re_L = \frac{V\ \bar{L}}{\nu_{air}} \tag{4.11}$$

where V (m/s) is the wind speed at the ground surface and ν_{air} (m^2/s) is the kinematic viscosity of air.

Thermal properties for the heat transfer analysis is provided in Table 4.1.

TABLE 4.1: Thermal properties for thermal analysis

Material	C (J/kgK)	k (W/mK)	ρ (g/c^3m)
Water	4188	0.6	1
Ice	2117	2.2	0.92
Soil Skeleton	868	2.6	2.65
Air	-	0.6	-

The verification of the numerical simulation is done by comparing the results to the temperature gauge data from a study at a Manitoba Hydro's pipeline site close to the city of St. Lazare, Manitoba that was carried out by Ferreira (2016). The pipeline in St. Lazare is a natural gas line made of steel with the diameter of 0.1683 m. The temperature gauge was attached to the pipe and was at the depth of 0.9 m. The temperature gauge was

installed in Sep. 20th, 2011 and was monitored hourly until Aug. 24th, 2016. The weather data of Brandon, MB for the same time period is used for the boundary conditions. The comparison is presented in Fig. 4.1. Accordingly, the ground temperature at the location of the temperature gauge is predicted fairly well with the thermal analysis. This verification shows that the assumption we made earlier that the ground temperature is mainly affected by the weather conditions is valid for the pipeline located in St. Lazare research site.

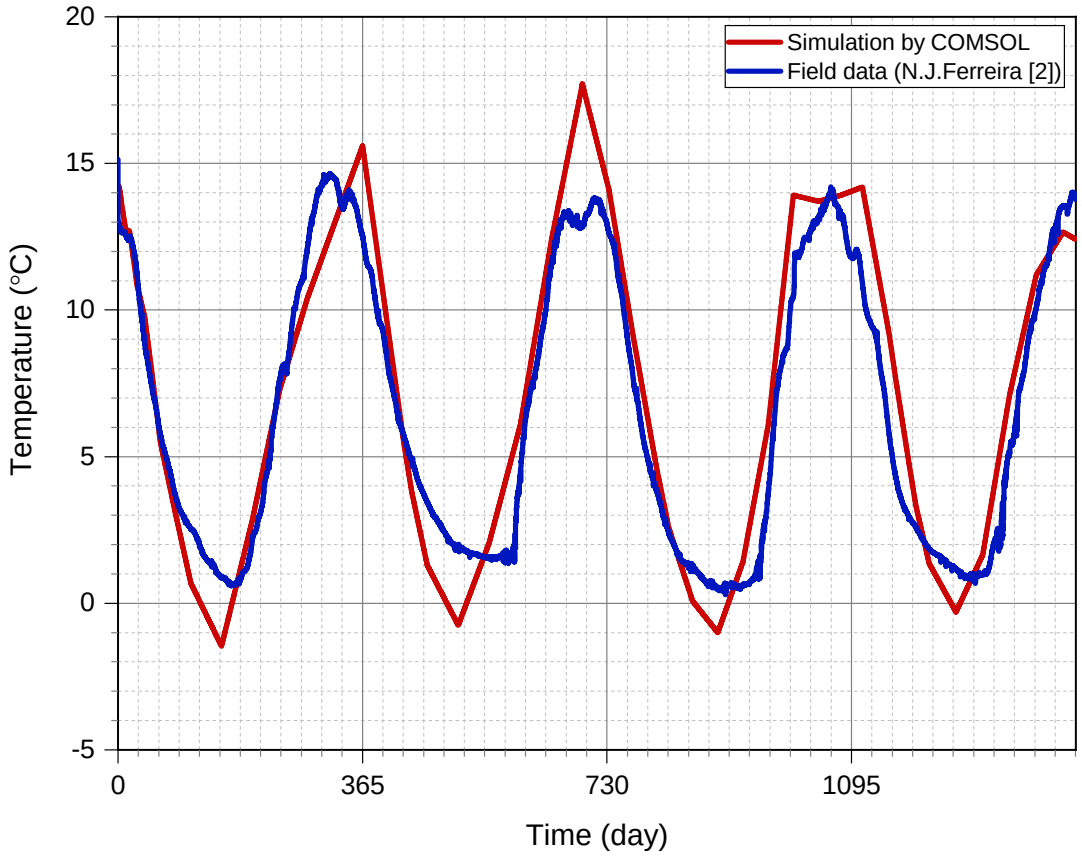

FIGURE 4.1: Comparing the numerical simulation to the field data

The temperature profiles of the ground in Winter and Summer for a typical year is shown in Fig. 4.2 based on Winnipeg weather data. The temperature variation is then used to calculate the thermal expansion in the pipeline. In buried pipelines, it is assumed that the

pipe is long enough so that the soil-pipeline interaction fully restrain the pipe. As a result, the thermal stress imposed on the pipeline due to thermal expansion can be calculated by Eq. 4.12:

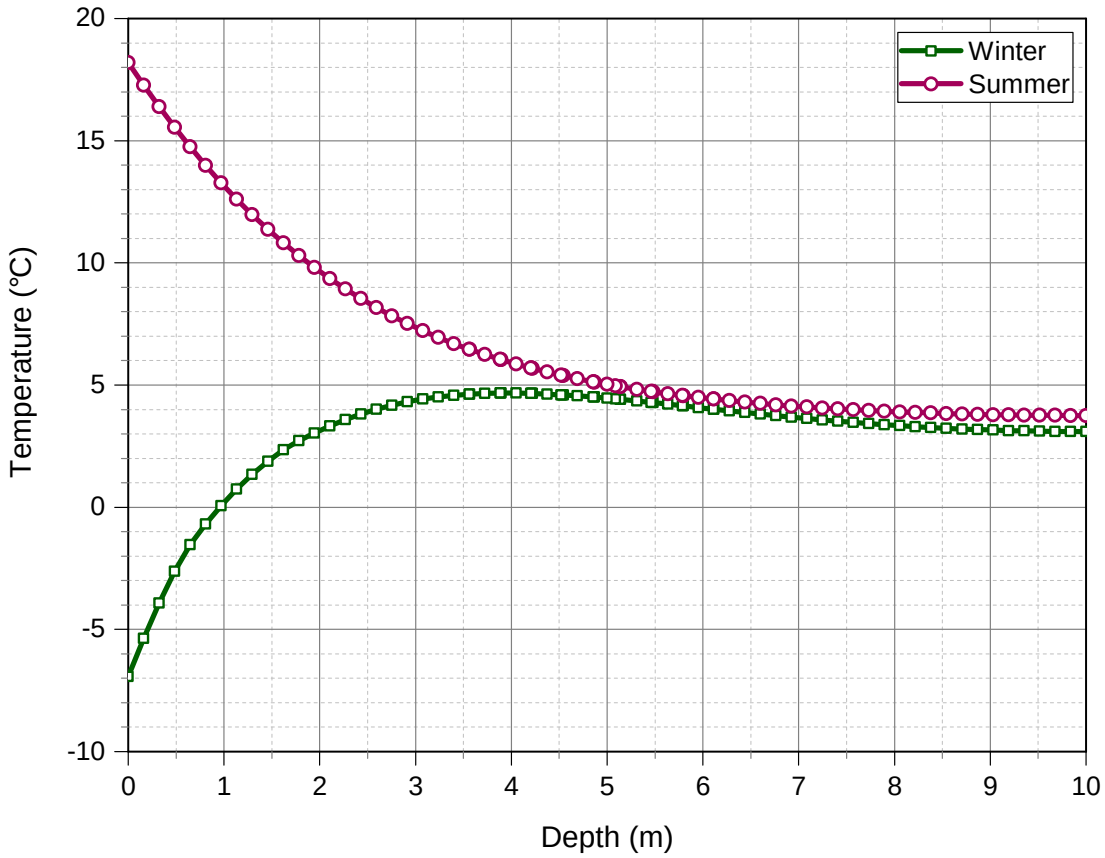

FIGURE 4.2: Temperature profile in the ground

$$\sigma_T = E\alpha\Delta T \tag{4.12}$$

where E is the Young's modulus of the pipe and α is the thermal expansion coefficient.

In this analysis, the Young's modulus and thermal expansion coefficient of the pipe material is assumed to be 207 GPa and 12×10^{-6}. The thermal stress induced in the pipeline

is presented in Fig. 4.3 and is estimated by a third degree polynomial function of depth as shown in Eq. 4.13.

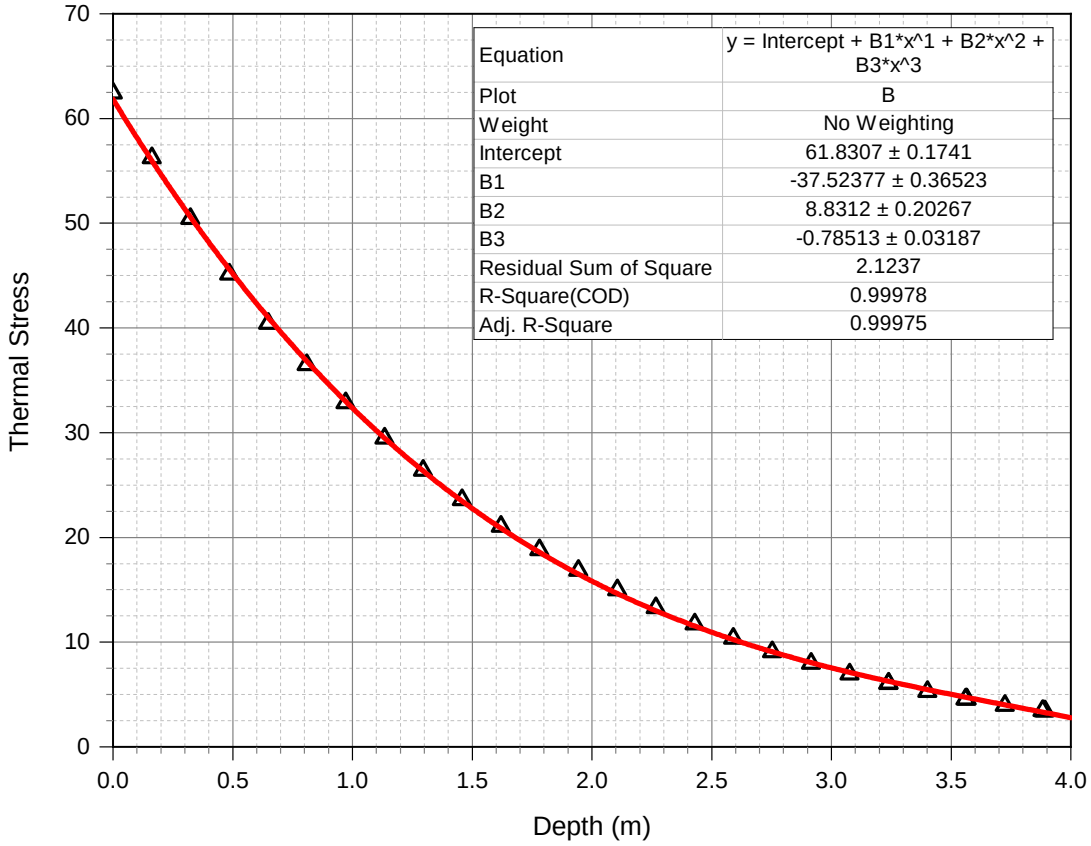

FIGURE 4.3: Maximum thermal stress induced in a pipeline

$$\sigma_T = -0.78513H^3 + 8.8312H^2 - 37.52377H + 61.8307 \tag{4.13}$$

4.3.1 Longitudinal soil displacement

The soil displacement in case of soil creep is assumed to be slow enough so that the excess pore water pressure dissipates through the soil-pipe interface. As a result, the drianed

soil-spring model, presented in Eq. 4.14, is used to estimate the interaction loading on the pipeline due to soil creep movements as introduced by ASCE (1984):

$$\begin{aligned} t_u &= \pi D \gamma' H (\frac{1+k_0}{2}) tan(\phi'_\mu) \\ x_u &= 2.5 \sim 5mm \end{aligned} \tag{4.14}$$

where t_u is the axial force applied per unit length of pipeline, D is the pipe diameter, γ' is the unit weight of soil, H is the burial depth, k_0 is the earth pressure coefficient at rest, ϕ'_μ is the effective soil friction angle of the interface, and x_u is the ultimate relative displacement.

Assuming that the soil-pipeline interaction is constant over the pipeline length, the stress induced in the pipeline can be written as Eq. 4.15:

$$\sigma_X = \frac{F}{A} = \frac{t_u \times L}{2\pi D t} = \gamma' L (\frac{1+k_0}{4t}) tan(\phi'_\mu) \times H \tag{4.15}$$

T, γ', L, k_0, t, and ϕ'_μ can be considered constant for a specific site so σ_X can be written as a function of burial depth by Eq. 4.16:

$$\begin{aligned} \sigma_X &= f \times H \\ f &= \gamma' L (\frac{1+k_0}{4t}) tan(\phi'_\mu) \end{aligned} \tag{4.16}$$

4.3.2 Summation of longitudinal stress in restrained pipe

The net longitudinal stress in restrained pipeline can be calculated by Eq. 4.17 according to clause 833.3 of ASME B31.8 (2003).

$$\sigma_L = \sigma_P + \sigma_T + \sigma_B + \sigma_X \tag{4.17}$$

where σ_P is axial loading due to internal pressure; σ_T is the thermal stress; σ_B is the bending stress; σ_X is the stress due to ground displacement.

The bending stress is not considered for this analysis due to the fact that the soil displacement is assumed parallel to the pipeline axis. We note that the earth pressure on the pipeline is insignificant compared to the internal pressure of the pipe and is neglected for design purposes according to ALA (2001). The derivative of the combined stress relative to H is set to zero as shown in Eq. 4.18 to find the optimal depth. It should be noted that since the hoop stress is not a function of depth, its derivative relative to depth is zero.

$$\frac{\partial \sigma_L}{\partial H} = -2.35539H^2 + 17.6624H - 37.52377 + f = 0 \tag{4.18}$$

The plot of Eq. 4.18 as shown in Fig. 4.4 can be used to find the optimal burial depth of a pipeline based on the extent of a landslide and interface properties. In the next section, Fig.4.4 is used to estimate the optimum burial depth in two pipeline locations of Manitoba Hydro prone to slow downslope movement of soil.

4.4 Examples

The optimum burial depth of the pipeline for two sites in Manitoba Hydro's pipeline network is estimated using the presented framework in Section **??**. The adequacy of the the presented framework is checked against an independent numerical analysis, presented in Section **??**. The first example is a pipeline 1 km south of the city of St. Lazare, MB and the second example

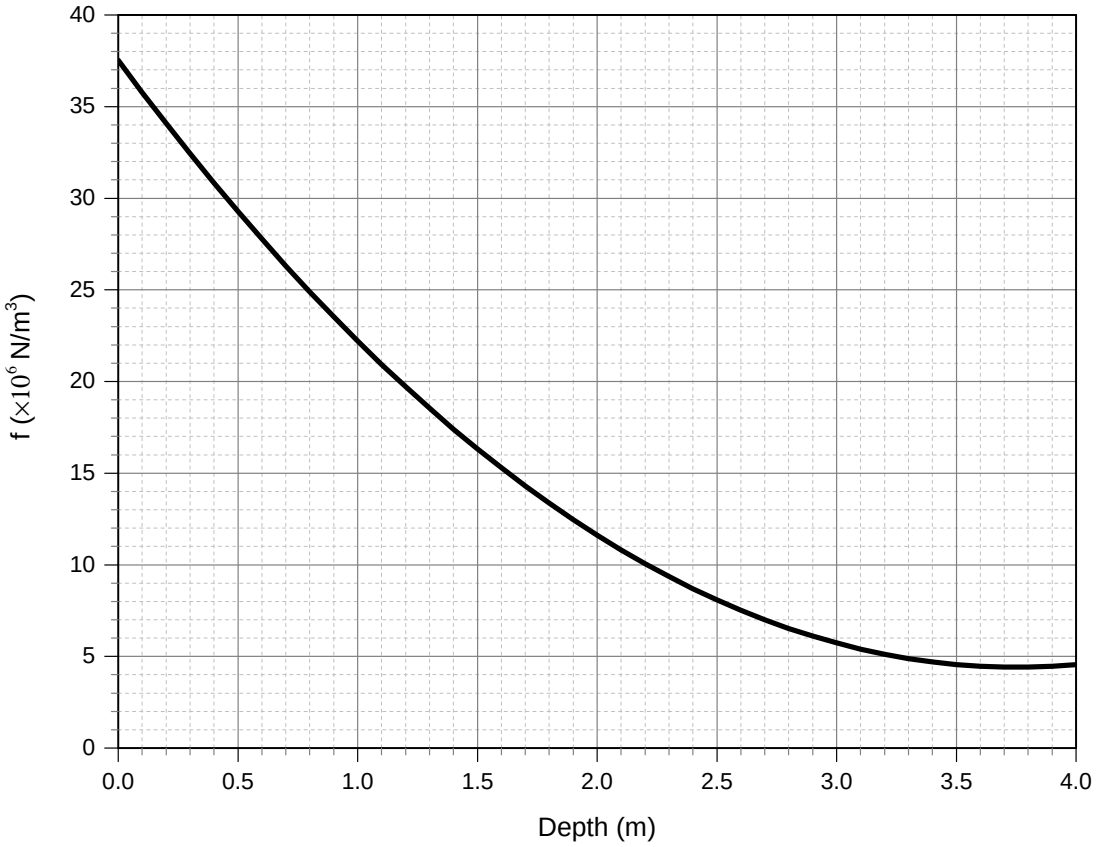

FIGURE 4.4: The curve of the optimal depth based on f values

is a pipeline about 10 km south of Morris, MB at Plum River crossing. The displacement of ground at St. Lazare site is estimated to be 40 mm per year by monitoring the movements of pins (12.5 mm rebar) with RTK GPS survey equipment according to the instrumentation program carried out from 2011 to 2016 by Ferreira (2016). The length of the slope at St. Lazare research site is 300 m. At the Plum River research site, the slope on the south of the river is 32 m long and it is 30 m long on the north of the river. The width of Plum River is 18 m. The pipeline at both research sites are buried at the depth of 0.9 m. However, along the slope and at river crossings, the burial depth varies from 0.75 m to 4 m at St. Lazare research site and from 0.7 m to 2.5 m at Plum River research site.

4.4.1 Burial depth estimation using the presented framework

According to Eq. 4.4, Table 4.2 and Table 4.3, the value of f is estimated to be $73 \times 10^6\,\mathrm{N/m^3}$ for St. Lazare research site and $16.5 \times 10^6\,\mathrm{N/m^3}$ for Plum River research site. Using Fig. 4.4, the interaction loading dominates the problem if f is greater than $37.5 \times 10^6\,\mathrm{N/m^3}$ so the minimum burial depth, which is 0.6 m according to CSA-Z662-15, should be used at St. Lazare research site. Similarly, the optimal burial depth at Plum River is estimated to be 1.5 m.

4.4.2 Burial depth estimation using the finite element modelling

In this section, a numerical analysis is performed using Abaqus to calcualate the induced stress in the pipeline due to the temperature variation and ground displacement for different burial depths. The soil-pipeline interaction is modeled by PSI (Pipe Soil Interaction) elements as elastoplastic springs. PSI elements have only displacement degree of freedom and can reflect the ground displacement effects on the pipeline through their stiffness. The stiffness of the PSI elements is defined according to ASCE (1984). It is assumed that the ground displacement is parallel to the pipe's longitudinal axis. The soil heave at the bottom of the valley, and soil settlement at the top of the valley is not modeled in the analysis. The pipeline is modeled by Timoshenko beam elements for a length of 2000 meters. The pipeline and soil parameters for the numerical simulations are presented in Table 4.2 and 4.3, respectively. The results for St. Lazare and Plum River research sites are presented in Fig. 4.5 and 4.6, respectively. The horizontal axis, X, is parallel to the pipeline axis that is crossing the valley from $X = 700$ m to $X = 1000$ m in St. Lazare research site and $X = 968$ m to $X = 1030$ m in Plum River research site. The width of the Plum River is 18 m that is from $X = 995$ m to $X = 1010$ m along the pipeline's right-of-way. The interceptions of the curves with the vertical axis show the thermal stress in the pipeline which is constant over the pipeline length. The thermal stress increases from 5 MPa to 48 MPa by decreasing the burial depth

from 4 m to 0.5 m as shown in Fig. 4.5. According to this figure, the minimum burial depth is the best option in St. Lazare even though the thermal stress is the highest. In Plum River research site, increasing the burial depth from H=0.5 m to H=1.5 m decreases the combined stress while increasing the burial depth from H=1.5 m to H=4 m increases the combined stress. According to Fig. 4.6, the optimum burial depth is H=1.5 m for Plum River that was estimate in Section **??**.

TABLE 4.2: pipeline properties used for the numerical simulation

Research sites	D (mm)	t (mm)	ν	α_L	E (GPa)	σ_y (MPa)
St. Lazare	168.3	4.78	0.3	12×10^{-6}	207	345
Plum River	88.9	3.17	0.3	12×10^{-6}	207	241

TABLE 4.3: soil properties used for the numerical simulation

Research sites	γ (kPa)	K_0	ϕ'	μ	E_a(m)
St. Lazare	17	0.8	15	0.6	0.005
Plum River	17	0.8	10	0.7	0.005

4.5 Conclusion

A heat transfer analysis is performed considering the phase change effects using COMSOL Multiphysics. The temperature varitation as a function of depth is estimated and coupled with the analytical solution of interaction loading from the ground displacement. The result is provided in a practical curve for an estimation of the optimum burial depth to be used for design purposes. The adequacy of the curve is examined with two real case examples of pipelines prone to soil creep that are solved numerically with Abaqus. According to the curve of Fig. 4.4, when the value of f is more than 37×10^6 N/m^3, the minimum soil cover for the pipeline should be considered because the interaction loading on the pipeline due to the ground displacement is more severe compared to the thermal stress imposed on the pipeline due to the seasonal temperature variation. On the other hand, as can be seen from the curve

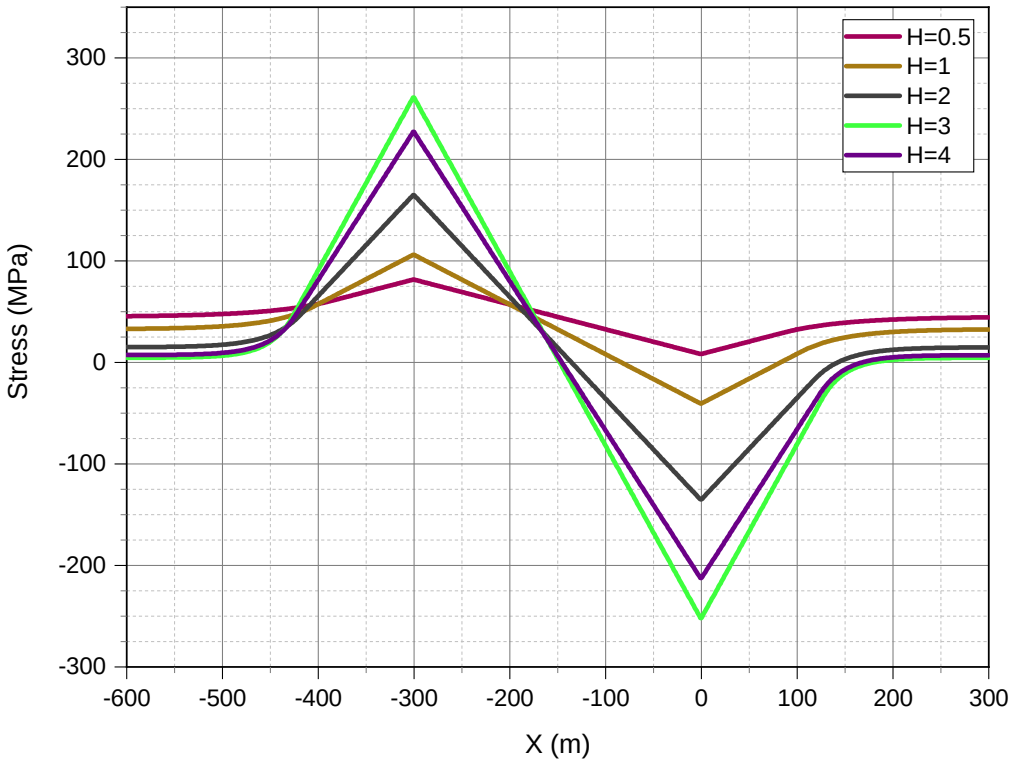

FIGURE 4.5: Numerical analysis of pipeline in St. Lazare research site

of Fig. 4.4, when the value of f is as low as $5 \times 10^6\,\mathrm{N/m^3}$, the optimum burial depth rises to 3.2 m to minimize the thermal stress on the pipeline; for this case, the interaction force is negligible compared to the thermal stress. Obviously, this curve is not a design curve but only a tool to show at what depth the combined thermal and longitudinal stress is minimum to facilitate the design process by engineers.

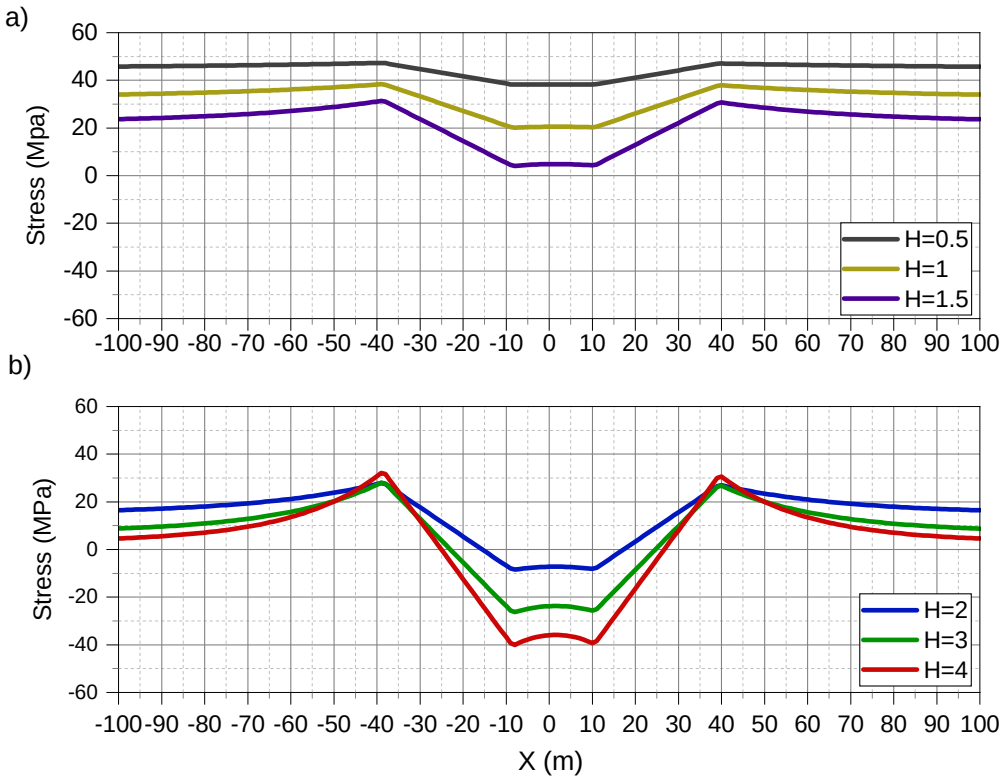

FIGURE 4.6: Numerical analysis of pipeline in Plum River research site

Chapter 5

Summary, conclusion and recommendations for future work

The main objective of this thesis was to characterize the (horizontal) soil springs in sloping ground for inclusion in pipeline guidelines such as PRCI (2017) and ALA (2001). This research project comprised of two other projects, in which the pipe behaviour was examined in landslides. A summary of each project with its major contributions are presented in the order of importance as follows.

5.1 Lateral force-displacement response of buried pipes in slopes

A preliminary numerical analysis elucidated that the horizontal soil springs offered by current guidelines such as ALA (2001) and PRCI (2017) significantly underestimate the pipe loading in landslides. The reason lies in the fact that the current guidelines were developed mostly based upon laboratory works in which the pipes were installed below the level ground. The assumption of level ground conditions is not always valid in real-life projects,

and the effects of ground inclination on pipeline performance are not well established in the literature. To understand soil-pipe interaction in slopes, a series of full-scale experiments were conducted at a large-scale testing facility at the University of British Columbia, Vancouver, Canada. The normalized force-displacement response of soil-pipe interaction was presented and compared to that in level ground. It was realized that the pipe loading could be increased 100% as the slope grade is changed from 0 to 40%. The experimental data showed that the pipe loading could be reduced 50% when the slope grade is changed from 0 to -40%. This is an important observation and a clear indication of the significant effects of ground inclination on soil-pipe interaction. It is important to note that the soil springs inside and outside the landslide boundaries are not distinguished in the current pipeline guidelines as the ground surface is symmetric relative to the pipe in level ground. The ground surface is asymmetrical relative to the pipe in sloping ground and so the soil-pipe interaction should be defined separately inside and outside the landslide boundaries. This distinctive definition of soil springs was presented based upon two sets of experiments: 1) pulling the pipe horizontally toward the toe of slopes to characterize the soil springs outside the landslide boundaries, and 2) pulling the pipe horizontally toward the crest of slopes to characterize the soil springs inside the landslide boundaries. A numerical model was calibrated against the experiential results, and was implemented in an extensive parametric study to extend the research to deep burial depth conditions for loose, medium and dense sands. The results of this study, including those from ten experiments and 110 numerical simulations, were presented in normalized graphs, which can be included in pipeline guidelines as a benchmark for the pipeline design.

5.2 Numerical analysis of pipeline response to slow landslides: case study

The behaviour of existing Manitoba Hydro pipelines subjected to slow landslides was examined with a beam-type finite element modelling using soil springs. The project was significant in the sense that four years of continuous hourly instrumentation data was available. This data includes the pipe-wall strain measured by 23 strain gauges, the ground displacement measured with RTK surveying equipment and seven inclinometers, groundwater conditions measured by ten VW piezometers and ground temperature measured by six temperature gauges. The effects of changing seasons and temperature variation on the pipe behaviour were studied using this instrumentation data. As explained in chapter 3, the pipe behaviour subjected to slow landladies was estimated by finite element modellings. The soil-pipe interaction was modelled using soil springs. The measured ground displacements were imposed on the pipe as the boundary conditions of soil springs. The results of the numerical simulations were compared to the field measurements. This comparison showed that the strain gauges did not capture the strain due to the ground displacement. By conducting thermal analysis on the pipe (presented in chapter 4), it was known that the pipe stress in the field was only representing the induced thermal stress due to the temperature variation. It was concluded that because the strain gauges were installed on the pipes after many years of operation, no landslide-related strain was captured by the strain gauges. In other words, the pipes had been deformed by the landslides before the installation of the strain gauges, and the continuation of the landslides did not result in pipe deformation. The numerical study suggested similar results; in fact, the soil-pipe interaction has an elastic perfectly plastic behaviour meaning that the pipe loading does not increase after the maximum capacity of the interface is reached. If the pipe can withstand the soil loading with its elastic capacity, the continuation of ground displacements does not result in the accumulation of strain in

the pipe wall. This phenomenon was numerically investigated by subjecting the pipes to various ground displacement profiles. During the instrumentation program, a pipe section was cut in one of the sites to measure the strain release and estimate the initial state of the pipe. The strain gauges captured no strain release while the personnel reported sudden pipe displacement after the cut. According to the thermal study, the sudden pipe movement was not related to the locked-in thermal strain. Therefore, it was a clear indication of the locked-in landslide-related strain on the pipe wall. By investigating the problem with the numerical simulations, it became evident that the strain gauges were far away from the cutting point such that the strain was dissipated in the soil-pipe interaction. This happens because the pipe is anchored in the soil, and reverse soil-pipe interaction is activated when the pipe loading is lifted. This reverse soil-pipe interaction absorbs the released energy along a specific length of the pipe depending on the strength parameters of the interface. As such, it was concluded that cutting the pipe and measuring the strain release is not a reliable method in determining the initial state of buried pipes subjected to ground displacements.

5.3 Effects of ground displacement and thermal loading on selecting pipe depth of cover in river crossings

A thermal analysis was conducted in COMSOL Multiphysics considering the phase change in the soil to determine the thermal loading on the pipe. This information was used to develop a simple graph for choosing the pipe burial depth in sloping ground such that the combined loading from the ground displacement and seasonal temperature variation is minimized. The thermal analysis was calibrated with the temperature measurements collected during the four years of instrumentation. As the thermal analysis was conducted with Winnipeg weather data, the presented graph can only be used in similar atmospheric conditions. The presented method is used to estimate the optimum pipe burial depth in

two case studies. These estimated pipe burial depths were used in a numerical simulation conducted in Abaqus/standard considering the temperature variations and ground displacements. The results were compared to deeper and shallower depth of covers to check the adequacy of the model in the prediction of an optimum soil cover. According to the numerical simulations, the pipe with the suggested optimum depth of cover, experienced minimum stress among all cases.

5.4 Recommendations for future work

- The soil springs offered by pipeline guidelines are mainly based upon experimental work in which the pipes were pulled in specific directions, and the force-displacement responses were measured. In real-life problems, a pipe can undergo complex loadings depending on the alignment of the pipe relative to the landslide. It is interesting to install strain gauges on a pipe subjected to such complex loadings and compare the results of the instrumentation with numerical estimation using independent soil springs. This would help to identify different factors that can affect the pipe behaviour in landslides and design experimental work to investigate and characterize such factors.

- The design graphs presented for the estimation of the lateral bearing capacity factor presented in chapter 2 are based upon an experimental-numerical study that requires further validation against real-life problems. It seems worthwhile to use the presented framework to estimate pipe behaviour in case-studies and compare the results of simulations to those of instrumentations.

- The slope grade effects on horizontal soil springs were examined for dry loose, medium and dense sands in this research program. The effects of slope grade on soil springs can be studied for different backfill materials.

- The effects of slope grade on horizontal soil springs are examined and characterized in this research. The effects of slope grade on axial, uplift or bearing soil-pipe interaction can be investigated. This would enable the practitioners to estimate the pipe behaviour subject to landslides with more complex loading conditions.

- The soil-pipe interaction in oblique directions such as horizontal-uplift, horizontal-axial and uplift-axial is addressed in the literature for level ground conditions. For sloping ground conditions, however, there is a lack of knowledge on how soil springs interact, and this is an emerging research opportunity.

- The sloping ground was characterized for the pipe diameter of 324 mm. The study can be extended to various pipe diameters in order to characterize the effects of pipe size on soil-pipe interaction in sloping ground.

- The pipe used in these experiments was rigid. The behaviour of flexible pipes installed in slopes can be investigated.

Appendix A

Additional information on the testing equipment

A.1 Testing chamber

The soil chamber is a steel-framed structure that is made up of fourteen W150×37 H-section welded to C250×30 channel base plates and reinforced with welded HSS 89×89×3.8 tubular braces. The base plates are bolted to the self-sustained steel foundation. The walls of the soil box are made up of 1.2 m × 2.4 m × 0.019 m treated plywood bolted to the steel columns. The 10 cm × 15 cm crossbeam timbers with an approximate length of 1.3 m are placed at a centre-to-centre distance of 300 mm to stiffen the walls and limit their deflection. The chamber's length can be extended to 5 m, if required, by adding another set of H-section columns on the north of the box.

A.2 Loading system

The loading of pipes embedded in soil was carried out using two double-acting hydraulic actuators with individual capacity and maximum working pressure of 418 kN and 21 MPa, respectively. The hydraulic actuators are manufactured by Royal Westcoast Cylinders Inc., New Westmister, BC, Canada. The full stroke of a given actuator is 610 mm, and the actuators are trunnion-mounted on loading pedestals, which are bolted in the self-sustained steel foundation. The actuator system is equipped with an LVDT—Temposonic Series E-model manufactured by MTS Systems Corp., Cary, NC, USA. This is a linear-position sensor with non-contact sensing technology and a resolution of 2 microns that provides linear measurement with repeatability of 0.001%.

A.3 Control system

RMC100-S2-ENET motion controller produced by Delta Computer Systems Inc., Vancouver, WA, USA, is used to control the actuators. It is a position and velocity controller with an ethernet connection type and asynchronous serial interface (SSI). The SSI transfers synchronized data between the controller and actuators. The controller is programmed with RMCWin, a Microsoft Windows-based software produced by Delta Computer Systems Inc.

A.4 Data acquisition system

A 16-channel signal conditioner-model SCXI-1001—manufactured by National Instruments, Austin, TX, USA, is used to collect the data from the transducers. A commercially available data acquisition software, DasyLab, produced by MCC Corporation (Norton, MA, USA), is used to record data at a rate of 4 Hz.

A.5 Instrumentation equipment

High capacity force transducers (MTS Model 661.22—manufactured by MTS Systems Corp., Cary, NC, USA) is used to measure the force. The load cells have a capacity of 250 kN and are threaded into the hydraulic cylinder. String potentiometers, Series SP2-50 (manufactured by Digi-Key Electronics, Thief River Falls, Minnesota, USA), are used to measure the pipe movements in a straight line.

A.6 Photography equipment

The soil deformation was captured using a camera in a continuous shooting mode. The camera was able to shoot with a maximum rate of 3.7 frames per second (fps). However, this maximum shooting rate was limited to the ability of the camera to store the captured images. An internal memory, called a buffer, enables a camera to fire with the maximum burst rate while the images are written to the external memory card. The size of the buffer and photo, rate of clearing the buffer, and writing speed of the memory card should be considered in order to maintain the maximum firing rate during the test.

Appendix B

Soil failure mechanism in physical tests and numerical modellings

Photos from the tests at the peak displacement are presented herein for an overview of the deformation pattern during the experiments. The soil deformation pattern is evident through the distortion of the horizontal white silica sand in the pictures. The contours of plastic strain from the numerical modelling are presented below each photograph for comparison. Accordingly, there is a good agreement between the deformation patterns in the physical tests and numerical simulations. Tests with negative slopes (tests 6 and 7; Fig. B.6, B.7) show larger failure zones while tests with positive slopes (tests 1, 2, 4, 5, 8, 9; Fig. B.1, B.2, B.4, B.5, B.8, B.9) show smaller failure zones. According to the results and the photographs, the extent of the deformation zone is reduced by changing the slope from negative to positive. The pipe load, on the other hand, is increased as the slope is changed from negative to positive. This is because in positive slopes, the weight of the soil is a resistant force while in negative slopes, the weight of the soil is a driving force. Therefore, in negative slopes, a fraction of the loading from the pipe can move a larger volume of the soil. In positive slopes, higher loads are required to move a smaller volume of the soil. This is one

of the fundamental findings of this research that can be implemented in design of pipelines in the sloping ground as it is carefully characterized in Fig. 2.15, 2.16, 2.17.

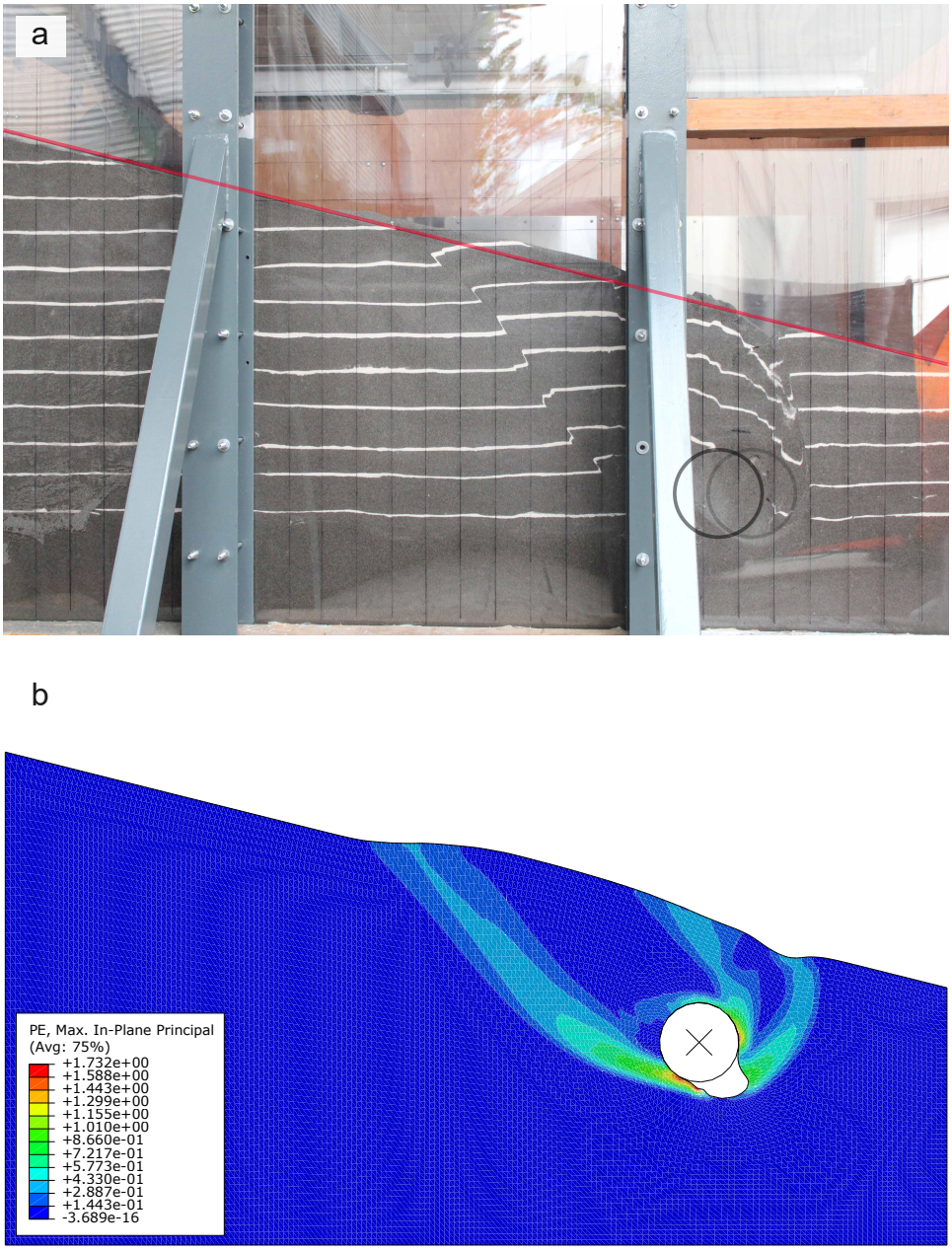

FIGURE B.1: Soil deformation in test 1 with slope grade of 25% and burial depth ratio of 1.6 a) experiment b) simulation

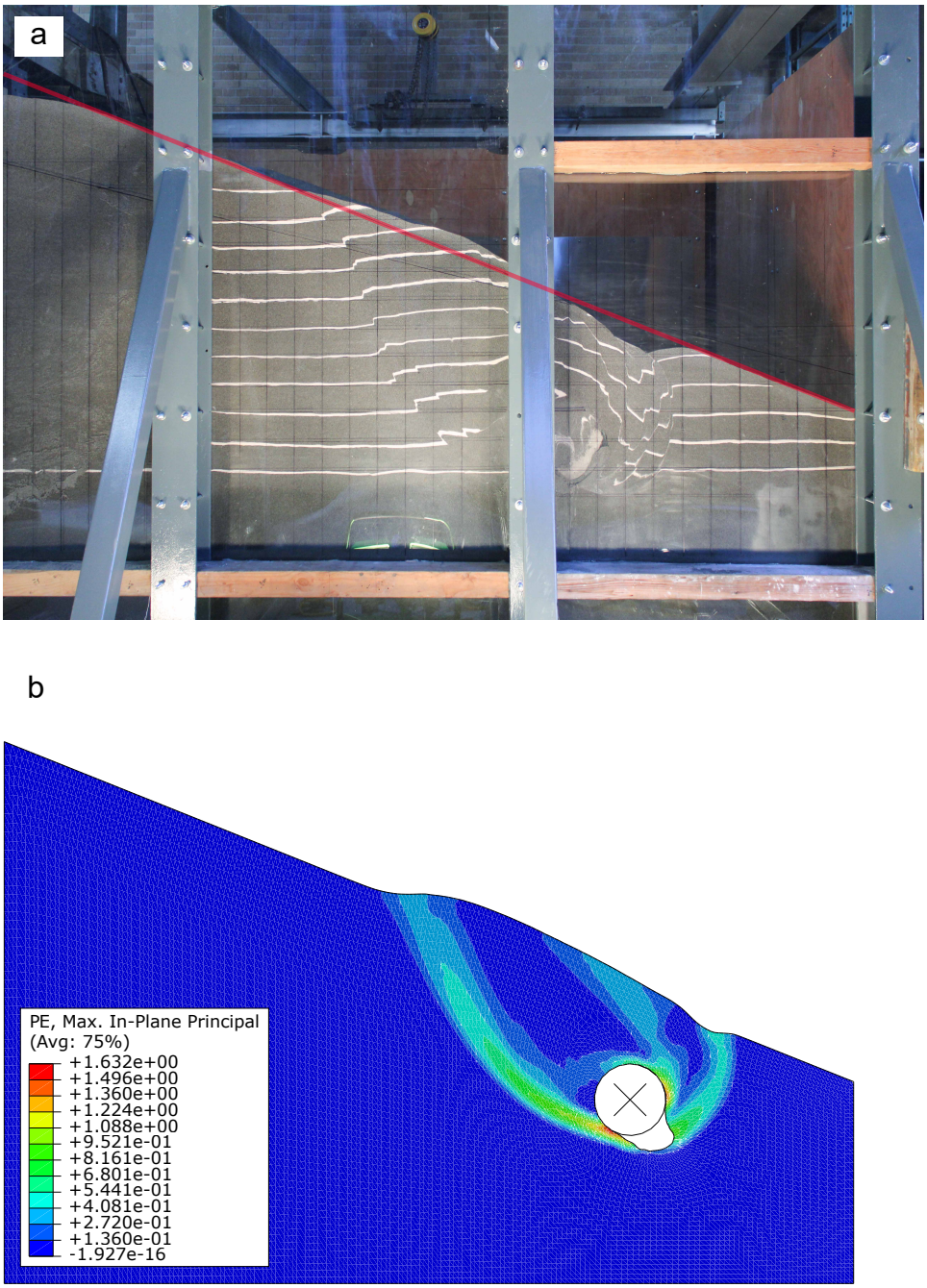

FIGURE B.2: Soil deformation in test 2 with slope grade of 40% and burial depth ratio of 1.6 a) experiment b) simulation

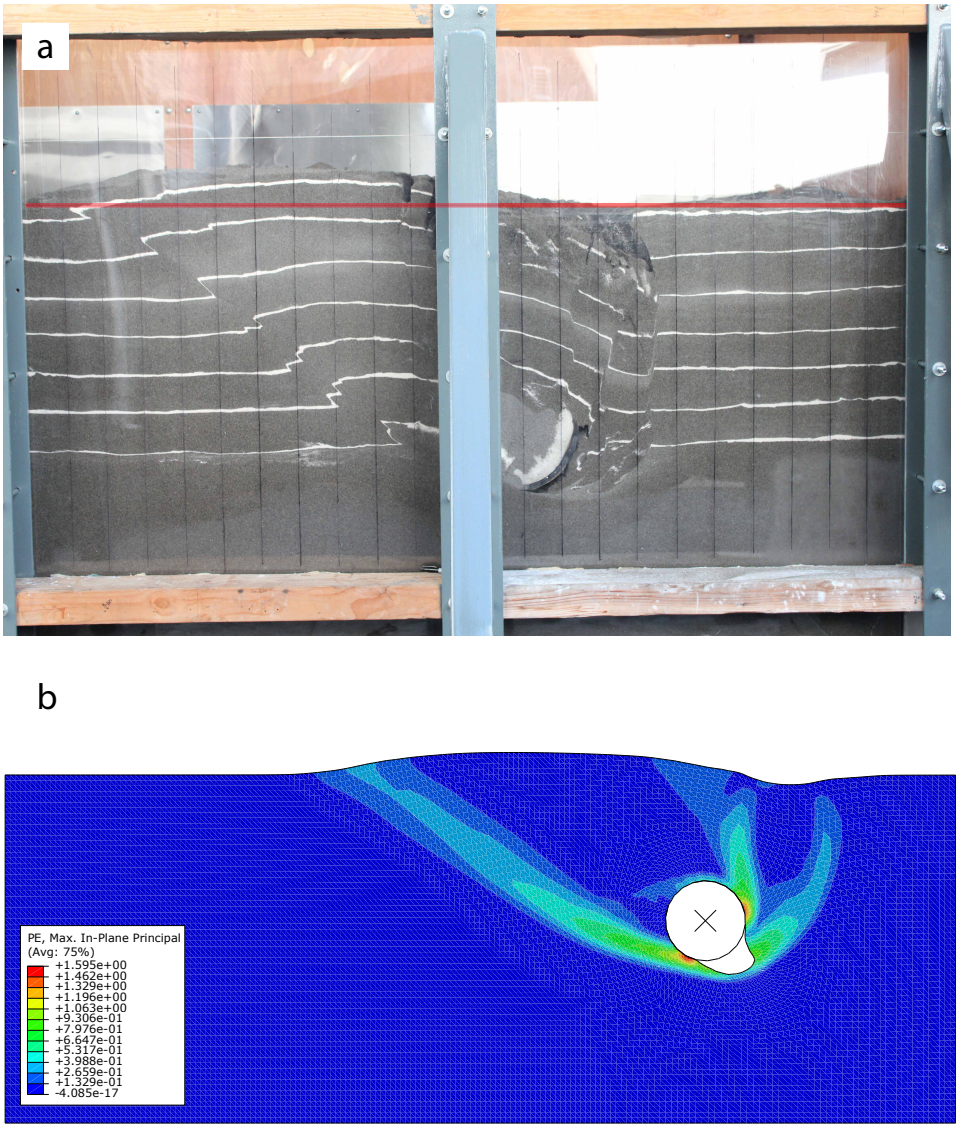

FIGURE B.3: Soil deformation in test 3 with slope grade of 0% and burial depth ratio of 2 a) experiment b) simulation

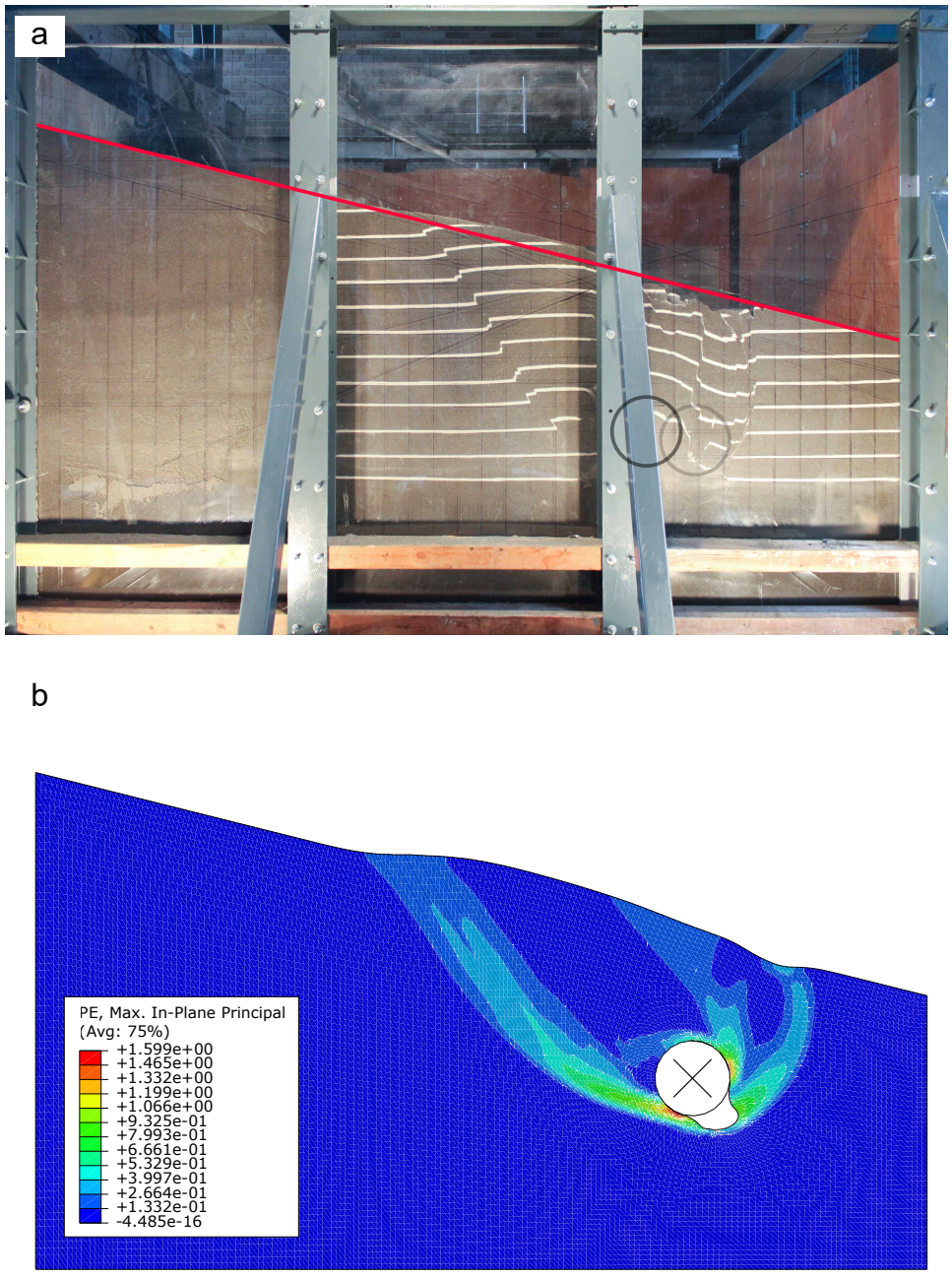

FIGURE B.4: Soil deformation in test 4 with slope grade of 25% and burial depth ratio of 2 a) experiment b) simulation

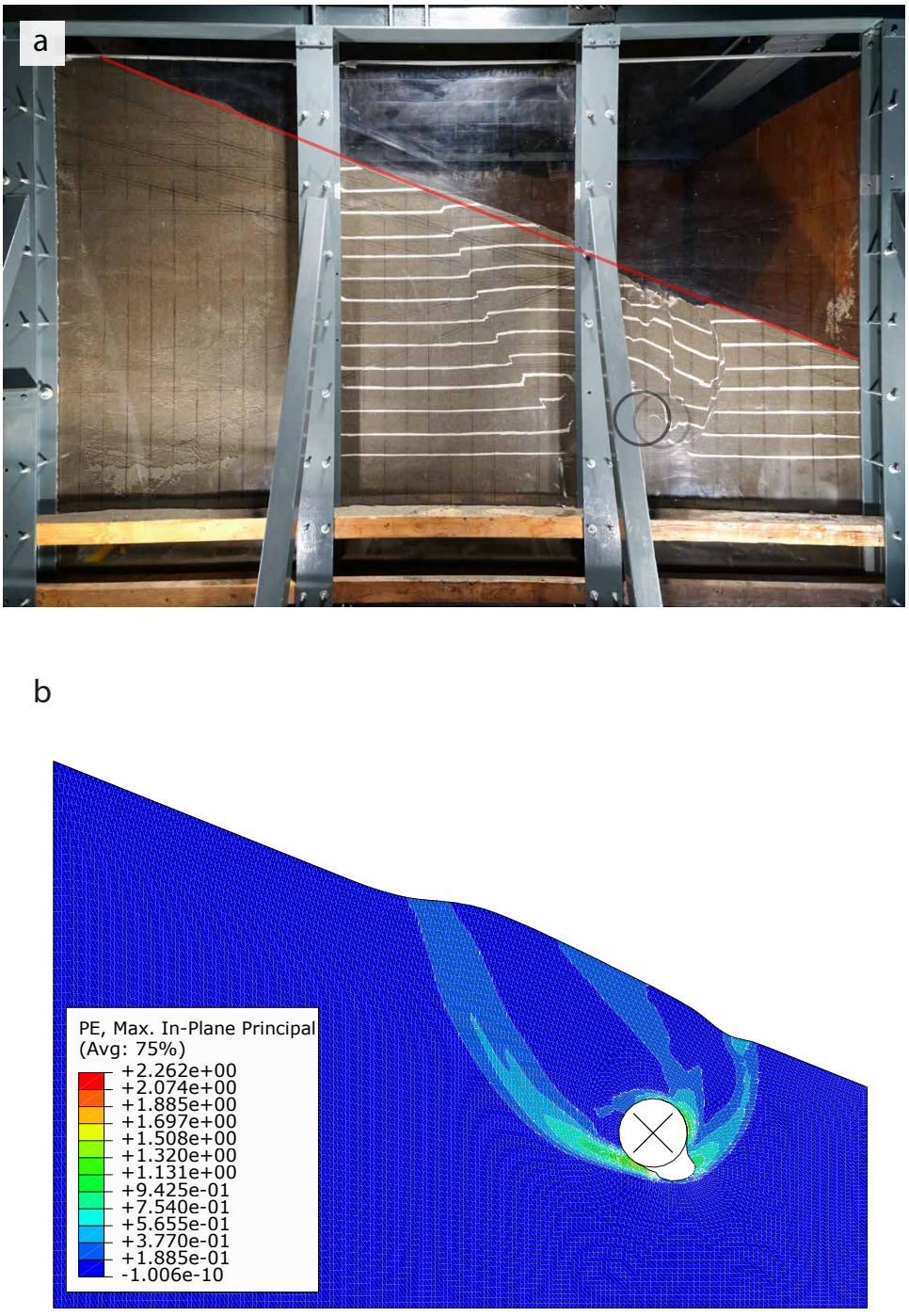

FIGURE B.5: Soil deformation in test 5 with slope grade of 40% and burial depth ratio of 2 a) experiment b) simulation

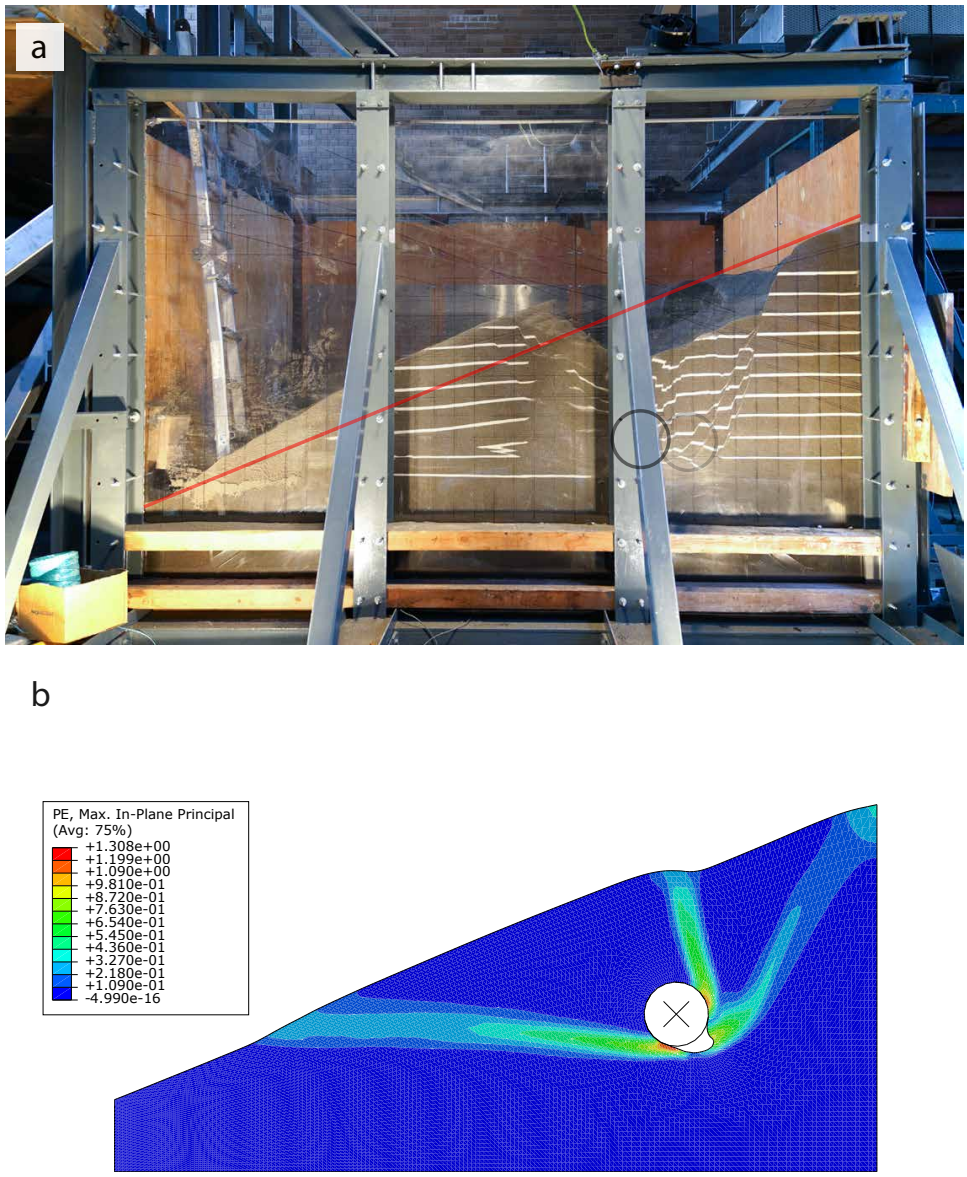

FIGURE B.6: Soil deformation in test 6 with slope grade of -40% and burial depth ratio of 2.4 a) experiment b) simulation

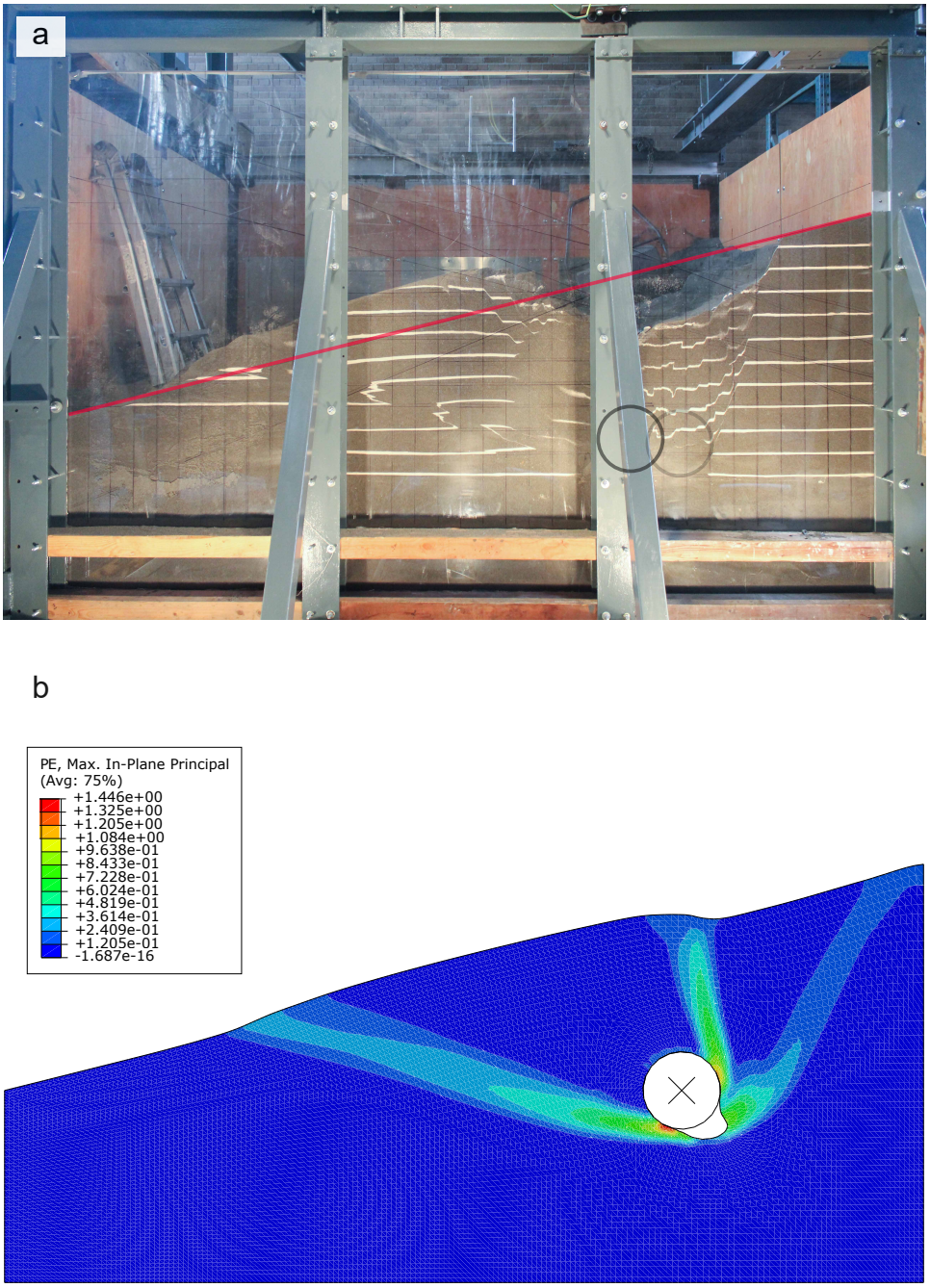

FIGURE B.7: Soil deformation in test 7 with slope grade of -25% and burial depth ratio of 2.4 a) experiment b) simulation

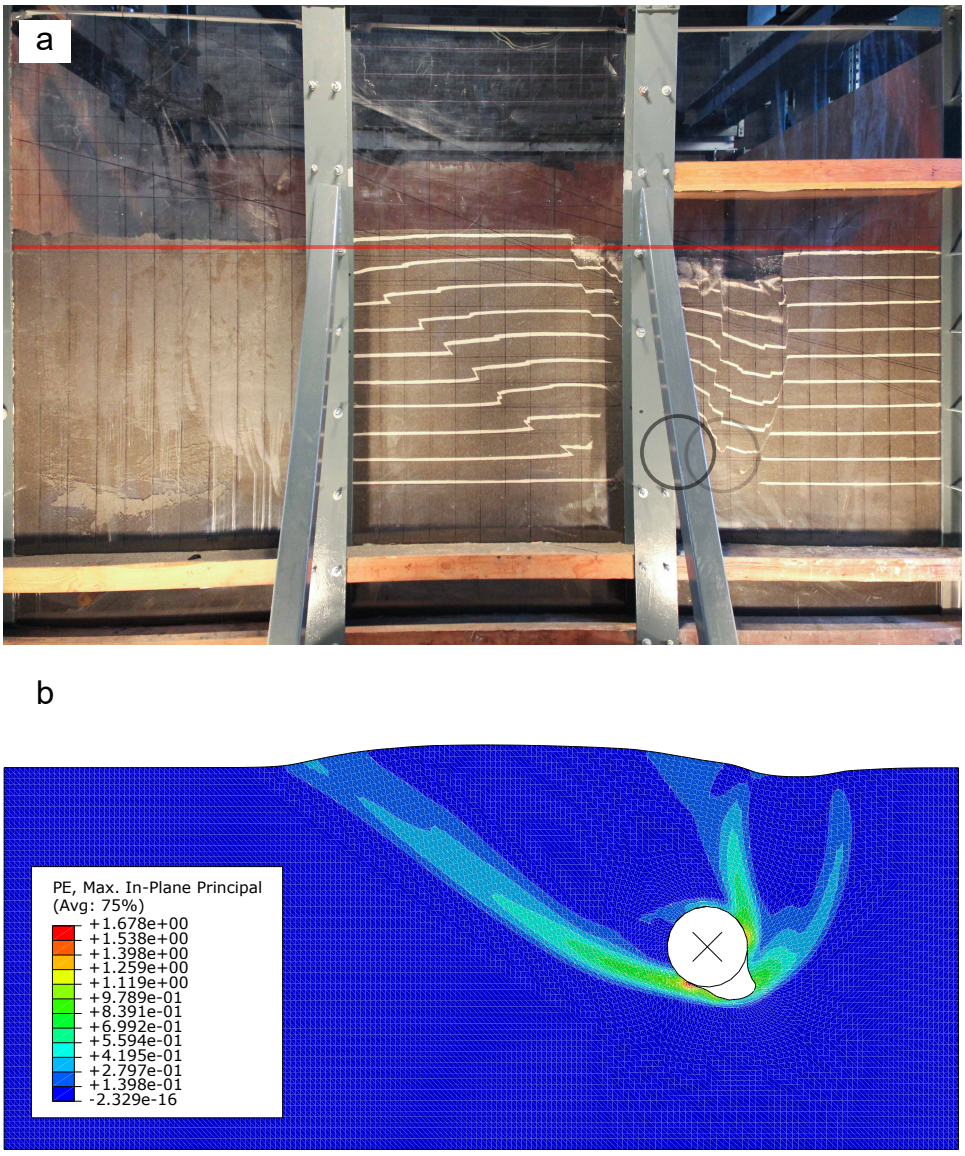

FIGURE B.8: Soil deformation in test 8 with slope grade of 0% and burial depth ratio of 2.4 a) experiment b) simulation

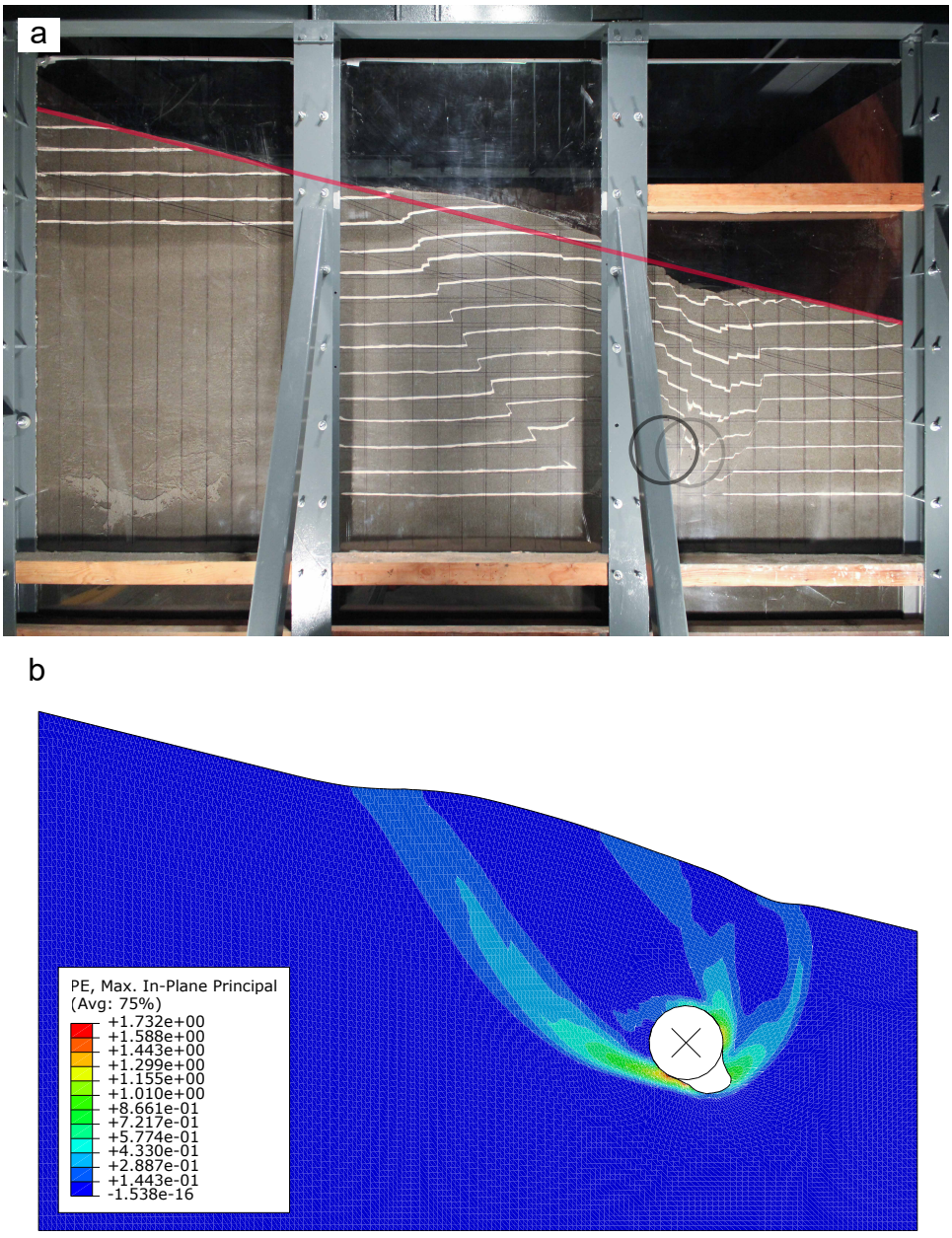

FIGURE B.9: Soil deformation in test 9 with slope grade of 25% and burial depth ratio of 2.4 a) experiment b) simulation

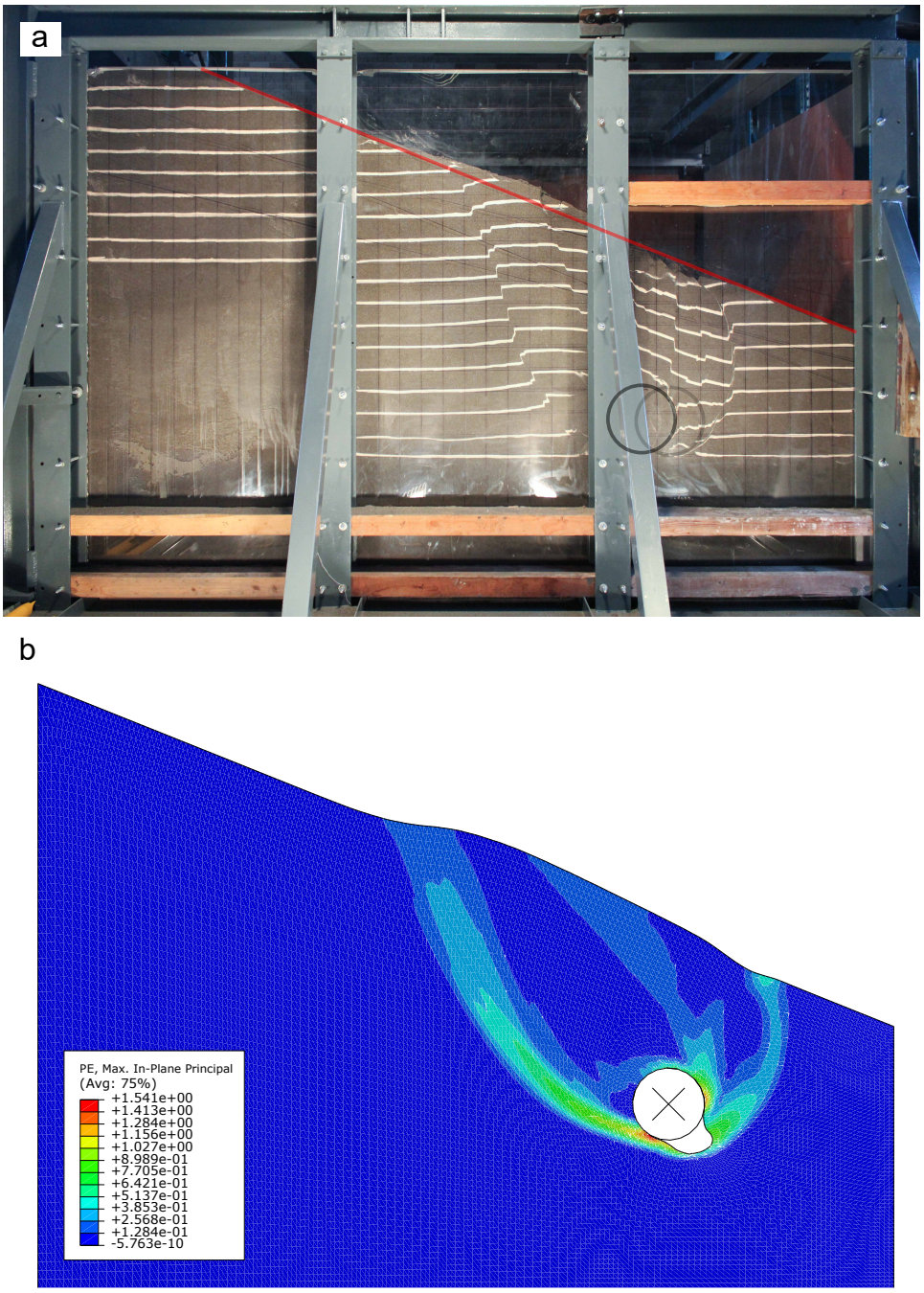

FIGURE B.10: Soil deformation in test 10 with slope grade of 40% and burial depth ratio of 2.4 a) experiment b) simulation

Appendix C

Advanced Soil-Pipe Interaction Research (ASPIRe™) facility

The ASPIRe™ facility at the University of British Columbia and the test preparation are presented herein through a series of photos. The plexiglass installation in the front face of the soil chamber, the access hole and conveyor belt, actuators and instrumentations such as load cells and string potentiometers, pipe connections, nuclear densometer, compaction equipment, and the process of filling and emptying of the sandbox are illustrated in these photos.

FIGURE C.1: Test preparation: plexiglass installation

FIGURE C.2: Test preparation: access hole and conveyor belt

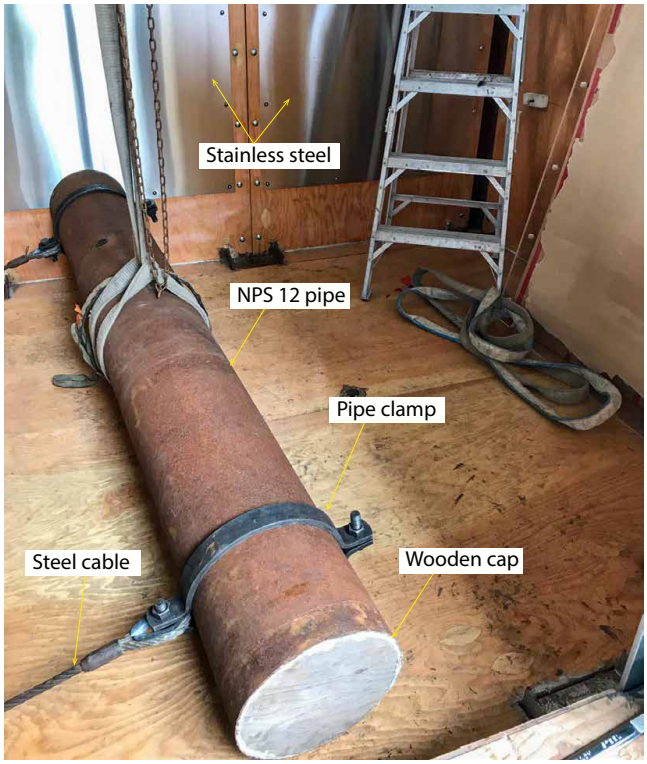

FIGURE C.3: Test preparation: pipe connections

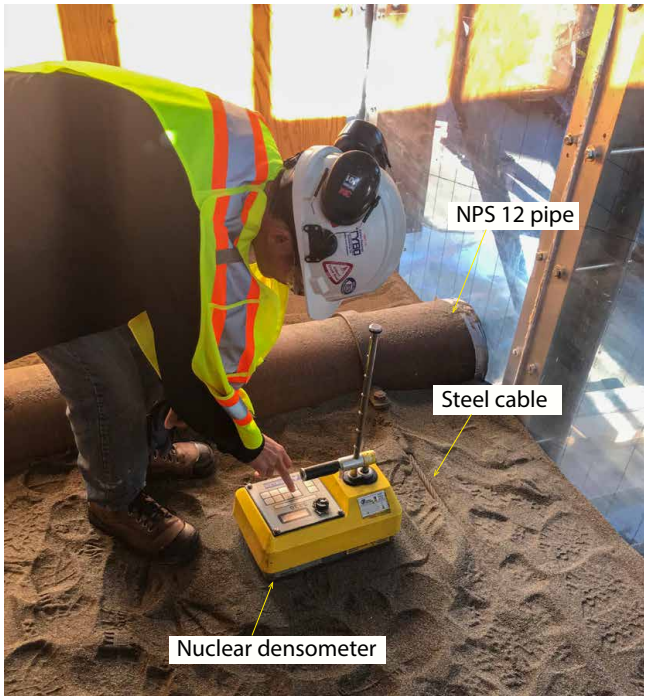

FIGURE C.4: Test preparation: nuclear densometer

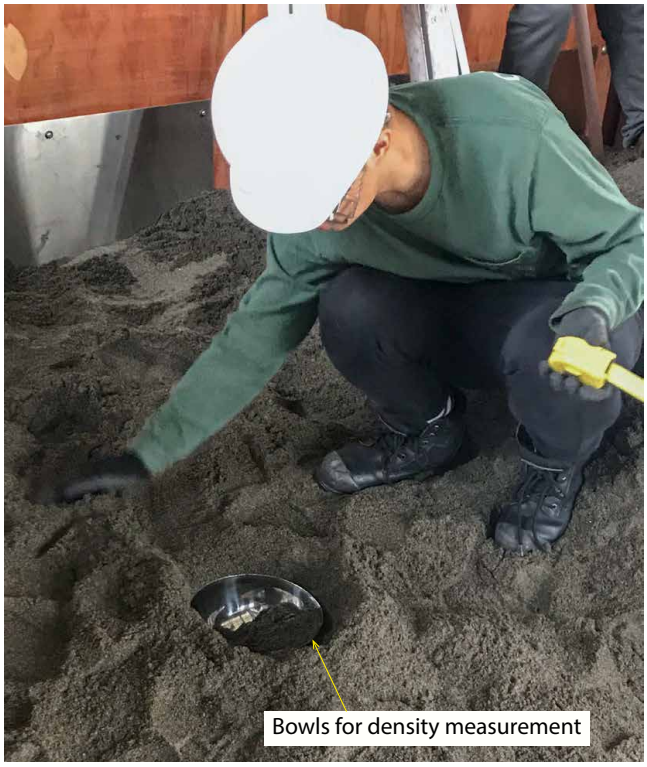

FIGURE C.5: Test preparation: using bowls for density measurements

FIGURE C.6: Test preparation: filling the sandbox

FIGURE C.7: Test preparation: dumping hopper

FIGURE C.8: Test preparation: a prepared test

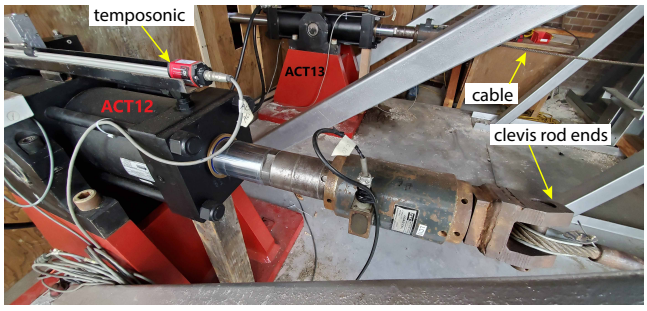

FIGURE C.9: Test preparation: actuators

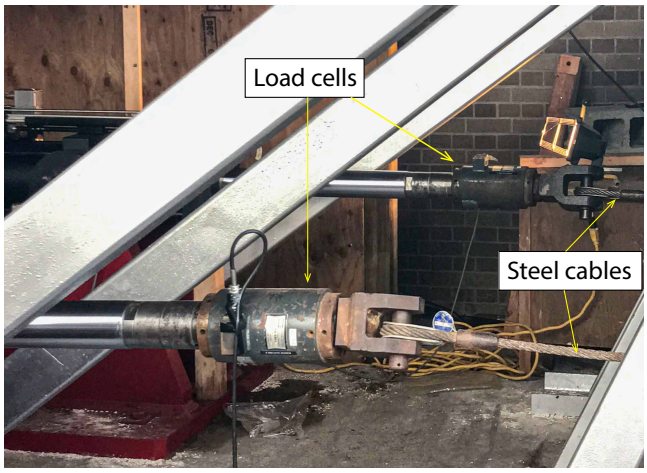

FIGURE C.10: Test preparation: load cells

FIGURE C.11: Test preparation: emptying soil chamber

FIGURE C.12: Test preparation: string potentiometers

FIGURE C.13: Test preparation: 100-kg static roller

FIGURE C.14: Test preparation: tamper

Appendix D

Force and displacement measurements over time

The displacement and force response of the pipe during the loading is plotted versus time. The pipe loading was measured using two load cells as illustrated in Fig. 2.3a; the results are presented with blue lines (loadcell 1 & 2). The pipe displacement is measured with two string potentiometers as shown in Fig.2.3a, results are presented with green lines (string pot 1 & 2). Note that the force measured by load cell 1 (western load cell) is higher than load measured by load cell 2 (eastern load cell). The reason for this difference is that the pipe is not placed symmetrically relative to the actuators. In other words, there was about a 0.1-m clearance from the pipe end to the western wall (see Fig. 2.3a), while almost no gap exists between the pipe end and plexiglass. This gap was intentionally provided to facilitate moving the pipe in the soil chamber during the test preparation. The normalized force was calculated with the assumption that the load was linearly distributed over the pipe length. The force-displacement curves presented in Fig. 2.7 to 2.10 are constructed using the information in these plots. It is noted that the total pipe load is the sum of the loads from both actuators. The pipe displacement is calculated by averaging the values of both string

pots. In some tests, the measured displacement of string pot 1 diverges from that of string pot 2. For example, in Fig. D.9, the maximum displacement measured by string pot 1 is 0.2 m while this value is 0.175 m for string pot 2. This means that the pipe rotated during the pull out. This rotations, however, was negligible as it was calcuated to be 0.6° in this example.

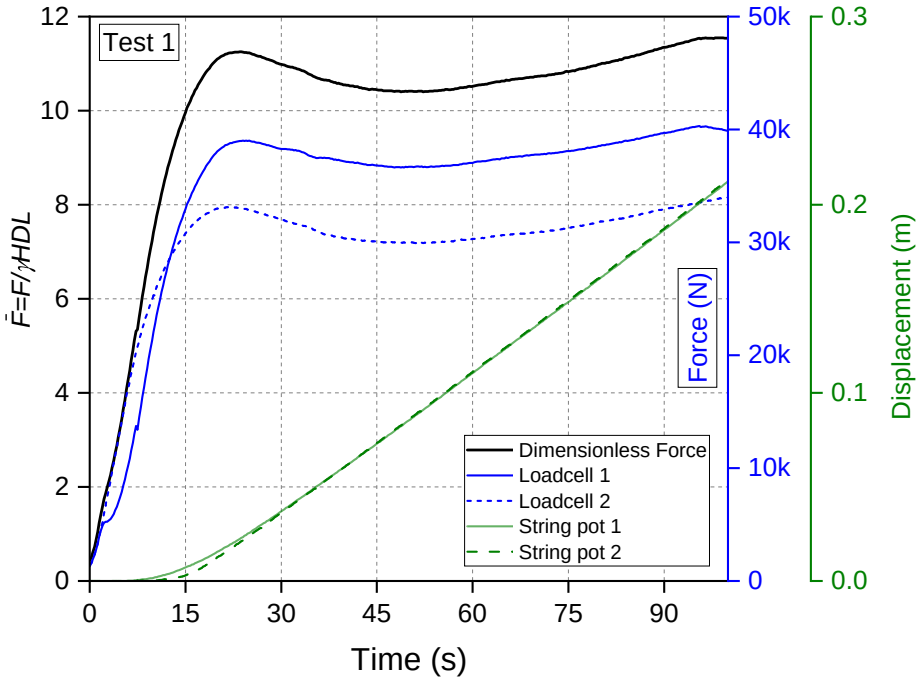

FIGURE D.1: Normalized force, force and displacement measurement over time for Test 1

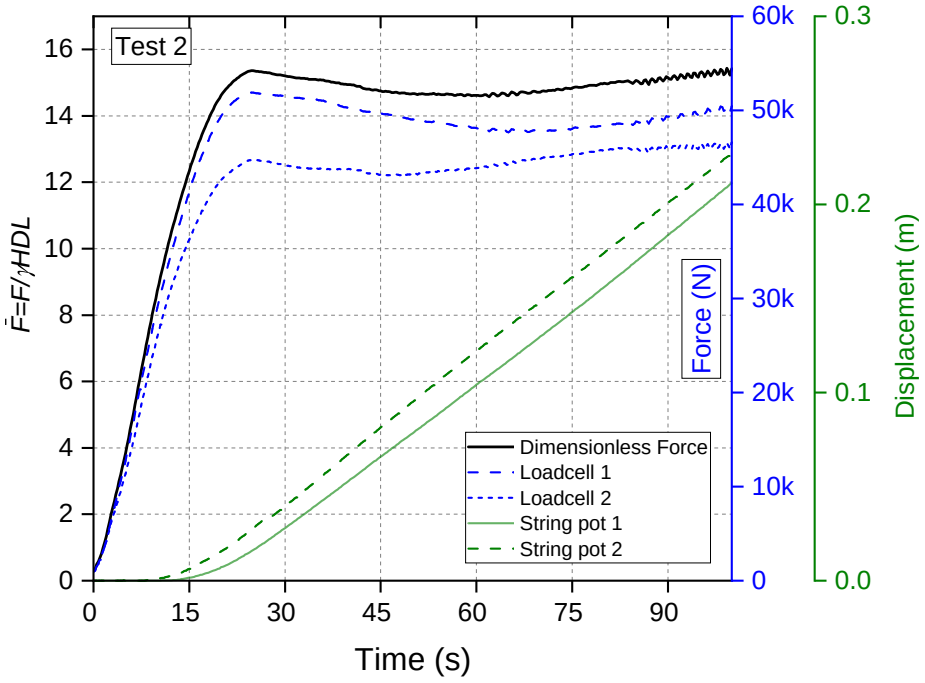

FIGURE D.2: Normalized force, force and displacement measurement over time for Test 2

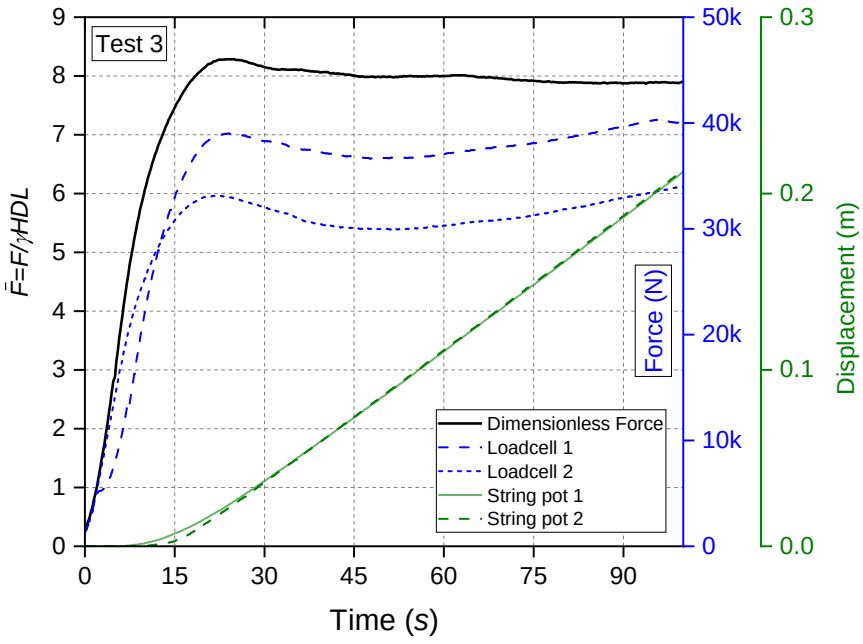

FIGURE D.3: Normalized force, force and displacement measurement over time for Test 3

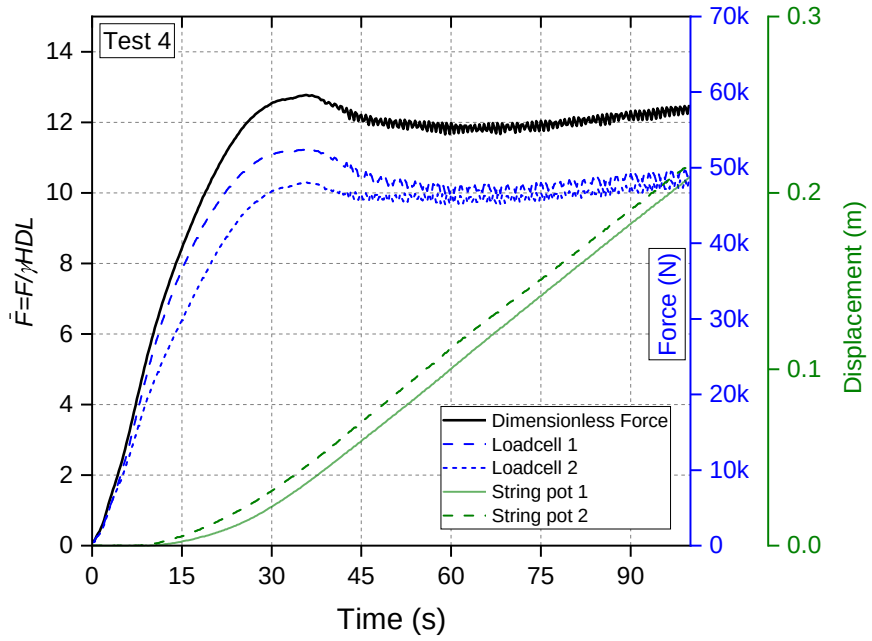

FIGURE D.4: Normalized force, force and displacement measurement over time for Test 4

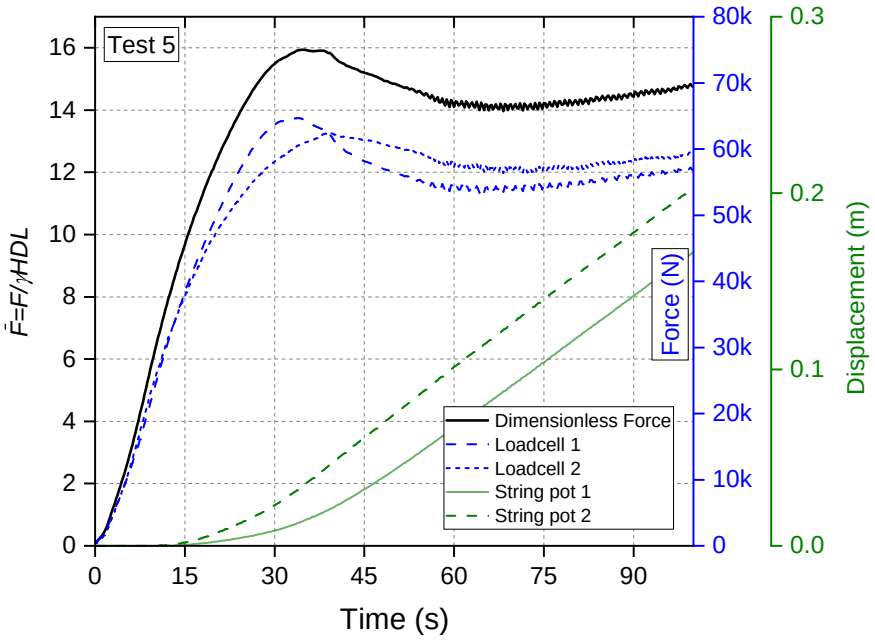

FIGURE D.5: Normalized force, force and displacement measurement over time for Test 5

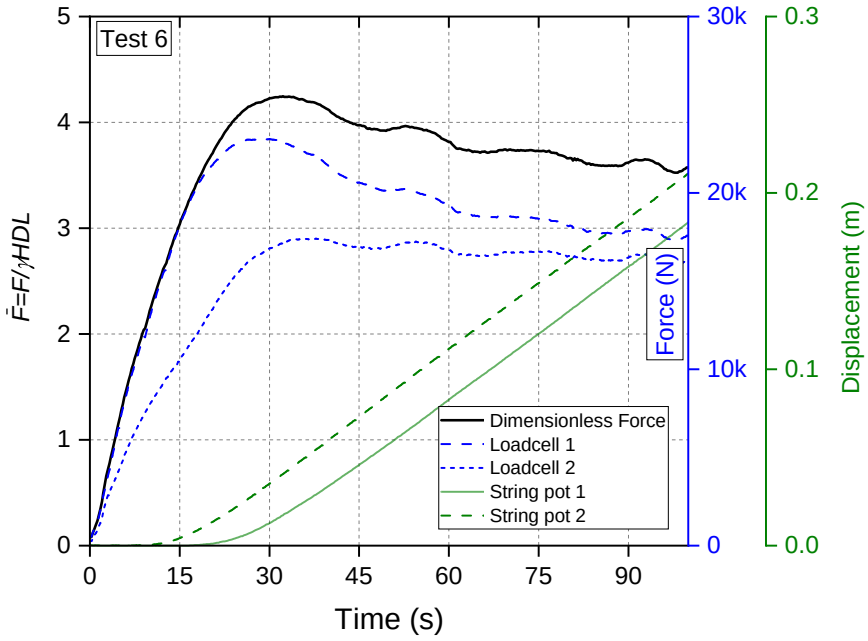

FIGURE D.6: Normalized force, force and displacement measurement over time for Test 6

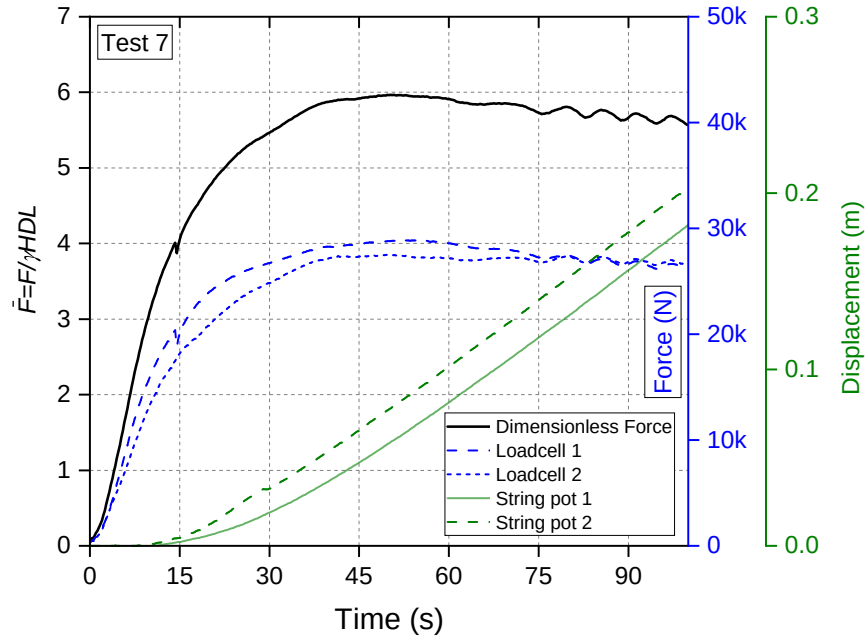

FIGURE D.7: Normalized force, force and displacement measurement over time for Test 7

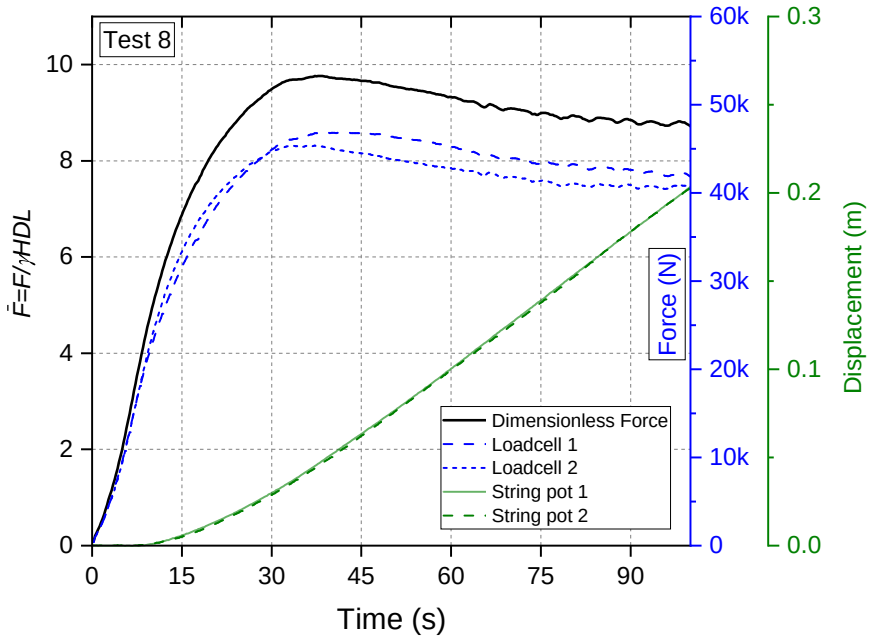

FIGURE D.8: Normalized force, force and displacement measurement over time for Test 8

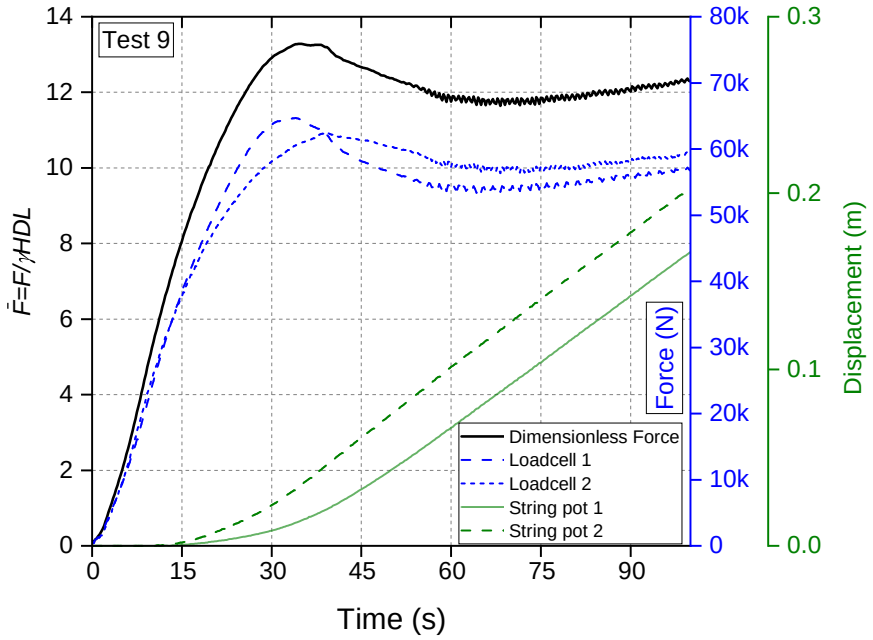

FIGURE D.9: Normalized force, force and displacement measurement over time for Test 9

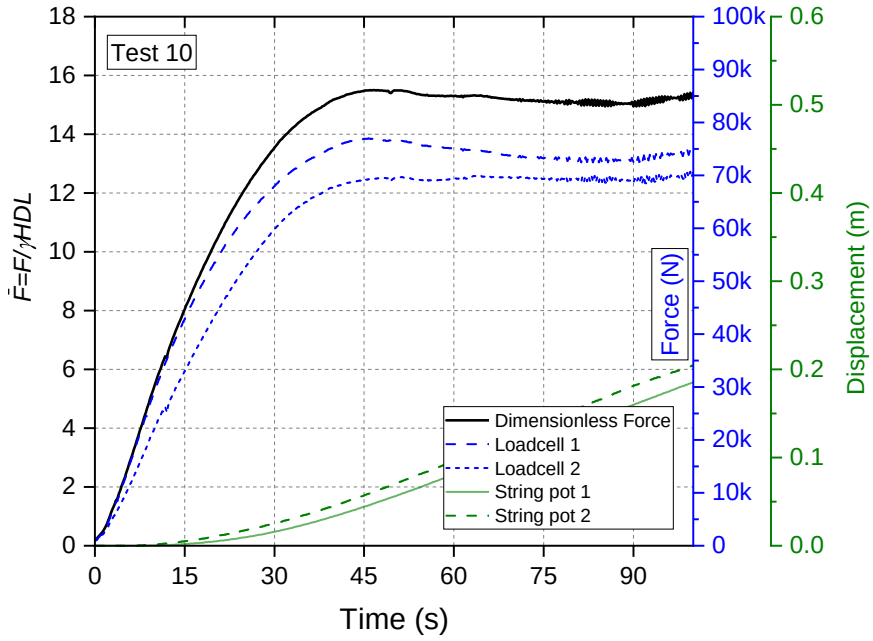

FIGURE D.10: Normalized force, force and displacement measurement over time for Test 10

Bibliography

ABAQUS (2017). *SIMULIA User Assistance*. Dassault Systèmes Simulia Corp., Johnston, RI, USA.

American Lifeline Alliance (2001). "Guidelines for the design of buried steel pipe". In: *American Society of Civil Engineers*.

Ansari, Y. et al. (2019). "Physical modelling of lateral sand–pipe interaction". In: *Géotechnique*, pp. 1–16.

ASCE (American Society of Civil Engineers) (1984). *Guidelines for the seismic design of oil and gas pipeline systems*. Committee on Gas and Liquid Fuel Lifelines.

Audibert, J. M. E. and Nyman, K. J. (1978). "Soil restraint against horizontal motion of pipes". In: *International Journal of Rock Mechanics and Mining Sciences & Geomechanics Abstracts* 15.2, A29.

Bolton, M. D. (1986). "The strength and dilatancy of sands". In: *Géotechnique* 36.1, pp. 65–78.

Burnett, A. J. (2015). "Investigation of full scale horizontal pipe–soil interaction and large strain behaviour of sand". PhD thesis. thesis, Queen's University, Kingston, Ont.

Byrne, P. M. et al. (1987). "Soil parameters for deformation analysis of sand masses". In: *Canadian Geotechnical Journal* 24.3, pp. 366–376.

Cappelletto, A. et al. (1998). "Field full scale tests on longitudinal pipeline-soil interaction". In: *2nd International Pipeline Conference*. American Society of Mechanical Engineers, pp. 771–778.

CSA Z662-15 (Canadian Standards Association) (2015). *Oil and Gas Pipeline Systems*.

Daiyan, N. et al. (2011). "Investigating pipeline–soil interaction under axial–lateral relative movements in sand". In: *Canadian Geotechnical Journal* 48.11, pp. 1683–1695.

Das, B. M. and Seeley, G. R. (1975). "Load-displacement relationship for vertical anchor plates". In: *Journal of Geotechnical and Geoenvironmental Engineering* 101.ASCE #11402 Proceeding.

Ferreira N, J. (2016). "Risk to Buried Gas Pipelines in Landslide Areas". PhD thesis. Department of Civil Engineering, The University of Manitoba, Winnipeg, MB.

Garrison, R. E. et al. (1969). "Early diagenetic cementation of recent sands, Fraser River delta, British Columbia". In: *Sedimentology* 12.1-2, pp. 27–46.

Guo, P. and Stolle, D. (2005). "Lateral pipe-soil interaction in sand with reference to scale effect". In: *Journal of Geotechnical and Geoenvironmental Engineering* 131.3, pp. 338–349.

Ha, D. et al. (2008). "Centrifuge modeling of earthquake effects on buried high-density polyethylene (HDPE) pipelines crossing fault zones". In: *Journal of geotechnical and geoenvironmental engineering* 134.10, pp. 1501–1515.

Hansen, J. B. (1961). "The ultimate resistance of rigid piles against transversal forces". In: *Bulletin 12, Danish Geotech. Institute*, pp. 1–9.

Hsu, T. W. (1996). "Soil restraint against oblique motion of pipelines in sand". In: *Canadian geotechnical journal* 33.1, pp. 180–188.

Hsu, T. W. et al. (2001). "Soil friction restraint of oblique pipelines in loose sand". In: *Journal of transportation engineering* 127.1, pp. 82–87.

Hsu, T. W. et al. (2006). "Soil restraint to oblique movement of buried pipes in dense sand". In: *Journal of transportation engineering* 132.2, pp. 175–181.

Incropera, F. P. et al. *Fundamentals of Heat and Mass Transfer, 2007, pp. A-5*.

Jung, J. K. et al. (2013). "Lateral soil-pipe interaction in dry and partially saturated sand". In: *Journal of Geotechnical and Geoenvironmental Engineering* 139.12, pp. 2028–2036.

Kanji, M. A. (1974). "The relationship between drained friction angles and Atterberg limits of natural soils". In: *Geotechnique* 24.4.

Karimian, H. (2006). "Response of buried steel pipelines subjected to longitudinal and transverse ground movement". PhD thesis. University of British Columbia.

Katebi, M. et al. (2018). "The optimum pipeline burial depth considering slow downslope soil movement and seasonal temperature variation". In: *12th International Pipeline Conference*. American Society of Mechanical Engineers, V002T02A015.

Katebi, M. et al. (2019a). "A study on the effects of slope grade on the soil-pipeline interaction loading". In: *Geostjohns2019 conference*.

Katebi, Mohammad et al. (2019b). "Numerical analysis of pipeline response to slow landslides: case study". In: *Canadian Geotechnical Journal* 56.12, pp. 1779–1788.

Kondner, R. L. (1963). "Hyperbolic stress-strain response: cohesive soils". In: *Journal of the Soil Mechanics and Foundations Division* 89.1, pp. 115–144.

Kostyukov, V. D. (1967). "Distribution of the density of sand in the sliding wedge in front of anchor plates". In: *Soil Mechanics and Foundation Engineering* 4.1, pp. 12–13.

Leonards, G. A. (1965). *Experimental study of static and dynamic friction between soil and typical construction materials*. Tech. rep. Purdue Univ Lafayette in School of Civil Engineering.

Mechanical Engineers (2003) ASME B31.8-2003, American Society of (2003). *Gas Transmission and Distribution Piping Systems*. Standard. American Society of Mechanical Engineers, New York.

Mesri, G. and Hayat, T. M. (1993). "The coefficient of earth pressure at rest". In: *Canadian Geotechnical Journal* 30.4, pp. 647–666.

Michalowski, R. L. (1993). "A constitutive model of saturated soils for frost heave simulations". In: *Cold regions science and technology* 22.1, pp. 47–63.

Mitchell, J. K. and Soga, K. (2005). *Fundamentals of soil behavior*. Vol. 3. John Wiley & Sons, New York.

Monroy-Concha, M. (2013). "Soil restraints on steel buried pipelines crossing active seismic faults". PhD thesis. University of British Columbia.

Murray, E. J. and Geddes, J. D. (1989). "Resistance of passive inclined anchors in cohesionless medium". In: *Geotechnique* 39.3, pp. 417–431.

Neely, W. J. et al. (1973). "Failure loads of vertical anchor plates in sand". In: *Journal of Soil Mechanics & Foundations Div* 99.Proc. Paper 9980.

Newmark, N. M. and Hall, W. J. (1975). "Pipeline design to resist large fault displacement". In: *Proceedings of US national conference on earthquake engineering*. Vol. 1975, pp. 416–425.

Nyman, K. J. (1984). "Soil response against oblique motion of pipes". In: *Journal of Transportation Engineering* 110.2, pp. 190–202.

Oliveira, J. R. M. S. et al. (2010). "Physical modeling of lateral clay-pipe interaction". In: *Journal of geotechnical and geoenvironmental engineering* 136.7, pp. 950–956.

O'Rourke, M. et al. (2005). "Centrifuge modeling of PGD response of buried pipe". In: *Earthquake Engineering and Engineering Vibration* 4.1, pp. 69–73.

Oswell, J. M. (2016). *Soil mechanics for pipeline stress analysis*. Naviq Consulting Inc.

Ovesen, N. K. (1964). "Anchor slabs, calculation methods and model tests". In: *Bulletin* 16, p. 39.

Ovesen, N. K. and Strømann, H. (1972). "Design method for vertical anchor slabs in sand". In: *Performance of earth and earth-supported structures*. ASCE, p. 1481.

Paulin, M. J. (1998). "An investigation into pipelines subjected to lateral soil loading". PhD thesis. Department of Civil Engineering, Memorial University of Newfoundland, Mount Pearl, NL.

PRCI (Pipeline Research Council International) (2017). *Pipeline Seismic Design and Assessment Guideline*. Catalogue No: PR-268-134501-R01.

Revie, R. W. (2015). *Oil and gas pipelines: integrity and safety handbook*. John Wiley & Sons.

Rowe, R. K. and Davis, E. H. (1982). "The behaviour of anchor plates in sand". In: *Geotechnique* 32.1, pp. 25–41.

Roy, K. et al. (2015). "Finite element modeling of lateral pipeline–soil interactions in dense sand". In: *Canadian Geotechnical Journal* 53.3, pp. 490–504.

Roy, K. et al. (2018). "Lateral resistance of pipes and strip anchors buried in dense sand". In: *Canadian Geotechnical Journal* 55.12, pp. 1812–1823.

Saiyar, M. et al. (2016). "Response of pipelines of differing flexural stiffness to normal faulting". In: *Géotechnique* 66.4, pp. 275–286.

Sivathayalan, S. (2000). "Fabric, initial state and stress path effects on liquefaction susceptibility of sands". PhD thesis. University of British Columbia.

Smith, J. E. (1962). *Deadman anchorages in sand*. Tech. rep. NAVAL CIVIL ENGINEERING LAB PORT HUENEME CALIF.

TERRAIN, DE. "A suggested method for describing the rate of movement of a landslide". In: ().

Tian, Y. and Cassidy, M. J. (2011). "Pipe-Soil Interaction Model Incorporating Large Lateral Displacements in Calcareous Sand". In: *Journal of Geotechnical and Geoenvironmental Engineering* 137.3, pp. 279–287.

Trautmann, C. H. (1983). "Behavior of pipe in dry sand under lateral and uplift loading". PhD thesis. Cornell Univ., Ithaca, NY.

Trautmann, C. H. and O'Rourke, T. D. (1985). "Lateral force-displacement response of buried pipe". In: *Journal of Geotechnical Engineering* 111.9, pp. 1077–1092.

Trautmann, C. H. et al. (1985). "Uplift force-displacement response of buried pipe". In: *Journal of Geotechnical Engineering* 111.9, pp. 1061–1076.

Tsatsis, A. et al. (2018). "Performance of a buried pipeline along the dip of a slope experiencing accidental sliding". In: *Géotechnique* 68.11, pp. 968–988.

Uthayakumar, M. (1996). "Liquefaction of sands under multi-axial loading". PhD thesis. University of British Columbia.

Vermeer, PA and Sutjiadi, W (1985). "The uplift resistance of shallow embedded anchors". In: *International conference on soil mechanics and foundation engineering. 11*, pp. 1635–1638.

Welty, J. et al. (2014). *Fundamentals of momentum, heat and mass transfer*. Wiley Global Education.

Wijewickreme, D. et al. (2009). "Response of buried steel pipelines subjected to relative axial soil movement". In: *Canadian Geotechnical Journal* 46.7, pp. 735–752.

Wijewickreme, D. et al. (2017). "Soil restraints on buried pipelines subjected to reverse-fault displacement". In: *Canadian Geotechnical Journal* 54.10, pp. 1472–1481.

Xie, X. (2008). "Numerical analysis and evaluation of buried pipeline response to earthquake-induced ground fault rupture". PhD thesis. Rensselaer Polytechnic Institute.

Yimsiri, S. et al. (2004). "Lateral and upward soil-pipeline interactions in sand for deep embedment conditions". In: *Journal of Geotechnical and Geoenvironmental Engineering* 130.8, pp. 830–842.

Zhang, W. and Askarinejad, A. (2019). "Behaviour of buried pipes in unstable sandy slopes". In: *Landslides* 16.2, pp. 283–293.

Zhou, M. et al. (2017). "Performance of buried HDPE pipes–part II: total deflection of the pipe". In: *Geosynthetics International* 24.4, pp. 396–407.